TDD based 5G networks performance analysis and radio resource dimensioning with different network geometry models

Jalal Rachad

INSTITUT POLYTECHNIQUE DE PARIS

NNT: 2019IPPAT008

Thèse de doctorat

TDD based 5G networks performance analysis and radio resource dimensioning with different network geometry models

Thèse de doctorat de l'Institut Polytechnique de Paris
Préparée à Telecom Paris

École doctorale n°626 de l'Institut Polytechnique de Paris (ED IPP)
Spécialité de doctorat : Mathématiques et informatique

Thèse présentée et soutenue à Palaiseau, le 17/12/2019, par

Jalal RACHAD

Composition du Jury :

M. Bartlomiej BLASZCZYSZYN Directeur recherche, ENS-INRIA (DYOGENE)	Président
M. Anthony BUSSON Professeur, ENS-Lyon (LIP)	Rapporteur
Mme. Lina MROUEH Professeur, ISEP-Paris (DSIT)	Rapporteur
Mme. Isabelle GUERIN-LASSOUS Professeur, ENS-Lyon (LIP)	Examinateur
M. Laurent DECREUSEFOND Professeur, Telecom Paris (INFRES)	Directeur de thèse
M. Ridha NASRI Docteur et Ingénieur recherche, Orange Labs (MRP)	Co-Directeur de thèse

PhD thesis

Institut Polytechnique de Paris & Telecom Paris

ED IPP 626: Mathématiques et informatique

Analyse des performances et dimensionnement des réseaux mobiles 5G basés sur TDD avec différents modèles géométriques

Jalal RACHAD

Encadré par:

Prof. Laurent DECREUSEFOND & Dr. Ridha NASRI

December 2019

Dedication

To my beloved parents, it's impossible to thank you adequately for everything you have done, from rising me to loving me unconditionally.

To my lovely wife, for your encouraging words and honest love.

To my brother Anas and my sister Nihal.

Acknowledgement

It is my pleasure to get the opportunity to express gratitude to all who contributed in the successful completion of my PhD thesis.

First of all, I would like to express my heartily thanks to my thesis supervisor Professor Laurent DECREUSEFOND for his constant guidance, supervision throughout the last three years, for his confidence, patience and support to overcome numerous obstacles I have been facing through my research work. I would also like to express special thanks to my co-supervisor Dr. Ridha NASRI for his invaluable guidance, fruitful ideas throughout the whole period of my PhD and careful editing helped me enormously to get results of better quality.

I would like to thank my managers Roufia YAHI and Benoit BADARD, my GDM/MRP team members, Alain SIMONIAN, Zwi ALTMAN, Sana BENJEMAA and all my colleagues in Orange Labs for providing a friendly working environment and facilities to complete this thesis in the best conditions.

Contents

Abstract **9**

Résumé étendu **11**

Publications **29**

List of figures **33**

List of tables **35**

List of acronyms **37**

1 Introduction **39**
1.1 Background and general context 39
1.2 Problematics and contributions 42
1.3 Thesis outline 45

2 Related works and state of the art **47**
2.1 Dynamic-TDD vs S-TDD performance analysis and interference coordination schemes 47
2.2 Full Dimension MIMO and Beamforming 49
2.3 OFDM radio resource dimensioning 51
2.4 Cellular network modeling and interference analysis 53

3 D-TDD interference tractability and performance analysis **57**
3.1 Introduction 57
3.2 System models and notations 58
3.2.1 Dynamic TDD model 58
3.2.2 Macro-cell deployment 58

3.2.3 Small-cell deployment . . . 59
3.2.4 Propagation model . . . 60
3.3 Dynamic TDD interference derivation in a macro-cell deployment . . . 62
3.3.1 Downlink *ISR* derivation $D(z_0)$ . . . 62
3.3.2 Uplink *ISR* derivation $U(z_0)$ . . . 64
3.3.3 Coverage probability . . . 66
3.4 Small-cells' network performance analysis . . . 68
3.4.1 DL coverage probability derivation . . . 70
3.4.2 UL coverage probability derivation . . . 72
3.4.3 Average spectral efficiency . . . 73
3.5 Simulation results . . . 73
3.6 Conclusion . . . 78

4 A 3D beamforming scheme based on the spatial distribution of users' locations 79
4.1 Introduction . . . 79
4.2 System model and notations . . . 79
4.2.1 Network model . . . 79
4.2.2 Beamforming model . . . 80
4.2.3 Propagation model . . . 82
4.3 Characterization of antenna beamforming radiation pattern . . . 83
4.4 Interference characterization . . . 86
4.5 Numerical results and discussion . . . 88
4.6 Conclusion . . . 91

5 D-TDD interference mitigation schemes 93
5.1 D-TDD based macro-cell deployment interference mitigation scheme . . . 93
5.1.1 Interference characterization . . . 95
5.1.2 Simulation results . . . 97
5.2 D-TDD interference mitigation in small-cell deployment . . . 102
5.2.1 DL to UL *ISR* derivation . . . 103
5.2.2 Coverage probability . . . 104
5.3 Conclusion . . . 105

6 OFDM based 5G-NR dimensioning approach 107
6.1 Introduction . . . 107
6.2 System model and notations . . . 108
6.2.1 Indoor users model . . . 108
6.2.2 Outdoor users model . . . 108
6.2.3 Network model . . . 110

6.3 Presentation of the dimensioning approach 113
6.3.1 Qualification of the total number of requested PRBs 113
6.3.2 Congestion probability and dimensioning approach 115
6.4 Numerical results 120
6.5 Conclusion 126

7 Conclusions and perspectives **129**
7.1 Conclusions 129
7.2 Perspectives 130

Abstract

Although LTE has been considered as a strong technology expected to be used in the upcoming years, the need for a new technology, capable to meet the huge growth in data traffic volume, to support diverse use cases and to empower new users' experience, is becoming a reality. A new generation of cellular networks, known as 5G new radio (NR), has been standardized through improvements in the current 4G/4G+ concepts and features in order to bring a new level of flexibility, scalability and efficiency. Time division duplex (TDD) is expected to be one of the key features of 5G NR since it offers more advantages than frequency division duplex (FDD) mode in terms of capacity, flexibility and implementation adequacy with other features, such as full dimension multiple input multiple output antenna (FD-MIMO) technology. A variant operational mode of TDD, known as D-TDD, is in the scope. It is designed to deal with uplink (UL) and downlink (DL) traffic asymmetry since it is based on instantaneous traffic estimation and offers more flexibility in resource assignment. However, the use of D-TDD requires new interference mitigation schemes to handle two additional types of interference called cross link interference (CLI) and stands for DL to UL and UL to DL interference.

The first part of this thesis is devoted to tackle the problem of interference modeling in D-TDD based macro-cell and small-cell deployments. We provide a complete analytical approach to derive relevant metrics, such as interference-to-signal-ratio (ISR) and the coverage probability formulas, considering adequate geometry models for each type of deployment: regular hexagonal model for macro-cells and spatial PPP based model for small-cells. In the second part, we investigate the feasibility of two interference mitigation schemes designed to reduce the strong DL to UL interference that affects D-TDD based systems. To this intend, we propose a new 3D beamforming scheme based on the spatial distribution of users' locations. This technique aims at exploiting the horizontal and the vertical dimensions to enhance the strength of antenna radiation patterns in a given location and reduce DL interference in neighboring cells. Then, we study the applicability of this scheme in the context of D-TDD based macro-cells and we compare performance to S-TDD with the aim of verifying the feasibility of D-TDD for macro-cells. Additionally,

we propose a tractable cell clustering scheme, based on the hexagonal tessellation, to reduce DL to UL interference in small-cell networks.

The third part of the thesis is dedicated to investigate another problematic which is Orthogonal Frequency Division Multiplex (OFDM) radio resource dimensioning. Since 5G NR takes in consideration a wide array of emerging use cases and also the possibility of having future requirements, the third Generation Partnership Project (3GPP) comes up with a variant of OFDM known as scalable OFDM and having different sub carriers' spacing. This feature appears to be an ideal choice for 5G NR since it offers a high spectral efficiency, robustness to selective fading channels, convenience with diverse spectrum bands and compatibility with other features. Therefore, dimensioning OFDM is a major task to accomplish in the context of NR. To this purpose, we provide an analytical model to dimension OFDM based systems, that remains valid also for scalable OFDM, with a proportional fair resources' allocation policy. We identify two kind of users: *i*) indoor users that we model with a spatial PPP in the cell coverage area. *ii*) To model outdoor users, we propose first a random model describing the distribution of roads in the studied area which is Poisson Line Process (PLP), then we consider the random distribution of users in each road according to a linear PPP. Hence, the distribution of users becomes doubly stochastic according to a process known as Cox. According to this model, we show that the total number of requested radio resource follows a compound Poisson distribution and we derive some analytical results regarding the congestion probability. The accuracy of this model is then verified through numerical results.

Keywords 5G NR, S-TDD, D-TDD, Interference, SINR, ISR, Coverage probability, 3D beamforming, FeICIC, Cell clustering, Hexagonal network, PPP, Cox Process, PLP, Dimensioning, Congestion probability, QoS, ASE.

Résumé étendu

Introduction

Une nouvelle génération des réseaux mobiles, connue sous le nom de 5G NR, est en cours de standardisation à travers des améliorations apportées à son prédécesseur 4G/4G+. 5G NR va introduire un nouveau niveau de flexibilité, scalabilité et efficacité afin de satisfaire plusieurs classes de services. Le mode de duplexage TDD est le plus favorable pour 5G NR grâce aux avantages qu'il représente par rapport au mode FDD en termes de capacité, flexibilité et convenance de déploiement avec les autres technologies attendues dans le cadre de la 5G comme FD-MIMO. Une variante du TDD, connue sous le nom du dynamique TDD (D-TDD), attire de plus en plus l'attention. D-TDD est désigné pour l'adaptation des configurations des sous-trames DL et UL en se basant sur une estimation instantanée du trafic. Cependant, l'utilisation de ce mode nécessite l'implémentation des mécanismes capable de réduire deux types d'interférence additionnelles : l'interférence générée par les stations de bases qui impacte le signal UL des utilisateurs et l'interférence générée par les mobiles en UL qui interfère avec le signal DL des stations de base.

La première partie de cette thèse est consacrée à l'analyse des performances du mode D-TDD en termes de ISR et de probabilité de couverture dans 2 types de déploiement : macro-cells et small-cells. Ensuite, nous proposons deux techniques de mitigation des interférences dont la première est destinée aux macro-cells et basée sur le 3D beamforming tandis que la 2ème est le cell clustering et appliquée au small-cells. Dans la 2ème partie de cette thèse, nous étudions la problématique du dimensionnement de l'OFDMA qui sera une technologie de base pour la 5G NR. Etant donné que le dimensionnement des ressources radio est une tâche primordiale dans l'ingénierie radio, nous proposons un modèle analytique qui permet la réalisation de cette tâche en considérant un scheduling proportional fair. Nous distinguons entre 2 types d'utilisateurs : utilisateurs indoor qui sont modélisés par un PPP spatial et utilisateurs outdoor qui sont modélisés selon un processus de Cox conduit par un PLP. Plusieurs résultats analytiques et numériques sont exposés afin de justifier l'exactitude et la précision de ce modèle.

Modélisation des interférences et analyse des performances des réseaux mobiles basés sur le dynamique TDD:

Afin de supporter la prolifération continue du trafic de données observée durant les dernières années, et qui va continuer à augmenter vu les différentes exigences des utilisateurs mobiles et des services demandés, une variante du mode de duplexage TDD, nommée dynamique TDD, est introduite dans le but de permettre aux cellules d'adapter la configuration des trames montantes (UL) et descendantes (DL) d'une manière dynamique selon le trafic observé. L'utilisation d'un tel mode résulte en deux types d'interférence additionnelles qui impacte le signal utile des utilisateurs:

- L'interférence UL to DL: quand une cellule est en transmission DL, le signal utile d'un utilisateur servi en DL est interféré par le signal des utilisateurs qui transmettent en UL dans les autres cellules Fig. 1.
- L'interférence DL to UL: quand une cellule est en transmission UL, le signal utile d'un utilisateur est interféré par le signal DL des stations de base des autres cellules qui transmettent en DL Fig. 2.

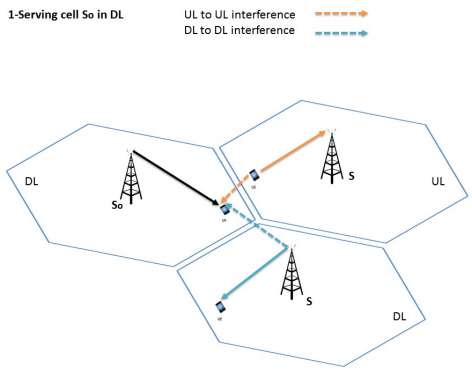

Figure 1 – L'interférence UL to DL

.

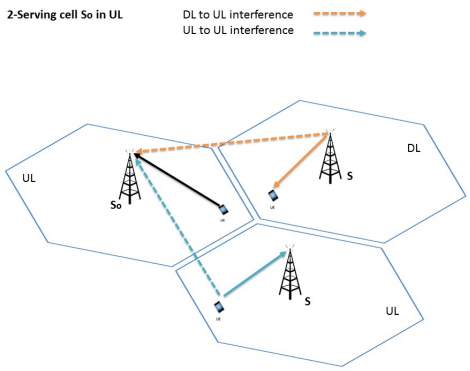

Figure 2 – L'interférence DL to UL

.

Ces deux types d'interférence sont en général difficiles à gérer surtout pour les macrocells car il se peut que les stations de base qui transmettent avec des puissances élevées se trouvent en visibilité directe entre eux et aussi les mobiles se déplacent d'une manière aléatoire.

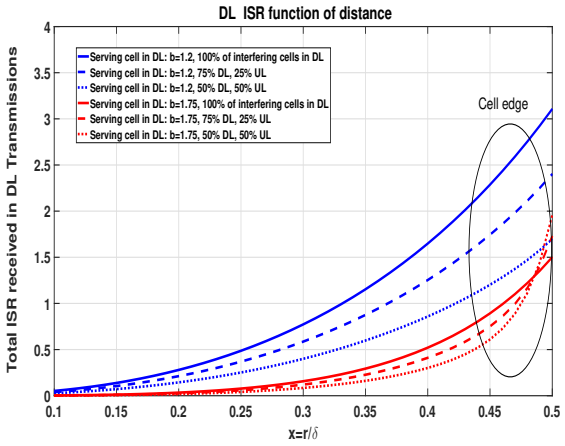

Figure 3 – DL ISR: Static TDD vs Dynamic TDD.

.

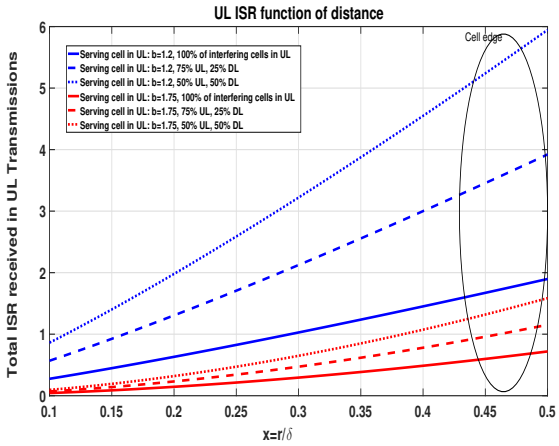

Figure 4 – UL ISR: Static TDD vs Dynamic TDD.

.

Dans ce contexte, nous proposons une approche analytique qui permet la modélisation des interférences générées par le mode D-TDD dans 2 types de déploiement :

- Un réseau de macro-cells: On le modélise par un réseau hexagonal régulier avec un nombre infini de cellules macro. On dérive les expressions de ISR (Interference to Signal Ratio) qui couvrent les 4 types d'interférence qui apparaissent selon le sens de transmission et on dérive aussi l'expression explicite de la probabilité de couverture en DL et en UL.

- Un réseau de small-cells: Étant donné que les small-cells prennent des positions non planifiées comme le cas des macro-cells, on choisit de modéliser leur distribution spatiale par un processus de poisson afin de pouvoir exploiter les résultats mathématiques basés sur la géométrie stochastique. Cela va permettre de dériver la probabilité de couverture en DL et en UL.

Pour un réseau de macro-cells, les résultats montrent que l'activation du mode D-TDD est en faveur de la transmission DL comme on peut voir sur Fig. 3. En effet, lorsque un certain nombre de cellules changent leurs sens de transmission du DL vers le UL, l'interférence qui provient du signal DL des stations de bases, qui est puissant par rapport au signal UL qui provient des mobiles, diminue et les performances s'améliorent par la suite. Cependant, le comportement est complètement différent durant la transmission UL. Lorsque le D-TDD s'active, on remarque que l'interférence augment d'une manière

significative, ceci provient du fait que le signal DL des stations de bases interfère et impacte beaucoup le signal UL du mobile dans sa cellule serveuse Fig. 4. Par conséquence, on peut conclure que le mode D-TDD ne peut pas s'appliquer à un réseau macro en UL sans techniques de mitigation d'interférence.

Les mêmes résultats peuvent être observés par simulation pour les deux types de déploiement macro-cells et small-cells. La seule différence c'est que le réseau de small-cells est moins vulnérable à l'interférence DL to UL car en général les small-cells sont considérées plus isolées les unes des autres.

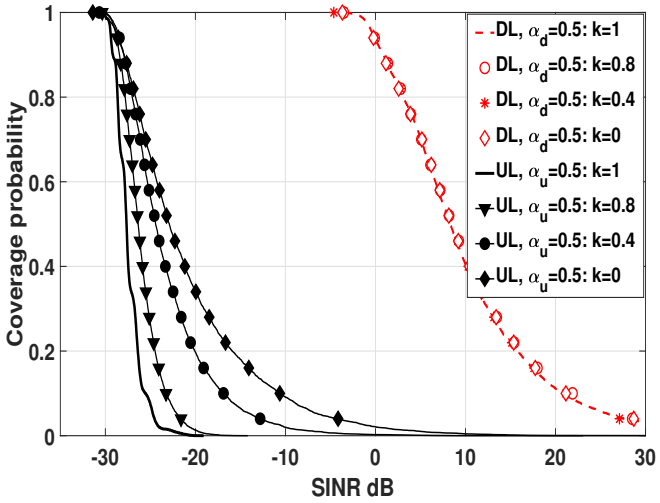

Figure 5 – Probabilité de couverture en DL et en UL pour un réseau macro avec différent facteur de control de puissance fractionnel.

Nous considérons pour le sens de transmission UL un mécanisme de contrôle de puissance appliqué au canal PUSCH et on le modélise par le contrôle de puissance fractionnel avec un facteur de compensation k. La figure Fig. 5 montre la probabilité de couverture en DL et UL en considérant différent facteurs de contrôle de puissance k pour un réseau de macro-cells dont le mode D-TDD est activé. Pour le DL, on peut voir que le contrôle de puissance en UL n'a quasiment aucun impact sur les performances car l'interférence qui domine durant le cycle de transmission DL est celle en provenance des stations de base qui transmettent en DL. Pour le UL, on peut constater qu'il y a une amélioration de la probabilité de couverture pour les petites valeurs de k. En effet, le contrôle de puissance fractionnel permet aux utilisateurs UL d'achever un SINR nécessaire pour leurs transmissions en contrôlant en même temps les interférences qu'ils génèrent. Pour un facteur k compris entre 0 et 1, l'affaiblissement du parcours est partiellement compensé. Ce qui

veut dire qu'il y a un compromis entre l'affaiblissement du parcours et le SINR requis i.e., avoir un affaiblissement de parcours élevé implique un signal UL moins élevé. Cela résulte en un compromis entre l'affaiblissement du parcours et le SINR qui permet de contrôler l'interférence UL dans le contexte du D-TDD.

Pour conclure, dans la première partie de cette thèse, nous avons proposé un modèle mathématique pour analyser les performances des réseaux macro-cells et small-cells avec le mode de duplexage D-TDD. Les résultats ont montré que ce mode est en faveur de la transmission DL par contre le UL est sévèrement impacté par l'interférence DL to UL. Dans la 2ème partie on propose un modèle 3D beamforming dédié à la mitigation des interférences en DL et on va montrer que l'application de ce modèle dans un réseau macro-cells permet de diminuer l'impact de l'interférence DL to UL et rendre le D-TDD faisable pour les déploiements macro.

Un modèle analytique 3D beamforming dont les rayonnements horizontal et vertical des antennes dépendent de la distribution spatiale des utilisateurs

FD-MIMO est une technologie qui est basée sur le fait d'arranger un grand nombre d'antennes dans un tableau 2D placé en tête des stations de base. Cela permet de surmonter les contraintes de taille en augmentant le nombre d'antenne dans le contexte de massive-MIMO ainsi que l'activation du 3D beamforming en exploitant la dimension verticale du rayonnement des antennes. Le 3D beamforming consiste à former un beam du signal aigu entre l'émetteur et le récepteur en jouant sur la largeur du beam dans le rayonnement horizontal et vertical de l'antenne. Cela permet d'augmenter la puissance du signal en le focalisant sur un endroit bien précis et en même temps diminuer l'interférence qui provient des autres stations de base.

Nous proposons dans cette 2ème partie un modèle analytique pour le 3D beamforming dont les rayonnements horizontal et vertical des antennes dépendent de la position géographique des utilisateurs considérés aléatoirement distribués dans le plan. Pour se faire, on considère un réseau hexagonal tri-sectoriel dont les stations de bases sont équipées par des antennes directionnelles. Pour modéliser leurs rayonnements horizontal et vertical, on adopte le modèle de Mogensen qui décrit les rayonnement comme suit

$$H(\alpha_{s,c}) = [\cos(\alpha_{s,c})]^{-2w_h} \tag{1}$$

$$V(\phi_{s,c}) = [\cos(\phi_{s,c})]^{-2w_v}, \tag{2}$$

avec $w_h = \frac{ln(2)}{\ln(\cos(\frac{\theta_{h3dB}}{2})^2)}$ et $w_v = \frac{ln(2)}{\ln(\cos(\frac{\theta_{v3dB}}{2})^2)}$. θ_{h3dB} et θ_{v3dB} sont les ouvertures 3dB horizontale et verticale.

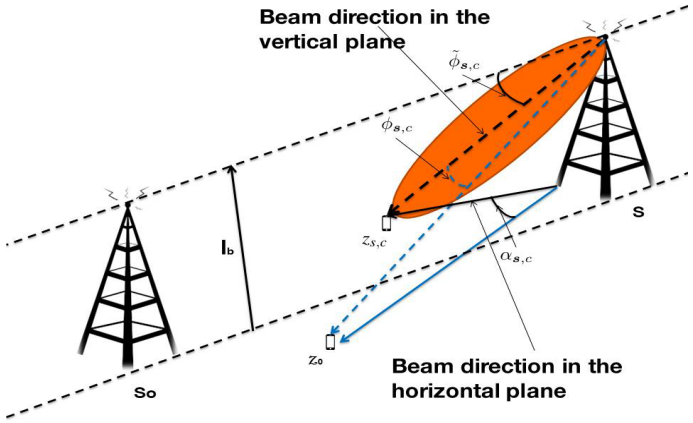

Figure 6 – Le modèle 3D beamforming

- L'angle $\alpha_{s,c}$ est l'angle dans le plan horizontal entre l'axe du beam dirigé vers un mobile $z_{s,c}$, qui se trouve dans un secteur c d'un site s, et la position du mobile z_0 qui se trouve dans le premier secteur du site serveur s_0.
- L'angle $\phi_{s,c}$ est l'angle dans le plan vertical entre le mobile l'axe du beam dirigé vers un mobile $z_{s,c}$ et l'orientation du mobile z_0 (Fig. 6).

En se basant sur la géométrie complexe on peut déterminer les expressions des angles $\alpha_{s,c}$ et $\phi_{s,c}$ comme suit:

$$\alpha_{s,c} = \psi(z_0, s) - \theta_{s,c}, \tag{3}$$

avec $\psi(z,s) = arg(z_0 - s)$ et $\theta_{s,c} = \psi(z_{s,c}, s)$ est l'argument complexe du $z_{s,c}$ relativement à s.

De même l'angle $\phi_{s,c}$ est exprimé par:

$$\phi_{s,c} = atan(\frac{l_b}{|z_0 - s|}) - \tilde{\phi}_{s,c}, \tag{4}$$

avec $\tilde{\phi}_{s,c} = atan(\frac{l_b}{r_{s,c}})$ est le downtilt de l'antenne qui est variable dans ce cas car il dépend de la position du mobile $z_{s,c}$.

Etant donné que les mobiles $z_{s,c}$ prennent des positions aléatoires dans les secteurs hexagonals des sites, on suppose que les angles $\theta_{s,c}$ sont uniformément distribuées dans l'interval $[\vartheta_c - \frac{\pi}{3}, \vartheta_c + \frac{\pi}{3}]$ avec $\vartheta_c = \frac{\pi}{3}(2c-1)$ est l'azimut de l'antenne du secteur c de chaque site s. Aussi, on suppose que les variables aléatoires $r_{s,c} = |z_{s,c} - s|$ sont uniformément distribuées dans l'intervalle $[0, \frac{2\delta}{3}U(\theta_{s,c} - \vartheta_c)]$ avec $U(\theta_{s,c} - \vartheta_c)$ c'est le rayonnement de l'antenne horizontal qui couvre tout le secteur hexagonal d'un site.

Le rayonnement des trois secteurs d'un site s reçu à la position z_0 d'un mobile dans le premier secteur de s_0 est donné par

$$G_s(z_0) = \sum_{c=1}^{3} \rho_{s,c} H(\alpha_{s,c}) V(\phi_{s,c}), \tag{5}$$

avec $\rho_{s,c}$ est une variable aléatoire de Bernoulli qui représente le pourcentage des ressources radio occupées par un mobile $z_{s,c}$.

En se basant sur ce modèle, on montre que le ISR est une série de variable aléatoire qui converge presque sûrement:

$$\mathscr{I}(z_0) = -1 + \sum_{s \in \Lambda} r^{2b} |s - z_0|^{-2b} G_s(z_0) 10^{\frac{\tilde{\gamma}_s}{10}}. \tag{6}$$

Ce résultat est intéressant car la convergence presque sûr implique la convergence en probabilité ce qui implique la convergence en distribution.

Les résultats de simulations montrent que le modèle 3D beamforming améliore les performances en termes de la probabilité de couverture. Comme on peut voir sur la figure Fig. 7, lorsqu'on prend des petites valeurs de l'ouverture 3dB horizontale, on constate une amélioration de la probabilité de couverture. Ceci est du au fait que l'application du 3D beamforming avec des beam aigus orientés vers les mobiles dans chaque secteur diminue l'interférence des stations de bases en DL et en même temps l'application du 3D beamforming pour le mobile dans la serveuse améliore sa puissance reçue et par la suite améliore son SINR.

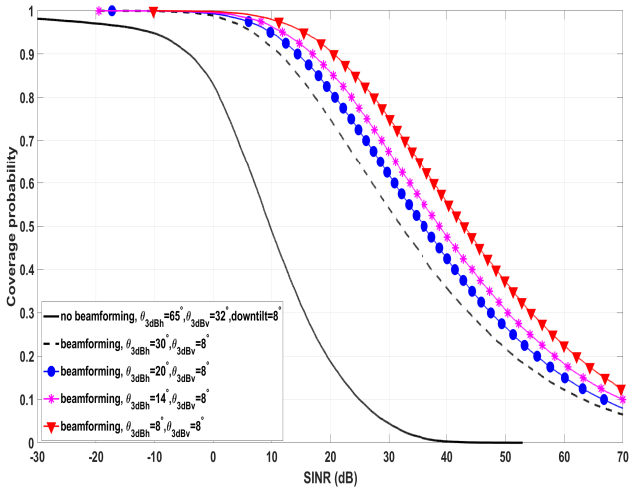

Figure 7 – Les variations de la probabilité de couverture avec différentes valeurs de θ_{h3dB}.

Aussi la comparaison entre le 3D beamforming et le 2D beamforming montre que les résultats sont bien meilleurs avec le 3D beamforming comme on peut voir sur la figure Fig. 8.

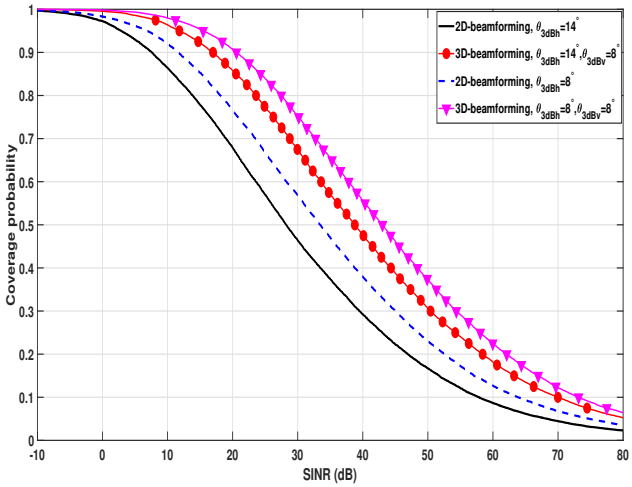

Figure 8 – Comparaison entre le 3D beamforming et le 2D beamforming.

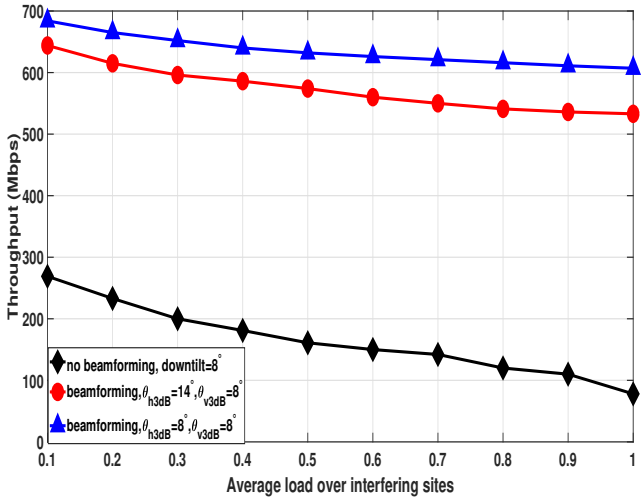

Figure 9 – Les variations du débit utilisateur avec la charge dans les sites qui interfèrent: comparaison entre le 3D beamforming et un réseau sans beamforming

Dans la figure Fig. 9, on trace le débit utilisateur en fonction de la charge dans les sites qui interfèrent afin de comparer le gain obtenu de l'application du 3D beamforming sur les performances. On peut constater qu'il y a une amélioration du débit quand le 3D beamforming est appliqué avec des petites valeurs de l'ouverture 3dB. Aussi, on peut voir que pour le cas du réseau sans beamforming, le débit devient sensible à l'augmentation de la charge dans les sites qui interfèrent. Cette sensibilité devient faible lorsque le 3D beamforming est considéré.

Ensuite, on étudie l'application de ce modèle 3D beamforming avec un réseau de macro-cells basé sur le mode de duplexage D-TDD afin de minimiser l'impact des interférences DL to UL et DL to DL et voir la faisabilité de ce mode de duplexage avec des déploiements macro-cells (Fig. 10 et Fig. 11).

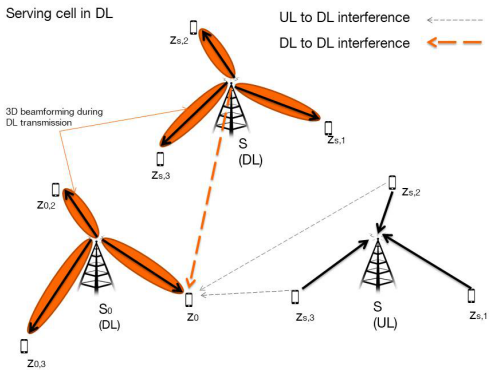

Figure 10 – D-TDD durant la transmission en DL

.

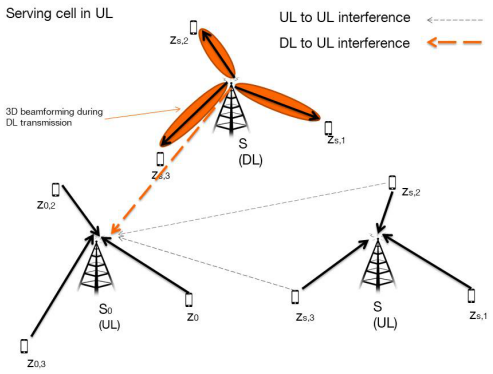

Figure 11 – D-TDD durant la transmission en UL

.

Pour se faire, on considère un réseau hexagonal tri-sectoriel dont les 3 secteurs de chaque site adoptent la même configuration des trames TDD. Une fois le D-TDD est activé, chaque site choisit le sens de transmission indépendamment des autres. Aussi, on considère que durant les sous-trames D-TDD, les stations de bases transmettent en DL considérant des mécanismes 3D beamforming selon le modèle présenté ci-dessus et le contrôle de puissance fractionnel est adopté pour les utilisateurs UL. Ce modèle nous a permis de dériver les expressions de ISR qui couvre les 4 types d'interférences en termes de séries convergentes et de séries qui convergent presque sûrement de variables aléatoires.

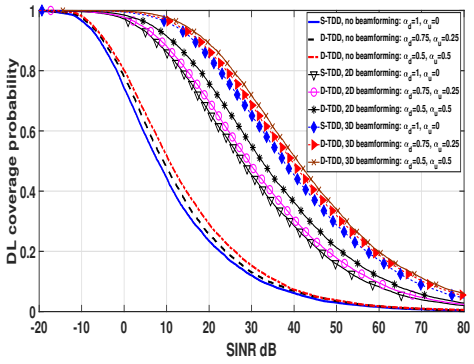

Figure 12 – Probabilité de couverture DL ($2b = 3.5$, $k = 0.4$).

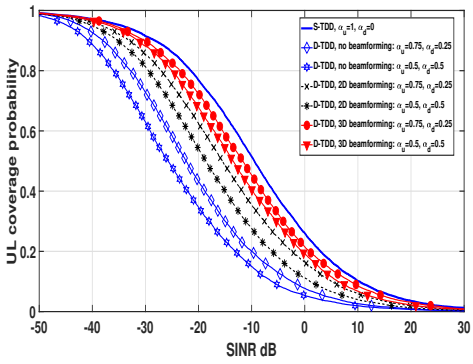

Figure 13 – Probabilité de couverture UL ($2b = 3.5$, $k = 0.4$).

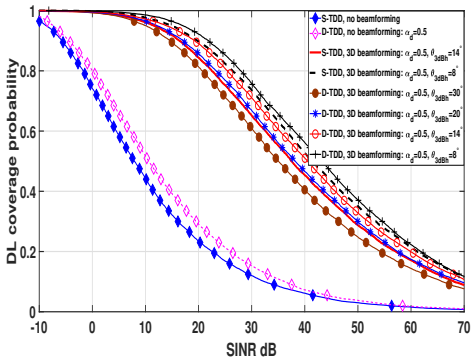

Figure 14 – Probabilité de couverture UL: D-TDD vs S-TDD with 3D beamforming avec des valeurs différentes des ouvertures 3dB ($2b = 3.5$, $k = 0.4$).

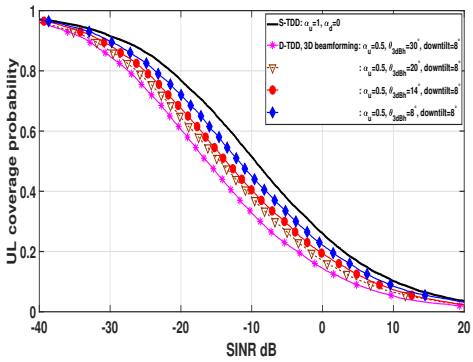

Figure 15 – Probabilité de couverture UL: D-TDD vs S-TDD with 3D beamforming avec des valeurs différentes des ouvertures 3dB ($2b = 3.5$, $k = 0.4$).

Les résultats numériques, présentés sur les figures 13,14,15, 16 et 17, montrent que le 3D beamforming améliore les performances en termes de la probabilité de couverture en DL puisque il permet la réduction de l'impact du signal DL des stations de base qui nuisent le plus aux performances durant le cycle DL. En UL, on peut remarquer que la probabilité de couverture d'un réseau basé sur le D-TDD avec le 3D beamforming est améliorée par rapport au cas sans beamforming. Aussi, avec des petites ouvertures 3dB horizontale et verticale, les performances s'approchent du Statique-TDD. D'une autre part, la combinaison du contrôle de puissance fractionnel avec le 3D beamforming améliorent plus les performances pour les mêmes raisons évoquées précédemment.

Pour conclure, le 3D beamforming réduit significativement les interférences générées par les signaux DL des stations de bases. Cela résulte en un gain significatif durant le cycle DL d'une station de base opérant dans un réseau basé sur le D-TDD. Pour le UL, on constate que les performances s'approchent du mode S-TDD quand le 3D beamforming est utilisé pour la transmission DL des stations de base qui sont dans le sens opposé à la serveuse. Cette amélioration est encore plus remarquable quand il y a une combinaison du 3D beamforming et le contrôle de puissance fractionnel avec des petites valeurs du facteur de compensation.

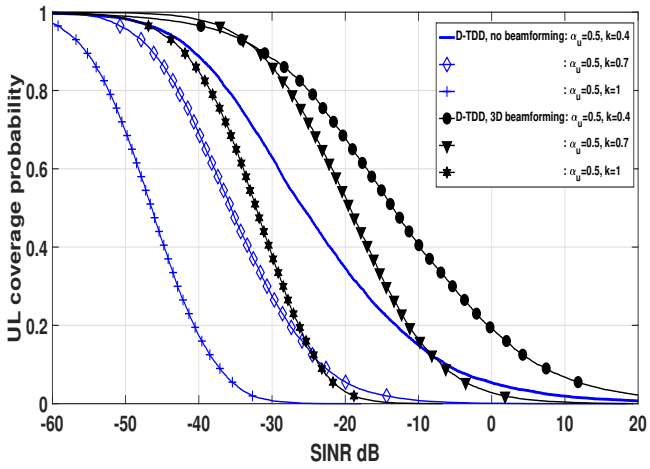

Figure 16 – L'effet du contrôle de puissance fractionnel sur la probabilité de couverture en UL: $2b = 3.5$, $k = 0.4$.

Dimensionnement des ressources radio d'un réseau basé sur l'OFDMA avec distinction entre les distributions aléatoires des utilisateurs outdoor et indoor

La dernière partie de cette thèse est consacrée à l'étude d'une autre problématique qui est le dimensionnement des ressources radio pour les réseaux mobiles basés sur l'OFDMA. L'analyse porte en particulier sur l'impact de la distribution aléatoire des utilisateurs dans la zone de couverture d'une cellule typique sur le nombre requis des ressources radio afin de satisfaire un service désiré. Ainsi, on distingue entre deux types d'utilisateurs:

- Des utilisateurs outdoor qui se situent généralement à l'extérieur sur des routes: on modélise leurs distribution par un processus aléatoire double stochastique dit processus de Cox basé sur le PLP (Poisson Line Process). En effet, la distribution aléatoire des routes a un impact significatif sur les performances des réseaux mobiles. Dans cette partie on modélise d'abord la distribution aléatoire des routes par un PLP, ensuite on considère une distribution aléatoire des utilisateurs sur chaque route selon un processus de poisson ponctuel (PPP) linéaire.

- Des utilisateurs indoor qui se localisent dans les bâtiments: on modélise leurs distribution par un PPP spatiale.

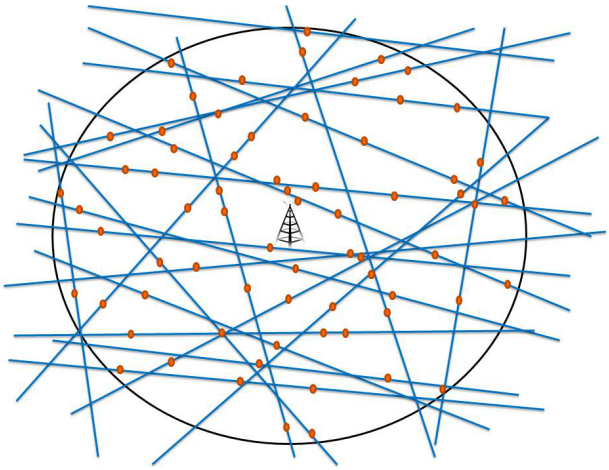

Figure 17 – Réalisation d'un processus de Cox basé sur un PLP dans la zone de couverture d'une cellule circulaire

D'une autre part, étant donné que le dimensionnement des ressources radio consiste à déterminer le nombre total des ressources radio nécessaire afin de gérer un trafic prédit tout en satisfaisant une qualité de service prédéfini au préalable par un opérateur, le choix d'une métrique significative qui décrit le mieux la qualité du service à respecter s'avère primordial. On choisi dans cette partie la probabilité de congestion comme fonction décrivant la qualité du service. Cette métrique est défini comme étant la probabilité que le nombre de ressource radio demandé par tous les utilisateurs dans la cellule dépasse le nombre de ressource disponible.

Afin de modéliser le réseau, on considère une cellule typique avec une station de base à son centre. Le débit de chaque utilisateur est déterminé en utilisant la borne supérieur de la formule de Shannon. On suppose que les utilisateurs sont schédulés d'une manière équitable i.e., celui qui perçoit des mauvaises conditions radio reçoit plus de PRBs afin de pouvoir accéder à une classe de service donnée (on suppose qu'il y a une seule classe de service avec un débit de transmission requis fixe et que l'allocation des PRBs se fait à chaque TTI). L'interférence est évaluée en termes de marge pour chaque région de la cellule.

En se basant sur ce modèle, pour chaque type d'utilisateur, la cellule pourra être divisée en plusieurs anneaux. la région entre chaque deux anneaux représente la région de la cellule dont les utilisateurs ont besoin d'un certain nombre de PRB. Ensuite, on montre que la somme totale des PRBs demandés dans la cellule suit une somme de Poisson composée.

Le modèle proposé permet de dériver une formule analytique de la probabilité de congestion conditionnellement au processus choisi et qui reste valide pour tout processus qui décrit la distribution spatiale aléatoire des utilisateurs:

Soit Λ une variable aléatoire tel que $\Lambda = \sum_{n=1}^{N} nV_n$, avec V_n sont des variables aléatoires de Poisson ayant des intensités w_n. La probabilité que Λ dépasse un seuil M est donnée par

$$\mathbb{P}(\Lambda \geq M) = 1 - \frac{1}{\pi} e^{-\sum_{n=1}^{N} w_n} \times \int_0^{\pi} e^{p_n(\theta)} \frac{\sin(\frac{M\theta}{2})}{\sin(\frac{\theta}{2})} \cos(\frac{M-1}{2} - q_n(\theta)) d\theta, \tag{7}$$

avec

$$p_n(\theta) = \sum_{n=1}^{N} w_n \cos(n\theta) \text{ and } q_n(\theta) = \sum_{n=1}^{N} w_n \sin(n\theta).$$

Cette formule peut encore être améliorée en introduisant un outil mathématique de l'analyse combinatoire dit Polynômes de Bell. Cela permet de déterminer la probabilité de congestion comme étant une somme finie des polynômes de Bell:

Soit Λ une variable aléatoire tel que $\Lambda = \sum_{n=1}^{N} nV_n$, avec V_n sont des variables aléatoires de Poisson ayant des intensités w_n. Soit x_j défini comme suit

$$x_j = \begin{cases} w_j j! & \text{si } 1 \leq j \leq N, \\ 0 & \text{sinon.} \end{cases}$$

La probabilité que Λ dépasse un seuil M peut s'exprimer comme étant une somme des polynômes de Bell exponentiels par

$$\mathbb{P}(\Lambda \geq M) = 1 - H \sum_{k=0}^{M-1} \frac{B_k(x_1, ..., x_k)}{k!} \tag{8}$$

avec $H = e^{-\sum_{n=1}^{N} w_n}$.

La formule analytique de la probabilité de congestion est comparée par la suite aux résultats des simulations Monte-Carlo comme s'affiche sur la figure 19 :

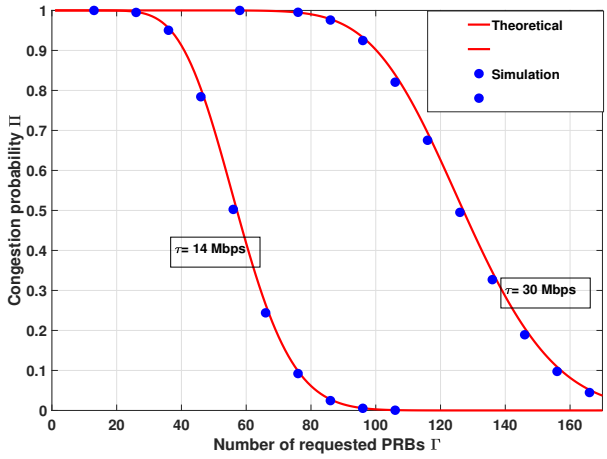

Figure 18 – Probabilité de congestion: théorique vs simulation pour deux valeurs de τ

On constate que les simulations correspondent bien aux résultats théoriques et aussi l'augmentation du débit moyen de la cellule génère une augmentation de la probabilité de congestion. Cela s'explique par le fait que le débit moyen cellule est directement lié à la densité des utilisateurs et la densité des routes dans la zone de couverture de la cellule.

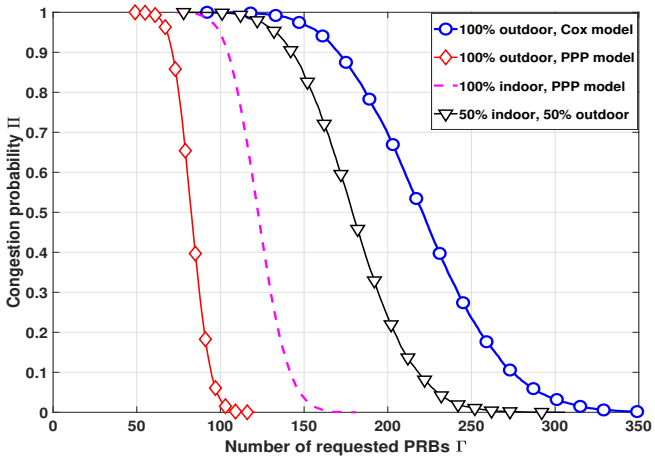

Figure 19 – Comparaison entre les différentes distributions aléatoires des utilisateurs

Dans la figure 20, on compare les différentes distributions aléatoires des utilisateurs en termes de la probabilité de couverture. On peut constater que le nombre de PRBs de-

mandé est toujours élevé, pour toute valeur cible de la probabilité de congestion, lorsque les utilisateurs sont distribués selon le processus de Cox. Cela veut dire que la géométrie aléatoire de la zone de couverture de la cellule a un impact très important sur les performances. Additionnellement, la grande demande de PRBs vient des utilisateurs indoor car ces derniers en général perçoivent des mauvaises conditions radio et l'environnement deep indoor est défavorable pour la propagation des ondes.

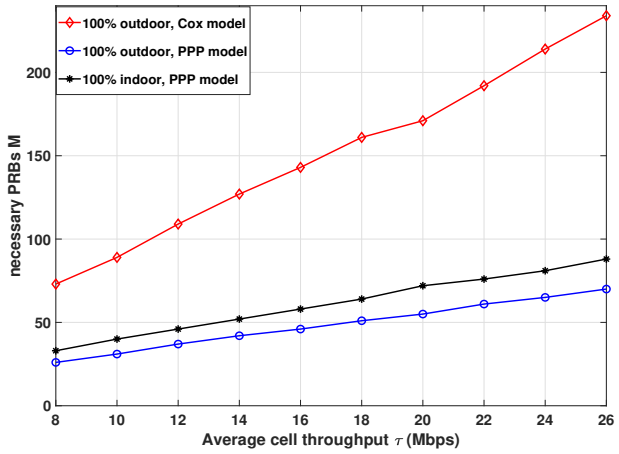

Figure 20 – Résultats de dimensionnement: comparaison entre les différents modèles

La figure 20 représente les résultats de dimensionnement avec une comparaison entre les différents modèles aléatoires des utilisateurs. On voit que le nombre de ressource dimensionné est toujours grand lorsque les utilisateurs suivent un processus de Cox géré par le PLP en comparaison avec le modèle PPP spatial ayant la même intensité. Lorsque l'intensité des routes est très élevé, les utilisateurs dans ce cas apparaissent distribués partout dans la cellule et non pas concentrés sur les routes, par conséquence, le processus de Cox peut être approximé par un processus de Poisson spatial ayant la même intensité. Avec une intensité des routes faible, les résultats deviennent optimistes avec un PPP spatial.

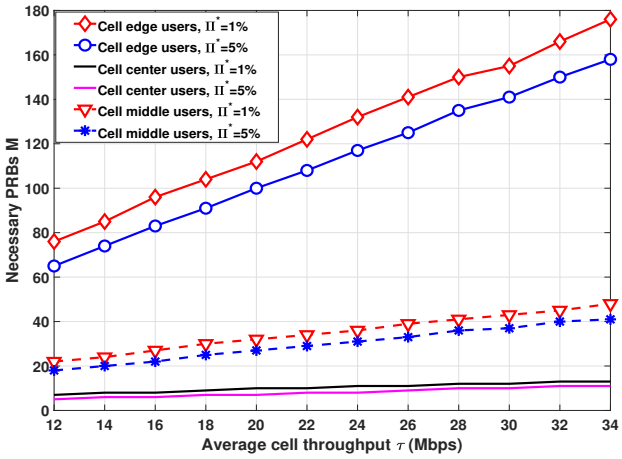

Figure 21 – Résultats de dimensionnement: comparaison entre les utilisateurs en cell edge, cell middle et cell center.

Pour analyser l'impact des interférences, la figure 22 montre es résultats de dimensionnement en considérant trois zones dans la cellule: cell center, cell middle et cell edge ayant chacune une marge d'interférence. On peut voir à partir des courbes de dimensionnement que la plus grande demande en terme de PRBs provient des utilisateurs en cell edge qui perçoivent un grand niveau d'interférence et un grand affaiblissement de parcours.

Le dimensionnement des ressources radio est une phase très importante car il permet aux opérateur d'avoir une vision très claire sur la manière dont ils peuvent manager le spectre radio afin de retarder des investissements dans l'acquisition des nouvelles bandes de fréquence. Si le nombre de ressource dimensionné dépasse le nombre disponible, l'opérateur par exemple peut faire appel à l'agrégation des porteuses pour élargir la bande de fréquence ou bien utiliser le mode de duplexage TDD qui permet d'exploiter la totalité de la bande de fréquence pour les deux sens de transmission DL et UL.

Publications

Journal papers

- Jalal Rachad, Ridha Nasri, Laurent Decreusefond. Dynamic-TDD Interference Tractability Approaches and Performance Analysis in Macro-Cell and Small-Cell Deployments. 2019. hal-02289230. Submitted to Annals of Telecommunications.
- Ridha Nasri, Jalal Rachad, Laurent Decreusefond. Radio Resource Dimensioning with Cox Process Based User Location Distribution Submitted to IEEE Transactions on Vehicular Technology.

Conference proceedings

- Rachad J, Nasri R, Decreusefond L. Interference analysis in dynamic TDD system combined or not with cell clustering scheme. In 2018 IEEE 87th Vehicular Technology Conference (VTC Spring) 2018 Jun 3 (pp. 1-5). IEEE.
- Rachad J, Nasri R, Decreusefond L. How to Dimension Radio Resources When Users Are Distributed on Roads Modeled by Poisson Line Process. In 2019 IEEE 90th Vehicular Technology Conference (VTC2019-Fall) 2019 Sep 22 (pp. 1-6). IEEE.
- Jalal Rachad, Ridha Nasri, Laurent Decreusefond. A 3D Beamforming Scheme Based on The Spatial Distribution of User Locations. IEEE PIMRC 2019, 2019, Istanbul, Turkey. hal-02164428.
- Jalal Rachad, Ridha Nasri, Laurent Decreusefond. 3D Beamforming based Dynamic TDD Interference Mitigation Scheme. Submitted to IEEE VTC 2020 (Spring).

List of figures

1 L'interférence UL to DL 12
2 L'interférence DL to UL 12
3 DL ISR: Static TDD vs Dynamic TDD. 13
4 UL ISR: Static TDD vs Dynamic TDD. 13
5 Probabilité de couverture en DL et en UL pour un réseau macro avec différent facteur de control de puissance fractionnel. 14
6 Le modèle 3D beamforming 16
7 Les variations de la probabilité de couverture avec différentes valeurs de θ_{h3dB}. 18
8 Comparaison entre le 3D beamforming et le 2D beamforming. 18
9 Les variations du débit utilisateur avec la charge dans les sites qui interfèrent: comparaison entre le 3D beamforming et un réseau sans beamforming 19
10 D-TDD durant la transmission en DL 20
11 D-TDD durant la transmission en UL 20
12 Probabilité de couverture DL ($2b = 3.5$, $k = 0.4$). 20
13 Probabilité de couverture UL ($2b = 3.5$, $k = 0.4$). 20
14 Probabilité de couverture UL: D-TDD vs S-TDD with 3D beamforming avec des valeurs différentes des ouvertures 3dB ($2b = 3.5$, $k = 0.4$). . . . 21
15 Probabilité de couverture UL: D-TDD vs S-TDD with 3D beamforming avec des valeurs différentes des ouvertures 3dB ($2b = 3.5$, $k = 0.4$). . . . 21
16 L'effet du contrôle de puissance fractionnel sur la probabilité de couverture en UL: $2b = 3.5$, $k = 0.4$. 22
17 Réalisation d'un processus de Cox basé sur un PLP dans la zone de couverture d'une cellule circulaire 23
18 Probabilité de congestion: théorique vs simulation pour deux valeurs de τ 25
19 Comparaison entre les différentes distributions aléatoires des utilisateurs . 25
20 Résultats de dimensionnement: comparaison entre les différents modèles . 26

21 Résultats de dimensionnement: comparaison entre les utilisateurs en cell edge, cell middle et cell center. 27

2.1 Poisson Point Process based cellular network. 53
2.2 Hexagonal grid based cellular network. 53

3.1 UL to DL interference. 59
3.2 DL to UL interference. 59
3.3 FeICIC technique in a heterogeneous deployment. 60
3.4 DL ISR: Static TDD vs Dynamic TDD. 65
3.5 UL ISR: Static TDD vs Dynamic TDD. 65
3.6 Parameters recapitulation. 69
3.7 Macro-cells network DL coverage probability. 75
3.8 Macro-cells network UL coverage probability. 75
3.9 Macro-cells network DL and UL coverage probability with different power control factors. 76
3.10 Small-cells DL coverage probability : $2b = 3.5$, $k = 0.4$ and $\lambda = 10$ small-cell$/km^2$. 77
3.11 Small-cells UL coverage probability : $2b = 3.5$, $k = 0.4$ and $\lambda = 10$ small-cell$/km^2$. 77
3.12 DL average spectral efficiency : $2b = 3.5$, $k = 0.4$. 77
3.13 UL average spectral efficiency : $2b = 3.5$, $k = 0.4$.. 77

4.1 3D beamforming illustration 82
4.2 Coverage probability variations: no beamforming vs 3D beamforming with different θ_{h3dB}. 88
4.3 Throughput variation with the average load over interfering sites: comparison between 3D beamforming model and hexagonal tri-sectorized network. 89
4.4 Coverage probability comparison: 3D beamforming vs 2D beamforming. 90
4.5 Downtilt $\tilde{\phi}_{s,c}$ impact: variable vs fixed downtilt. 91

5.1 D-TDD DL transmission cycle 94
5.2 D-TDD UL transmission cycle 94
5.3 DL Coverage probability ($2b = 3.5$, $k = 0.4$). 98
5.4 UL coverage probability ($2b = 3.5$, $k = 0.4$). 99
5.5 DL coverage probability: D-TDD vs S-TDD with 3D beamforming considering different half power beam-widths ($2b = 3.5$, $k = 0.4$). 100
5.6 UL coverage probability: D-TDD vs S-TDD with 3D beamforming considering different half power beam-widths ($2b = 3.5$, $k = 0.4$). 101

5.7 UL coverage probability: fractional power control effect: $2b = 3.5$, $k = 0.4$. 101
5.8 Cell clustering model 102
5.9 D-TDD DL to UL ISR with cell clustering scheme 105

6.1 Line parametrization. 109
6.2 A realization of Cox Point Process driven by PLP. 109
6.3 Congestion probability theoretical vs simulation for two values of τ . . . 121
6.4 Comparison between different user distributions 122
6.5 Required PRB M as a function of cell Throughput τ, for fixed transmission rate $C^* = 500kbps$. 123
6.6 Dimensioned PRBs comparison: outdoor users with Cox model, outdoor users with spatial PPP and indoor users with spatial PPP, for a fixed transmission rate $C^* = 500kbps$ 124
6.7 Interference impact ($\tau = 30Mbps$). 125
6.8 Interference impact on dimensioned PRBs M. 126
6.9 Comparison between dimensioned PRBs M for cell edge, cell middle and cell center users. 126

List of tables

3.1 D-TDD simulation parameters. 74

5.1 3D beamforming based D-TDD network simulation parameters. 98

6.1 Chapter 6 notations. 110

List of acronyms

3GPP	Third Generation Partnership Project
4G	Fourth Generation
5G	Fifth Generation
ABS	Almost blank sub-frames
ASE	Average spectral efficiency
AWGN	Additive white Gaussian noise
BS	Base station
CCDF	Complementary cumulative distribution function
CQI	Channel Quality Indicator
CLI	Cross link interference
CSI	Channel state information
DL	Downlink
D-TDD	Dynamic Time Division Duplex
eICIC	enhanced Inter-cell interference coordination
eIMTA	enhanced Interference Mitigation and Traffic Adaptation
eMBB	enhanced Mobile Broadband
FDD	Frequency Division Duplex
FD-MIMO	Full Dimension Multiple-in Multiple-out
FeICIC	Further enhanced Inter-cell interference coordination
FPC	Fractional power control
HetNet	Heterogeneous Network
HPBW	Half Power Beam Width
HPPP	Homogeneous Poisson Point Process
i.i.d	Independent and identically distributed
IM	Interference margin
ISR	Interference to Signal Ratio
LOS	Line of sight
LTE	Long term evolution

MCL	Mutual coupling loss
MCS	Modulation and Coding Schemes
MIMO	Multiple input multiple output
mMTC	massive Machine Type Communication
mmWave	Millimeter wave
NLOS	No line of sight
NR	New Radio
OFDM	Orthogonal frequency division multiplexing
PDT	Poisson Delaunay Tessellation
PGFL	Probability generating functional
PLP	Poisson Line Process
PPP	Poisson Point Process
PRB	Physical Resource Block
PVT	Poisson Voronoi Tessellation
QoS	Quality of service
RSRP	Reference Signal Receive Power
RV	Random Variable
SE	Spectral efficiency
SINR	Signal-to-interference-plus-noise ratio
S-TDD	Static Time Division Duplex
TTI	Time transmit interval
UL	Uplink
URLLC	Ultra Reliable Low Latency Communications

Chapter 1

Introduction

1.1 Background and general context

The upcoming 5th generation (5G) of mobile networks is promising to deliver a big leap in performance, spectral efficiency and capacity. 5G radio interface, known as new radio (NR), has been designed by considering flexibility in features definition in order to support the huge proliferation of mobile data traffic and to satisfy different use cases with different users' requirements. In the context of 5G, one can usually talk about three general classes of use cases: enhanced mobile broadband (eMBB), massive machine-type communication (mMTC) and ultra-reliable and low-latency communication (URLLC) [1]. To meet the requirements of those use case classes, 5G NR needs to exploit the potential of new technologies and also to get the most out of the wide array of frequency spectrum. Since bands at different frequencies have different characteristics due to propagation properties, 5G NR is expected to expand spectrum exploitation to bands at low frequencies below 1 Ghz, which are convenient for wide area coverage, mid-bands between 1 Ghz and 6 Ghz and high frequency bands above 24 Ghz known as millimeter waves (mmWave), mainly dedicated to enhance capacity in dense small-cell deployments. Furthermore, Time Division Duplex (TDD) mode is expected to be a key feature for 5G NR. Actually, TDD alternates downlink (DL) and uplink (UL) frame portions in time and allows them to share the same frequency band contrary to Frequency Division Duplex (FDD) mode based on paired frequency channels and a guard band to avoid interference between DL and UL. This gives an increase in frequency diversity and more resource assignment flexibility. Moreover, one of the major advantages of TDD is channel reciprocity. It allows the transmitter to estimate the channel on the outward link based on the estimated channel on the return link. Such properties make TDD more convenient with 5G NR features, such as massive multiple-in multiple-out (massive MIMO), 3D beamforming and dense small-cell deployments in

mmWave frequency bands, than FDD.

Additionally, TDD can be used with two mode of operation: static and dynamic. In static TDD (S-TDD) systems, cells allocate UL and DL subframes using time domain partitioning in order to avoid overlapping transmissions. The ratio of dedicated subframes in each direction is based on the average perceived traffic statistics measured over a period of time. To meet the continued growth in data traffic volume, Dynamic-TDD (D-TDD) has been introduced as a solution to deal with UL and DL traffic asymmetry, mainly observed for dense heterogeneous network deployments, since it is based on instantaneous traffic estimation and provide more flexibility in resource assignment. However, D-TDD system is severely limited by a strong mutual interference between the UL and DL transmissions because those two directions share the same frequency band. Hence, two types of interference appear: DL to UL (impact of DL other cell interference on UL signal received by the studied cell) and UL to DL (impact of UL mobile users transmission, located in other cells, on DL signal received by a mobile user located in the studied cell). Those additional interference, mainly DL to UL, are usually more difficult to deal with because of the LOS (Line Of Sight) between highly elevated base stations (BSs) transmitting with high power level and also because the mobiles can move around randomly. Thus, this duplexing mode can be more convenient with heterogeneous networks (HetNet) as small-cells are considered well isolated from each others and also from the macro-cells' layer.

Furthermore, in order to mitigate interference in D-TDD system, 3GPP (3rd Generation Partnership Project) standard advices new approach for enhanced Interference Mitigation and Traffic Adaptation (eIMTA) in dynamic environment [2]. Cell clustering scheme is an efficient technique that can be used to deal with D-TDD interference. Cells that suffer from high DL to UL interference level between each others can be gathered in the same cluster and use the same UL-DL configuration. In the same time, transmission directions in different clusters can be dynamically adapted. This technique can be very efficient for HetNet when it is combined with enhanced Inter Cell Interference Coordination (eICIC), introduced in 3GPP Release 10, or Further eICIC, introduced in 3GPP Release 11. eICIC and FeICIC are based on time domain partitioning: macro-cell BSs reduce the transmitted power level during some sub-frames called Almost Blank Sub-frames (ABS) so that small-cells can adjust UL-DL portions dynamically during those sub-frames according to the traffic variations. FeICIC and cell clustering are rather dedicated to minimize D-TDD interference in small-cell networks. Recently, the applicability of massive antenna technologies, such as Full Dimension MIMO (FD-MIMO) and 3D beamforming, with D-TDD has drawn the attention of telecommunication actors. Actually, beamforming consists in forming a signal beam between the transmitter and the receiver by using an array of anten-

nas. It enhances the signal strength at the receiver and minimize interference level so that high average data rate and high spectral efficiency can be achieved. Most existing base stations (BSs) are equipped with directional antennas that provides radiation patterns in the horizontal dimension, considering only the azimuth angle, and having a fixed vertical pattern and downtilt. By taking into account also the impact of the elevation and combining the horizontal and the vertical dimensions, the signal strength at the receiver location could be further improved and interference from neighboring cells could be minimized [3]. Therefore, the applicability of this feature with D-TDD can effectively reduce the strong DL to UL interference impact and thus make D-TDD feasible for macro-cell deployments.

Additionally, 5G NR will be also made through improvements in the current 4G/4G+ key features by taking in consideration the wide array of emerging use cases and also future requirements. Hence, The 3GPP has chosen an optimized OFDM based waveform for 5G NR known as scalable OFDM and having different subcarriers' spacing ($\Delta f = 2^{\nu}15$ kHz, where $\nu = 0$ to 4) [4]. This technology appears to be an ideal choice for 5G NR for many reasons such as the robustness to channel selective fading, the high provided spectral efficiency and also the compatibility with other techniques. A set of OFDM subcarriers constitutes the basic unit of radio resources that a cell can allocate to a mobile user. This set of subcarriers is called Physical Resource Block (PRB) in the 3GPP terminology. Furthermore, the allocation of PRBs to users is performed at each Time Transmit Interval (TTI) according to a predefined scheduling algorithm. The choose of this latter is mainly related to the fairness level between users, i.e., the way that resources are allocated to users according to their channel qualities and their priorities, defined by the operator [5–7]. Consequently, OFDM dimensioning will be certainly a major task in the context of 5G NR. It aims at finding the number of radio resources required to carry a forecast data traffic at a target users Quality of Services (QoS). Hence, it is of utmost importance to define a relevant metric for QoS and develop an accurate mathematical model for dimensioning capable to give the desired results by taking into account different system parameters. Besides, a key parameter for network dimensioning and performance analysis is Signal-to-Interference-plus-Noise-Ratio (SINR). This parameter, in turn, is related to the perceived interference which makes their modeling vital.

Actually, interference in cellular networks represents a major issue that obstructs the achievement of high performance in terms of data rate and spectral efficiency. Telecommunication actors continuously attempt to minimize it during all the phases of a technology conception, since it is related to network performance. In radio engineering, one can use interference margin, known also as noise rise, to perform link budget tools. However, this notion does not describe the real perceived interference and does not take into account the geometry of the studied area that impacts in one way or another performance. Thus,

the analytical tractability of interference is of prime importance. Having a mathematical model can always give better results and avoid recourse to extensive simulations. In effect, interference are related to the network geometry and the spatial distribution of users. Most considered models that can be found in literature are the regular hexagonal model [8] and random models based on spatial point processes [9] and [10]. Hexagonal network is the basis model for network design in radio engineering. It is considered effective for network having fixed cell radius such as macro-cell deployments. However, this model is not useful for heterogeneous network topology. Small-cells usually occupy unplanned random positions. It appears that stochastic point processes are practical to model their random distribution in dense urban environment. Homogeneous Poisson Point Process (HPPP) is a very popular model in cellular networks in which BSs and mobile users spatial distribution are modeled according to a PPPs. Despite the tractability of HPPP, this model can not fit with the geometry of real cellular networks because of the repulsive behavior of transmitting nodes. Also, with this model, one cannot evaluate interference at each arbitrary user location and only its distribution that can be determined [8] and [11]. Nevertheless, spatial PPP may not always be suitable for all spatial configurations of nodes. Actually, the spatial distribution of BSs and users is mainly related to the geometry of the studied area. This latter is related, in turn, to the spatial distribution of roads and buildings. For instance, indoor users, often distributed in buildings, can be modeled by a spatial PPP. However, outdoor users (e.g., pedestrians or vehicular) are generally distributed along roads. Hence, to model such a system, one should consider two sources of randomness: *i*) the random location of users on each road that can be modeled by a linear PPP and *ii*) the road system itself that can be considered as a random realization of a line process. Several approaches to model road systems can be found in the scientific literature such as Manhattan model that uses a grid of horizontal and vertical streets, Poisson Voronoi Tessellations (PVT) and Poisson Delaunay Tessellations (PDT) [12–14]. A well-known and tractable model that gives a quite good presentation of road systems in dense urban environment is Poisson Line Process (PLP). PLP is a random process mathematically derived from PPP. Instead of points, PLP is based on a random set of lines distributed in the plane $\mathbb{R}^2$. The distribution of nodes belonging to each line is modeled according to a linear PPP. Hence, the combination of roads and nodes distributions results in a doubly stochastic process often known as Cox process [15].

1.2 Problematics and contributions

The major contributions of this thesis are threefold:

1. D-TDD interference tractability approaches and performance analysis in macro-cell and small-cell deployments:

   As the number of mobile users is set to continue increasing in the upcoming years, D-TDD is expected to be one of the major keys of 5G NR. D-TDD enables the dynamic adjustment of UL and DL resource transmissions based on instantaneous traffic variations. The problem of this duplexing mode is two additional types of interference, called cross link interference (CLI), that stands in the way of the useful transmitted DL and UL signals: *i*) when the serving cell transmits to a given mobile location, DL and UL interferences' effect on DL useful transmission appears; *ii*) when the serving cell receives signals from mobiles, UL and DL interferences' impact on UL transmission rises. The first objective of this work is to provide a complete analytical framework for interference tractability in macro-cell and small-cell deployments. Macro-cells are modeled by using a regular hexagonal network with infinite number of sites whereas small-cells are modeled according to a spatial PPP, in order to exploit the mathematical framework based on stochastic geometry and to satisfy in the same time D-TDD assumptions. Moreover, to analyze the feasibility of D-TDD for macro-cells, the study treats in particular the explicit evaluation of Interference to Signal Ratio (ISR) in each position of the network by covering the four types of interference generated in D-TDD based network. This metric is very useful for link budget tools in which the average perceived interference is required in each mobile location. The second objective is to analyze performance of D-TDD based macro-cell and small-cell networks, in terms of the coverage probability expressed as a function of different system parameters, and its comparison with performance of existing S-TDD based networks. This metric is related to the throughput and it is useful for throughput dimensioning.

2. D-TDD interference mitigation schemes in macro-cell and small-cell networks:

   D-TDD based macro-cell networks undergo strong interference, mainly coming from DL transmitting BSs, that severely degrade performance. Actually, macro-cell BSs often transmit with high power levels and are likely to be in LOS condition. Therefore, D-TDD cannot be used with macro-cell deployments without interference mitigation schemes. FD-MIMO has been introduced as an efficient technique to enhance mobile network performance in terms of users' throughput and spectral efficiency. It is based on a 2D array of antennas that offers the possibility to increase the number of transmit antennas and gives extra degrees of freedom. Also, it makes possible to adapt the signal beams in the horizontal and the vertical dimensions. Consequently, applying 3D beamforming in D-TDD based macro-cell systems can effectively reduce the strong DL to UL interference impact and thus make D-TDD

feasible for macro-cell deployments.

The first part of this second contribution is dedicated to propose a new analytical approach to model 3D beamforming in a regular tri-sectorized hexagonal network. It aims at characterizing the antenna radiation patterns, in both the horizontal and vertical dimensions, by considering the random locations of users in the cells. Some analytical results regarding the explicit derivation of ISR and its mathematical expectation are provided. Also, 3D beamforming based system performance in DL transmission are analyzed through system level simulations to make sure that this feature enhances the coverage probability and reduces the perceived interference in DL. Finally, a comparison between 3D beamforming and 2D beamforming is given. The second part is devoted to investigate the applicability of 3D beamforming with D-TDD based systems and its comparison with S-TDD. Results show that 3D beamforming further enhances performance in DL and minimize significantly DL to UL interference during the UL transmission cycle of a typical cell. Different numerical results are provided to justify this interference mitigation approach.

On the other hand, small-cells are likely to be well isolated from each others, which makes D-TDD more convenient with HetNet deployments. As it is mentioned previously, cell clustering is an efficient technique devoted to minimize interference in a D-TDD environment. The main idea of cell clustering is to gather small-cells in different clusters based on specific metrics e.g., Mutual Coupling Loss (MCL) threshold between them. Small-cells in the same cluster adopt the same UL-DL frame configurations and the transmission inside a cluster can be coordinated by a central unit, which decides the more convenient frame configuration according to traffic conditions. Moreover, cells belonging to different clusters can choose the configuration independently from each others. However, the problem of CLI still exists even with cell clustering scheme. Actually, the dense deployment of small-cells certainly induces severe interference between small-cells belonging to neighboring clusters when they transmit in opposite directions. Hence, users served by small-cells located in the cluster edges can experience bad performance. So, the second part of this contribution is devoted to provide a tractable cell clustering scheme based on the hexagonal tessellation to see how this feature can reduce the DL to UL interference in a D-TDD based small-cell network.

3. OFDM based system radio resources dimensioning approach with a comparison between Cox process driven by PLP and Poisson Point Process:

   Radio resources dimensioning is a major task in cellular network development that aims at maximizing the network resources efficiency. Dimensioning process consists in assessing the necessary resources that permit to carry a predicted data traf-

fic in order to satisfy a given QoS. So, an accurate traffic estimation is one of the major issues to consider for dimensioning problem and for that, it is of utmost importance to choose a relevant QoS metric to evaluate system performance. To this purpose, the third contribution of this thesis aims at providing an analytical model to dimension OFDM based systems with a proportional fair resources' allocation policy. This dimensioning model is very useful for operators since it gives a vision on how they should manage the available spectrum. If the dimensioned number of resources exceeds the available one, the operator can, for instance, aggregate fragmented spectrum resources into a single wider band in order to increase the available PRBs, or activate capacity improvement features like dual connectivity between 5G and legacy 4G networks, in order to delay investment on the acquisition of new spectrum bands. Moreover, the proposed model can be applied to the scalable OFDM based 5G NR with different subcarriers' spacing in order to enable different types of deployments and network topologies and support different use cases. Furthermore, instead of considering only the random distribution of users, often modeled by a spatial PPP in the cell, we consider two types of users: *i)* indoor users distributed in buildings and modeled by a spatial PPP. *ii)* for outdoor users (e.g., pedestrians or vehicular), we characterize at first the random distribution of roads in a typical cell coverage area by a PLP and then we consider the random distribution of users in this system of roads according to a linear PPP. This model allows the operator to evaluate and compare performance between outdoor and indoor environments in terms of required radio resources. Finally, We show that the total number of the requested PRBs follows a compound Poisson distribution and we derive the explicit formula of the congestion probability as a function of different system parameters by using a mathematical tool from combinatorial analysis called the exponential Bell polynomials. This metric is defined as the risk that the requested resources exceed the available ones. It is often considered primordial for operators when it comes to resources dimensioning since it is related to the guaranteed quality of service. Then by setting a target congestion probability, we show how to dimension the number of PRBs given a forecast cell throughput.

1.3 Thesis outline

The structure of this thesis is as follows:

- Chapter 2: In this chapter, an extensive state of the art on Dynamic-TDD, Interference mitigation schemes in dynamic environment, FD-MIMO, 3D beamforming and radio resources dimensioning is provided. Also, a review of cellular network

modeling and interference tractability approaches is given.

- Chapter 3: This chapter is dedicated to investigate the analytical tractability of interference in D-TDD based macro-cell and small-cell deployments. Different analytical results, regarding the explicit derivation of ISR and the coverage probability, are provided. This is followed by a performance analysis part through system level simulations.

- Chapter 4: The aim of this chapter is to provide a new analytical model for 3D beamforming, in the context of FD-MIMO, in a tri-sectorized hexagonal network. A characterization of antenna beamforming radiation patterns, in both horizontal and vertical dimensions, is given considering the spatial distribution of user locations. Analytical and simulation results are stated to justify the accuracy of this scheme.

- Chapter 5: In the first part of this chapter, we investigate the applicability of 3D beamforming scheme, presented in chapter 4, in a D-TDD based macro tri-sectorized hexagonal network. Through system level simulations, we analyze performance in terms of the coverage probability of D-TDD and its comparison with S-TDD. In the second part, we present a cell clustering scheme based on the hexagonal tessellation that aims at minimizing interference in a D-TDD based small-cell deployments.

- Chapter 6: This chapter is devoted to present a new approach for radio resource dimensioning considering the congestion probability, qualified as a relevant metric for QoS evaluation. We distinguish between two types of users: indoor users modeled by a spatial PPP and outdoor users modeled by a linear PPP in a random system of roads described by PLP. Different analytical and simulation results are provided to justify this approach.

- Chapter 7: This chapter concludes the study and summarizes the different results. Also, it gives new potential perspectives for future works.

Chapter 2

Related works and state of the art

In this chapter, we provide a survey of related works, existing in the scientific literature, regarding the topic of dynamic TDD and the different proposed interference mitigation schemes. Also, we review the state of the art on FD-MIMO and 3D beamforming. Moreover, we summarize different related works to the topic of OFDM radio resources dimensioning before concluding with a review on cellular network modeling and existing approaches for interference tractability.

2.1 Dynamic-TDD vs S-TDD performance analysis and interference coordination schemes

TDD and FDD are the two fundamental duplexing schemes in wireless communication systems. FDD is based on paired spectrum bands to separate DL from UL transmission whereas TDD is based on unpaired band and the separation between DL and UL transmissions is performed in time. Additionally, TDD represents some characteristics that make it more desirable for the upcoming 5G NR. For instance, using an unpaired band allows the exploitation of the whole bandwidth whether for UL or DL, which leads to capacity enhancement. Moreover, channel reciprocity is a key advantage of TDD over FDD. TDD system can obtain the channel state information in DL from the measurements in the UL link [16]. Besides, TDD mode can be used with static frame configurations or dynamic adjustment of UL/DL frame portions. With the huge proliferation of mobile data traffic volume, D-TDD appears to be a good solution to optimize the adjustment of UL/DL sub frames since it is based on instantaneous traffic estimation.

D-TDD has been widely investigated in the available scientific literature; see for in-

stance [17–26]. The first study dates back to 2002 with the work in [17] where performance of a D-TDD fixed cellular network in UL transmission was investigated. Authors in [17] proposed a time slot assignment method to improve the UL outage performance. In [24], authors have studied the possibility of using dynamic adjustments of TDD UL/DL configurations in a pico-cells based HetNet. Even if the study lucks analytical analysis, simulation have shown that enabling dynamic adjustment is in the favor of DL transmission since it reduces the number of DL transmitting pico-cells. However, the UL transmission performance undergoes huge degradation because of the strong interference coming from DL transmitting pico-cells. Similar approach has been adopted in [19]. Authors have shown that applying interference mitigation between macro-cells and pico-cells leads to a significant improvement of the average packet throughput especially in low to medium traffic load situations. In [27], authors have studied performance of D-TDD based small-cell deployment. They have focused on a particular small-cell architecture known as phantom cells. This architecture is based on configuration split between the control plane, supported by macro-cells in low frequencies, and user plane supported by phantom cells in high frequencies. By using some well-known results from stochastic geometry regarding spatial PPPs, authors have derived the DL and UL outage probability formulas considering the four types of interference generated by D-TDD based systems. As expected, they have reached the conclusion that UL transmission cycle performs worst than DL in terms of outage probability. Moreover, they have proposed a frequency domain inter-cell-interference-coordination technique that leads to an enhancement in system performance. Similarly in [28], the coverage probability and the area spectral efficiency of a dense small-cell network based on synchronous D-TDD has been studied. Authors have derived a closed-form expressions of the DL/UL time resource utilization. Also, they have derived a closed-form expression of the coverage probability and the area spectral efficiency for both DL and UL transmission directions, by modeling BSs and users spatial distributions as two independent homogeneous PPPs. They have reached the conclusion that D-TDD performs better than S-TDD in terms of time resource utilization. Also, they have shown that D-TDD achieve better area spectral efficiency than S-TDD in DL. In [29], a two-tier Device to Device enhanced HetNet operating with D-TDD has been studied. Authors have proposed an analytical framework to evaluate the coverage probability and network throughput using stochastic geometry. Likewise in [30], authors have provided a comparison between static and dynamic TDD in millimeter wave (mm-wave) cellular network, in terms of *SINR* distributions and mean rates, considering synchronized and unsynchronized access-backhaul. From this survey, it is obvious that most of research works focus on the feasibility of D-TDD in small-cell deployments. However, performance of D-TDD based macro-cell deployments has not been well investigated.

In order to make D-TDD implementation feasible, some interference mitigation techniques based on cell clustering and mainly dedicated to small-cell deployments, have been proposed in literature; see for instance [31, 32]. All discussed cell-clustering schemes gather small-cells that highly interfere each others in the same cluster and force them to use the same configuration. Such schemes reduce D-TDD interference, although the problem is not completely solved since inter-cluster interference still exists especially between cells located in the edge of clusters. Also, it can force small-cells in the same cluster, with different traffic ratios, to choose the same frames' configurations which reduces the efficacy of D-TDD. To enhance the efficiency of cell clustering schemes, it was discussed in [32] a soft reconfiguration method based on cell clustering devoted to mitigate D-TDD interference in femto-cell deployments. This technique use a transition map constructed based on the ratio DL/UL with DL (UL) refers to the number of DL (UL) sub-frames in a TDD frame. The aim of this method is to allow cells in the same cluster to change dynamically the UL/DL configuration while saving a low interference level between them. This can be done by making femto-cells to choose by turns their configurations based on the transition map. Numerical results showed that this model outperforms the classic cell clustering schemes but the study lacks analytical modeling. Always in the same context, it can be found several works that have discussed radio resource management and optimization approaches to deal with cross slot interference generated by D-TDD. For instance in [25], authors have proposed a centralized clustering based coordination scheme for D-TDD with interference cancellation. The objective of this work was performing joint UL/DL user scheduling rate and MIMO rank allocation for each resource block.

2.2 Full Dimension MIMO and Beamforming

Multiple antenna technologies and beamforming were the subject matter of many existing works in the scientific literature. Massive MIMO technology known also as FD-MIMO offers a lot of advantages. It can enhance the capacity by increasing the number of installed antennas in sites' BSs [33–37]. Actually, according to the current LTE standard, most existing BSs have up to 8 antennas arranged linearly at the top. Since the array size is proportional to the number of antennas, increasing this latter linearly to fit massive MIMO requirements seems impractical. Consequently, research community and telecommunication actors come up with FD-MIMO as an alternative. The aim of this feature is to arrange antennas in a 2D array. By using intelligently this set of antennas, it enables the use of 3D beamforming by adapting also antenna radiation patterns in the elevation plane with extra degrees of freedom [38]. Moreover, FD-MIMO is very convenient with TDD duplexing mode since increasing the number of antennas does not increase the feedback overhead

thanks to TDD channel reciprocity property [39].

The applicability of massive MIMO and beamforming can be found in many works. In [35], authors analyzed performance of UL and DL non-cooperative multi-cell TDD networks. They have opted for a realistic system by taking in consideration imperfect channel estimation, pilot contamination, antenna correlation and path loss. Also, they have studied the asymptotic behavior of the system when the number of antennas increases, by using different precoding schemes, in order to achieve a given percentage of rate. Their model seems accurate comparing to realistic systems. In [40], authors have studied multi-level beamforming by developing a methodology to design a multi-level codebook of beams in an environment with low numbers of multi-path. They have focused on how beams can be generated with reduced interference from side lobs. Also, they have provided an algorithm to select beams during scheduling based on users CQI (Channel Quality Indicator). The applicability of this model to LTE use cases have shown that it seems good and attractive in terms of low implementation complexity and performance enhancement. It has been provided in [41] a channelization code of wideband CDMA (Code-Division-Multiple-Access) mobile communication systems based on sectored beamforming antenna arrays in BSs. To quantify the relationship between the number of antenna arrays and capacity gain, authors have provided through system level simulations a comparison between pedestrians and vehicular users. They have shown that it exists a compromise between the number of beams and antenna gain that avoid pilot overhead and does not results in low antenna gain. The proposed solution is based on cell splitting in terms of spatially isolated scrambling codes regions. In [42], it has been proposed a general framework to evaluate coverage and rate in mmWave cellular networks. Authors have considered three categories of BSs: indoor BSs, outdoor BSs that are in LOS condition and outdoor BSs that are NLOS to the users. BSs and users equipment are considered to be equipped with directional beamforming antennas modeled by using sectored antenna model to provide an approximation of beamforming patterns. The analytical approach is based on stochastic geometry. Also in [43], sectorized gain pattern has been considered to model beamforming radiation patterns in a self backhauled mmWaves' network. In [44], authors have proposed a new analytical model as a mixture of the inverse Gaussian [45] model and the inverse Weibul model [46], to model interference power distribution. They have established methods to estimate parameters for both rich and limited scattering environments. They have applied this model to evaluate performance of cellular network with joint transmit and receive beamforming.

Additionally, the impact of the vertical dimension in beamforming has been investigated throughout many works. In [47] authors investigated the impact of adapting the vertical pattern of antennas to user locations through conducted lab and field trial measure-

ments. They showed that, either in outdoor or indoor environments with Line Of Sight (LOS) and Non Line Of Sight (NLOS) conditions, adapting the vertical pattern improves performance. Interference restraint using dynamic vertical beam steering has been studied in [48]. authors have focused on the potential of dynamic vertical beam steering in an interference-limited macro-cell network. They have considered beam coordination methods for interference avoidance with and without requirements of communication between BSs. Through system level simulations and field measurements, they have shown, based on 3GPP standard specification, that performance are better with 3D antennas. In [49] authors have analyzed the impact of antenna radiation pattern and the downtilt on the performance of a DL cellular network in terms of the coverage probability and the area spectral efficiency. For the analytical approach, they have used tools from stochastic geometry to model the spatial distribution of nodes. Also, they have shown that there exists an optimal antenna downtilt that depends on the LOS and NLOS conditions. This optimal downtilt maximizes the coverage probability and improves the area spectral efficiency. Similarly in [50], the effect of antenna downtilt in a MIMO system has been studied through system level simulations. Authors used the 3GPP antenna radiation pattern model to show that the maximal cell throughput depends on the antenna downtilt. Finally, in [51] it has been proposed an analytical model for 3D beamforming in a tri-sectorized network. Authors have studied the impact of varying the horizontal and vertical half power beam-widths on performance enhancement.

Furthermore, the marriage between FD-MIMO and D-TDD is not well investigated in the available scientific literature. To the best of our knowledge, the only work that focuses on the feasibility of implementing 3D beamforming as an interference mitigation scheme for D-TDD based macro-cell networks is the study provided in [52]. In this work, based on random matrix theory, authors have shown that equipping BSs with a large number of antennas (massive MIMO), removes effectively the DL to UL interference in macro-cell deployments.

2.3 OFDM radio resource dimensioning

One of the principal decisions to make for 5G NR design is choosing an adequate waveform. OFDM seems to be an accurate technology for 5G NR since it represents numerous advantages such as low complexity of implementation, high provided spectral efficiency and low power consumption. Additionally, to meet with requirements and emerging class of services predefined in the context of 5G, NR design will introduce the scalable OFDM

to support diverse spectrum bands and different deployment models [53]. Furthermore, dimensioning OFDM is a major task to perform for 5G NR. It aims at assessing the necessary radio resources to guarantee a predefined QoS. This task is mainly related to different factors such as scheduling algorithm, the level of fairness between users, channel quality, traffic estimation and also the network geometry.

The available scientific literature of OFDMA based systems is quite rich and many aspects have been widely discussed such as resource allocation and dimensioning methods; see for instance [6,7,54–60]. In [54], an adaptive resource allocation for multiuser OFDM system, with a set of proportional fairness constraints guaranteeing the required data rate, has been discussed. The analysis is simplified by a low-complexity algorithm in order to separate sub-channel allocation from power allocation. Authors have shown that it offers more fairness and flexibility in terms of sum capacity. Similarly, authors in [6] surveyed different adaptive resource allocation algorithms and provided a comparison between them in terms of performance and complexity. Furthermore, OFDMA dimensioning has been always considered as a hard task especially with the presence of elastic data services. It was provided in [59] an analytical model for dimensioning OFDMA based networks with proportional fairness in resource allocation between users requiring different transmission rates. For a spatial Poisson distribution of mobile users in a typical cell coverage area, authors in [59] showed that the required number of resources follows a compound Poisson distribution. In addition, an upper bound of the blocking probability was given. Likewise in [60], authors have proposed an OFDMA dimensioning approach considering an Erlang's loss model and Kaufman-Roberts algorithm to evaluate the blocking probability. The aim of this study was to build a method that determines the minimum density of BSs assuring a given quality of services. The accuracy of their model has been verified through numerical results that showed that the proposed method induces only up to 10% loss of the capacity. Also in [61], it has been proposed an analytical method to evaluate the QoS for a DL OFDMA system considering real-time and elastic traffic with a dimensioning approach illustration. In [62], authors have proposed a method to dimension OFDM based cellular networks by using the so-called exponential effective SINR. This method consists in extending the single SINR based planning to multi-carrier systems through a redefinition of the link outage probability. Also, they have introduced a Gaussian approximation for the exponential effective SINR. Numerical results showed that for practical number of sub-carriers, this approximation can be used to set up a simplified panning procedure through calculating only two moments of the single-carrier SINR. They have derived also an upper bound of the outage probability considering interference.

2.4 Cellular network modeling and interference analysis

Interference characterization is one of the main concept of cellular networks. It is related to the SINR and thus the capacity, which are the prime concern to enhance when it comes to performance analysis of mobile network communications. Interference modeling is mainly related to the geometry of the network. It has always been a challenging problem even with single tier networks. Hence, choosing an accurate tractable models is of utmost importance since it saves time by avoiding to have recourse to extensive simulations.

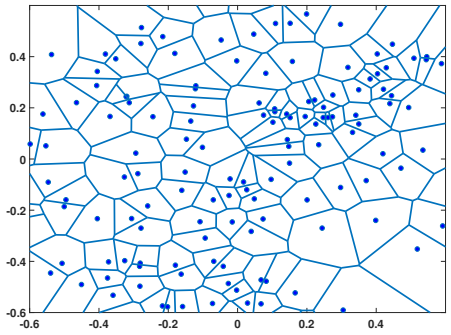

Figure 2.1 – Poisson Point Process based cellular network.

.

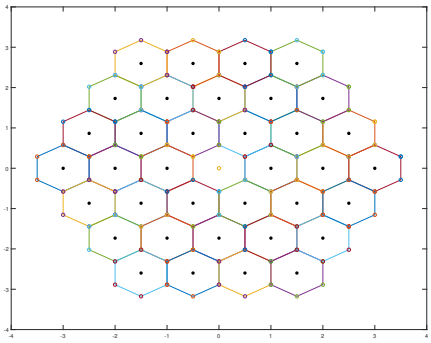

Figure 2.2 – Hexagonal grid based cellular network.

.

The most frequent models that can be found in literature are deterministic and random models [8, 9, 15, 63–72]. One of the most popular models is the spatial PPP. This model assumes that BSs are distributed in a given area of the plane according to a spatial PPP. Users are assumed to connect with the nearest BSs and follow a uniform distribution in their coverage areas represented by voronoi cells; see Fig. 2.1. Stochastic geometry is a strong mathematical tool that leads to explicit results in the analysis of random models and especially spatial PPP based models. It has been provided in [9] a complete analysis of a DL transmitting cellular macro-cells' network. Authors have derived a general explicit expression of the coverage probability. Also, they have provided an explicit formula of the mean achievable rate. Moreover, the study contains some simplifications of the derived formulas considering different special cases. Finally, they have verified the accuracy of their model, through some numerical results, by comparing it to the grid models and real deployment of BSs. In [68], it has been provided a complete analytical analysis of a DL k-tiers cellular network to model HetNet deployments. BSs of each tier are modeled according to a homogeneous PPP and tiers are assumed to be independent from each others.

From numerical results, it can be observed that the coverage probability of an actual 4G deployment lies between the PPP model and the grid model, such that PPP model provides a lower band whereas grid model offers an upper bound. To analyze the performance of an UL network, it has been discussed in [71] an interesting approach. Since interference in UL comes from mobiles that are randomly distributed in the network contrary to DL where interference comes from fixed transmitting nodes, the modeling of an UL network requires some fundamental changes. The study of [71] assumes that mobile locations are distributed according to a spatial PPP and the BS corresponding to each mobile user is uniformly distributed in the voronoi cell of this mobile. To simplify the analytical analysis, authors have demonstrated that the distances between mobiles and BSs are weak in terms of dependence that comes from the use of fractional power control model [73]. With this assumption, the proposed model has led to an explicit derivation of the UL coverage probability.

Actually, despite the tractability of spatial PPP based models, they cannot fit with the geometry of real macro-cell wireless networks because of the repulsive behavior of sites. Also, with random models one cannot evaluate the received interference in each mobile location of a cell, which is very important for link budget tools, and only its distribution is determined. The regular hexagonal network (Fig. 2.2) is the basic model for radio engineering. However, this model has been widely considered intractable. With the work of [8], numerous analytical results regarding the explicit derivation of ISR and the coverage probability are provided. In particular, authors have proved that the ISR in a regular hexagonal network with infinite number of sites equipped with omni-directional antennas, is a function of mobile location in a typical cell. This function can be written in terms of convergent series on the distance between the mobile location and its serving BSs. Also, they have derived the explicit expression of the coverage probability considering different mobile user locations scenarios especially uniform and log-normal distributions. In [11] a comparison between a regular hexagonal network and a spatial PPP based network has been discussed. From this comparison, one can conclude that the hexagonal model approximates well the geometry of real macro-cell layout and it is tractable as well as HPPP based models. Also, the regular hexagonal model can deal with non-uniform user location distributions contrary to spatial PPP.

Furthermore, it becomes very hard to model a cellular network where BSs are distributed according to a random point process and equipped with sectorized antennas. For instance in [10], it has been proposed a cell sectorization model based on a homogeneous PPP to model the spatial distribution of BSs. Authors have proposed an approach to model the horizontal and the vertical antenna radiation patterns of each sector considering the randomness and the geometry of the network. Numerical results shows that this model fits well with measurements obtained from an operational network. To the best of our knowl-

edge, this study is the only one that tackle the problematic of sectorization in random cellular network models. With deterministic model such as regular hexagonal network, this problematic becomes much easier. For instance in [8], a tractable approach for interference derivation in a tri-sectorized hexagonal network with infinite number of sites has been proposed. By considering only the horizontal antenna radiation patterns, authors have used the complex geometry to show that ISR can be written in terms of a convergent Fourier series.

Recently with the new emerging technologies such as vehicular communication known as V2X and V2V, it becomes important to consider also the geometry of the studied area and the random distribution of roads in cellular network performance analysis. Several models can be found in literature; see for instance [15, 64, 72, 74, 75]. In [72], Morlot has introduced a new population model that takes the geometry of cities into account by adding the random distribution of roads. In order to derive the UL coverage probability, he modeled the system of roads according to a PLP and he provided a comparison between two types of users: walkers and drivers. A similar model can be found in [15]. To perform the canonical coverage analysis of a vehicular network, authors have considered a doubly stochastic model for wireless nodes. They have assumed that the irregularity of roads can be modeled by a PLP and the irregularity of wireless nodes can be modeled by independent linear PPPs on each road. They have derived the SIR (Signal-to-Interference-Ratio) metric in Nakagami-m fading channel and the expression of the coverage probability as a function of different system parameters. Through simulations, they have provided a comparison between their model and a spatial PPP model. The main conclusion reached from this study is that PPP model gives optimistic results comparing to Cox process driven by PLP and results become similar between the two models only for big values of roads' density. This model seems accurate and interesting and merits more investigation considering other aspects of cellular networks performance analysis such as radio resources dimensioning.

Chapter 3

D-TDD interference tractability and performance analysis

3.1 Introduction

Meeting the continued growth in data traffic volume, Dynamic Time Division Duplex (D-TDD) has been introduced as a solution to deal with the uplink (UL) and downlink (DL) traffic asymmetry, mainly observed for dense heterogeneous network deployments, since it is based on instantaneous traffic estimation and provide more resource assignment flexibility. However, the use of this feature requires new interference mitigation schemes capable to handle two additional types of interference between cells in opposite transmission direction: DL to UL and UL to DL interference. Those interference are difficult to deal with especially DL to UL.

The aim of this chapter is to provide a complete analytical framework for interference tractability in macro-cell deployments and dense small-cell networks. We model macro-cells by using a regular hexagonal network with infinite number of sites. We treat in particular the explicit evaluation of *ISR* in each position of the network, in terms of convergent series, that covers the four types of interference generated in D-TDD based network. To model small-cells, we adopt the widely used spatial PPP and we show how to exploit the mathematical framework based on stochastic geometry and satisfy in the same time D-TDD assumptions. Additionally, we derive the explicit expressions of the coverage probability (SINR distribution) for a typical cell in DL and UL for both macro-cell and small-cell networks. This metric is related to throughput distribution and it is useful for cell throughput dimensioning. Finally, we analyze, through system level simulations, performance of D-TDD based network and its comparison with S-TDD considering different system parameters.

3.2 System models and notations

3.2.1 Dynamic TDD model

To model the D-TDD system, we assume that all cells initially operate synchronously in DL or UL. This setup can be considered as a baseline scenario characterizing performance of existing synchronous TDD system i.e., S-TDD. After a period of time, it is assumed that all cells select randomly UL or DL frame portions based on traffic conditions. Four types of interference henceforth appear depending on the transmission direction: *i*) when the serving cell transmits to a given mobile location, DL and UL interferences' effect on DL useful transmission appears; *ii*) when the serving cell receives signals from mobiles, UL and DL interferences' impact on UL transmission rises (Fig. 3.1 and Fig. 3.2). It is considered hereafter that the scheduler does not allocate the same spectral resources to different mobile users in one cell at the same time (e.g., TD-LTE scheduling). So, intra-cell interference is not considered. Therefore in a given cell, we consider that during a sub-frame of interest (i.e., when D-TDD is activated), there is one active transmission whether on DL or UL with full-buffer traffic model. To characterize the transmission directions of cells, denoted by s, we consider two Bernoulli random variables (RVs) $\chi_d(s)$ and $\chi_u(s)$ such that $\mathbb{P}(\chi_d(s)=1)=\alpha_d$ and $\mathbb{P}(\chi_u(s)=1)=\alpha_u$. $\chi_d(s)$ refers to the DL transmission cycle of a cell s and $\chi_u(s)$ refers to the UL transmission cycle of a cell s during a D-TDD sub-frame. It is important to mention that a cell s cannot be in DL and UL during the same TTI. Hence, to avoid this case, we add the following condition $\chi_u(s)=1-\chi_d(s)$. This means that $\alpha_d=1-\alpha_u$.

3.2.2 Macro-cell deployment

To model macro-cells, we consider a hexagonal cellular network denoted by Λ with an infinite number of macro-cells having an intersite distance between them denoted by δ. The hexagonal model means that for each node $s\in\Lambda$, there exists a unique $(m,n)\in\mathbb{Z}^2$ such that $s=\delta(m+ne^{i\frac{\pi}{3}})$. We denote by s_0 the serving cell located at the origin of $\mathbb{R}^2$ ($\mathbb{R}^2$ is isomorphic to $\mathbb{C}$). Antenna in each site is assumed to have an omni-directional radiation pattern and covers a geographical area named Voronoi cell, having a cell radius denoted by R. Furthermore, the location of a mobile served by s_0 is denoted by z_0 such that $z_0=re^{i\theta}$ where (r, θ) are the polar coordinates in the complex plane. We denote also by z the geographical location of a mobile served by a cell $s\in\Lambda^*$ in the plane, where Λ^* is the lattice Λ without the serving cell s_0. Location z is written in the complex plane by

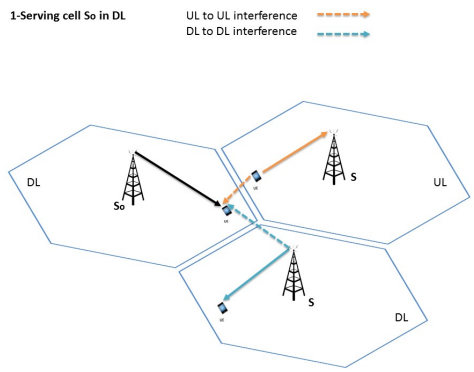

Figure 3.1 – UL to DL interference.

.

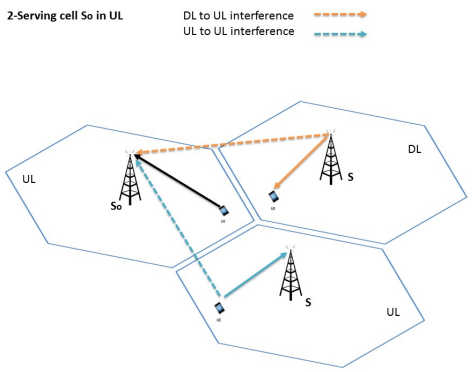

Figure 3.2 – DL to UL interference.

.

$z = s + \rho e^{i\phi}$, where ρ and ϕ represents respectively the distance and the angle between z and s. Moreover, it is assumed that the locations of mobile z in the plane are uniformly distributed.

3.2.3 Small-cell deployment

Since small cells usually occupy unplanned random positions, it appears that stochastic point processes are practical to model their random distribution in a dense urban environment. The most common approaches model the DL cellular network with a BSs distribution according to a spatial PPP and uniform users' distribution in BS Voronoi cells [9]. For the UL transmission, it has been proposed in [71] an interesting approach considering a spatial PPP distribution of users in the plane with a uniform distribution of each BS in the Voronoi cell of the associated mobile. However, with D-TDD, for each transmission direction there is two sources of interference: BSs and mobiles. In order to be able to exploit the mathematical framework based on stochastic geometry and satisfy in the same time the D-TDD assumptions, we model the set of active mobiles z served by the small-cells, denoted hereafter by $\tilde{s}$, by a PPP Φ of intensity λ. This implies that z are uniformly distributed in the studied area.

As we have mentioned previously, each small-cell $\tilde{s}$ has one active mobile transmitting whether in DL, with probability α_d, or in UL with probability α_u. Thus, we can assume that each mobile is associated with the nearest small-cell. Furthermore, the position of each small-cell can be expressed in the complex plane by $\tilde{s} = z + \rho_z e^{i\phi_z}$, with (ρ_z, ϕ_z) are the polar coordinates of $\tilde{s}$ relatively to z. This means that also the set of small-cells forms a PPP obtained by a displacement of Φ (Displacement theorem [63]), i.e., the process of

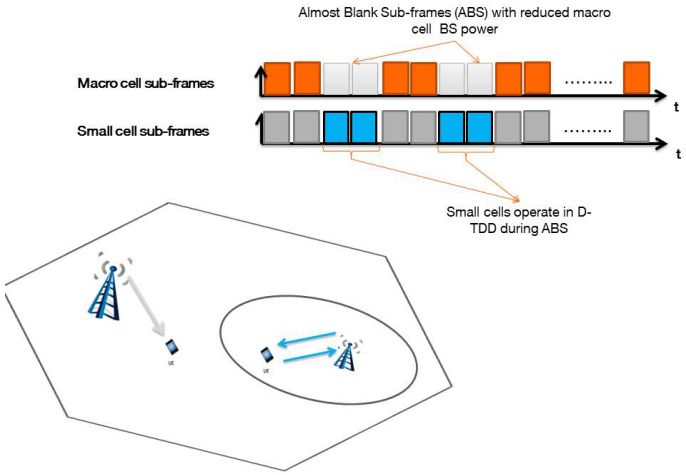

Figure 3.3 – FeICIC technique in a heterogeneous deployment.

mobiles and small-cells are two dependent PPPs.

Additionally, to reduce strong macro-cell layer interference impact on users served by small-cells, especially in small-cells range expansion, we assume that FeICIC is implemented; see Fig. 3.3. With this feature, macro-cells reduce their transmitted power level during some specific sub-frames called Almost Blank Sub-frames (ABS) so that small-cells use those sub-frames to configure dynamically the UL-DL frame portions. Moreover, we assume that all macro cells are well synchronized and adopt the same S-TDD configuration. Hence, macro-cell BSs interference can be neglected.

3.2.4 Propagation model

To model the wireless channel, we consider the standard power-law path loss model based on the distance between a mobile z and a BS s such that the path loss $L(s,z)$ is given by

$$L(s,z) = a|s-z|^{2b}, \tag{3.1}$$

with $2b$ is the path loss exponent and a is a propagation factor that depends on the type of the environment (Indoor, Outdoor...).

In addition to the path loss, the received power by a mobile depends on the random channel effects, especially shadowing and fast fading. Shadowing refers to the attenuation

of the received signal power caused by obstacles obstructing the propagation between the transmitter and receiver. In this chapter, shadowing effect is not considered for reasons of tractability. Readers can refer to [8] in which a way of how shadowing can be included in calculations is provided.

Likewise, fast fading random model is not considered for the macro-cell deployment in order to simplify calculations. Actually, fading effect can be compensated through link level performing that maps the *SINR* to the throughput (Th). Also, for an AWGN (Additive Gaussian Noise Channel), Shannon's formula provides the relation between *SINR* and Th. Hence, the fast fading effect can be compensated by using a modified Shannon's formula to have $Th = K_1 log_2(1 + K_2 SINR)$, with K_1 and K_2 are constants calibrated from practical systems [76]. However, for the heterogeneous system analysis, multi-path Rayleigh fading effect is considered. We denote by H_i and G_i, with $i = \tilde{s}$ or $i = z$, the fading coefficients between, a transmitting node i and a typical receiving mobile, and between i and a typical receiving BS. We assume also that the RVs H_i and G_i are independent and identically distributed (i.i.d) for each propagation link and follow an exponential distribution of mean 1.

In UL transmission, power control is applied to PUSCH (Physical Uplink Shared Channel) channel in order to set the required mobile transmitted power. In this study, it is modeled by the fractional power control model (FPC), i.e., the path loss is partially compensated by the power control [77]. The transmitted power by the mobile location z to its serving cell s is then written

$$P(z,s) = P^*(s) \left(|z-s|^{2b} \right)^k \tag{3.2}$$

where $P^*(s)$ is the target power cell specific and $k \in [0\ 1]$ is the power control compensation factor. When $k = 1$ the power control scheme totally indemnifies the path loss in order to reach the target power $P^*(s)$. For the case $0 < k < 1$ the path loss is partially compensated and mobile users in cell edge create less interference because their transmitted power is reduced.

Without loss of generality, we consider that $P^*(s)$ is the same for all the cells. Power values P and P^* are supposed to include the path loss constants and antenna gains of BSs and user equipments. It is important to note that section 3.3 and section 3.4 are independent. So, to avoid confusion, we denote by $\tilde{P}$ and $\tilde{P^*}$ respectively the transmitting power and the target power cell specific of small-cell BSs.

3.3 Dynamic TDD interference derivation in a macro-cell deployment

We define the Interference to Signal Ratio *ISR* as the received power from an interfering source (interfering mobile or BS) divided by the useful power received by z_0 from the serving cell. The average *ISR* experienced in DL transmission by a mobile location z_0 connected to s_0 is

$$D(z_0) = \alpha_d \, D_{\downarrow}(z_0) + \alpha_u \, D_{\uparrow}(z_0) \tag{3.3}$$

with $D_{\downarrow}$ and $D_{\uparrow}$ are respectively DL to DL and UL to DL average interference to signal ratios experienced during the DL cycle.

Likewise, the average *ISR* experienced by cell s_0 in UL transmission cycle is

$$U(z_0) = \alpha_u \, U_{\uparrow}(z_0) + \alpha_d \, U_{\downarrow}(z_0) \tag{3.4}$$

where $U_{\uparrow}$ and $U_{\downarrow}$ are respectively UL to UL and DL to UL interference to signal ratios experienced during the UL cycle.

3.3.1 Downlink *ISR* derivation $D(z_0)$

Expression of DL to DL *ISR* $D_{\downarrow}(z_0)$

In [8], it has been shown that the DL *ISR* function of a location $z_0 = re^{i\theta}$ in a hexagonal cellular network with infinite number of cells admits a series expansion on r and θ and is a very slowly varying function on θ. Taking $x = \frac{r}{\delta}$ such that $x < 1$ ($x < 1/\sqrt{3}$ condition always satisfied in hexagonal network), the expression of $D_{\downarrow}$ is recalled from [8]

$$D_{\downarrow}(z_0) = \frac{6x^{2b}}{\Gamma(b)^2} \sum_{h=0}^{+\infty} \frac{\Gamma(b+h)^2}{\Gamma(h+1)^2} \omega(b+h) x^{2h} \tag{3.5}$$

where $\Gamma(.)$ is the Euler Gamma function and

$$\omega(z) = 3^{-z} \zeta(z) \left(\zeta(z, \frac{1}{3}) - \zeta(z, \frac{2}{3}) \right), \tag{3.6}$$

with $\zeta(.)$ and $\zeta(.,.)$ are respectively the Riemann Zeta and Hurwitz Riemann Zeta functions [78].

Expression of UL to DL *ISR* $D_{\uparrow}(z_0)$

The UL to DL interference is generated from mobile users located at other cells, mainly from those located at the border of cells adjacent to cell s_0. Since there is only one mobile user transmitting at the same time in UL for each cell, the total UL to DL *ISR* can be evaluated by averaging over locations $z \in s$ and then summing over $s \in \Lambda^*$. So, if we assume that location z is uniformly distributed in s, $D_{\uparrow}(z_0)$ is mathematically written as

$$D_{\uparrow}(z_0) = \frac{1}{\pi R^2} \int_0^R \int_0^{2\pi} \sum_{s\in\Lambda^*} \frac{P^*\ \rho^{2bk}\ r^{2b}}{P\left|s+\rho e^{i\phi}-re^{i\theta}\right|^{2b}} \rho d\rho d\varphi \tag{3.7}$$

To evaluate equation (3.7), we can proceed analogously to the proof of *ISR* formulas in hexagonal omni-directional networks provided in [8]. We start by taking $z^{'} = re^{i\theta} - \rho e^{i\phi}$. It is obvious that $\left|z^{'}\right| < |s|$. It follows from [8] that the sum over s inside the double integral admits a series expansion on $\left|z^{'}\right|/\delta$ as in (3.5). Using formula (3.5) and writing $\left|z^{'}\right|$ in terms of r, θ, ρ and ϕ, (3.7) becomes

$$\begin{aligned} D_{\uparrow}(z_0) = \frac{6P^*x^{2b}}{P\pi R^2\,\Gamma(b)^2} \int_0^R \int_0^{2\pi} \sum_{h=0}^{+\infty} \frac{\Gamma(b+h)^2\omega(b+h)}{\Gamma(1+h)^2\delta^{2h}} \times \\ (r^2+\rho^2)^h (1-\frac{2r\rho}{r^2+\rho^2}\cos(\phi))^h \rho^{2bk+1} d\rho d\phi \end{aligned} \tag{3.8}$$

The sum and integrals of (3.8) can be switched and the inside integral can be evaluated by expanding $(1-\frac{2r\rho}{r^2+\rho^2}\cos(\phi))^h$ as a binomial sum. After few derivations of known special integrals and simplifications, the UL to DL *ISR* $D_{\uparrow}(z_0)$ can be evaluated by the following convergent series on $x = r/\delta$

$$\begin{aligned} D_{\uparrow}(z_0) = \frac{6P^*x^{2b}R^{2bk}}{P\,\Gamma(b)^2} \sum_{h=0}^{+\infty} \sum_{n=0}^{\lfloor \frac{h}{2} \rfloor} \sum_{i=0}^{h-2n} \frac{\Gamma(b+h)^2\omega(b+h)}{\Gamma(n+1)^2\Gamma(h+1)} \times \\ \frac{(\frac{R}{\delta})^{2n+2i}\ x^{2h-2n-2i}}{\Gamma(i+1)\Gamma(h-2n-i+1)(n+i+bk+1)} \end{aligned} \tag{3.9}$$

Since $x < 1/\sqrt{3}$ for hexagonal model, it is obvious that the first elements of this series are sufficient to numerically evaluate $D_{\uparrow}$. Furthermore, after few simplifications, (3.9) can be written as an entire series on x^2 as follows

$$D_{\uparrow}(z_0) = \frac{6P^* x^{2b} R^{2bk}}{P} \sum_{h=0}^{+\infty} \beta_h x^{2h} \tag{3.10}$$

with

$$\beta_h = \sum_{n=0}^{h} \sum_{i=0}^{+\infty} \frac{\Gamma^2(b+h+n+i)\omega(b+h+n+i)}{\Gamma(b)^2\Gamma^2(n+1)\Gamma(i+1)} \times \frac{(\frac{R}{\delta})^{2n+2i}}{\Gamma(h-n+1)\Gamma(h+n+i+1)(n+i+bk+1)} \tag{3.11}$$

3.3.2 Uplink *ISR* derivation $U(z_0)$

In this part, we derive the analytical expression of the UL interference to signal ratio. The UL signal received from location z_0 at cell s_0 experiences interference coming from cells transmitting in DL and also from mobiles in adjacent cells which are in UL transmission cycle. The following results may be proved in much the same way as $D_{\downarrow}$ and $D_{\uparrow}$ in the previous section.

UL to UL *ISR* $U_{\uparrow}(z_0)$

The UL interference is generated by mobiles in neighboring cells which are randomly distributed in the network as opposed to the DL direction where cells' positions are fixed. Thus recalling the fact that mobile location z is uniformly distributed in cell s and taking into account the definition of the transmitted power with fractional power control model given by equation (3.2), $U_{\uparrow}(z_0)$ can be expressed as

$$\begin{aligned} U_{\uparrow}(z_0) =& \frac{1}{\pi R^2} \int_0^R \int_0^{2\pi} \sum_{s \in \Lambda^*} \frac{\rho^{2bk} \left| s + \rho\ e^{i\phi} \right|^{-2b}}{r^{2b(k-1)}} \rho d\rho d\phi \\ =& A_1(b)\ x^{2b(1-k)} \end{aligned} \tag{3.12}$$

where

$$A_1(b) = \frac{6(R/\delta)^{2bk}}{\Gamma(b)^2} \sum_{h=0}^{+\infty} \frac{\Gamma(b+h)^2\ \omega(b+h)}{\Gamma(h+1)^2\ (bk+h+1)} (R/\delta)^{2h}$$

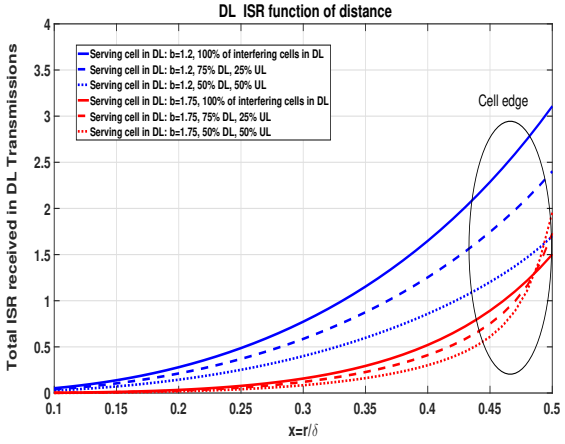

Figure 3.4 – DL ISR: Static TDD vs Dynamic TDD.

.

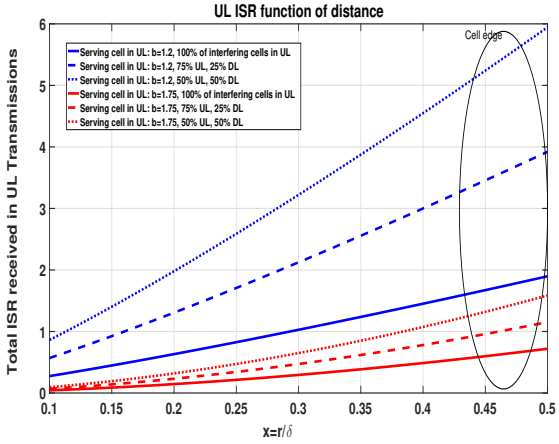

Figure 3.5 – UL ISR: Static TDD vs Dynamic TDD.

.

It is interesting to note that when a mobile is located at the same position as the serving BS, the UL to DL interference expression becomes similar to the expression of the UL to UL interference. From equation(3.11) we have

$$\beta_0 = \sum_{i=0}^{+\infty} \frac{\Gamma(b+i)^2\ \omega(b+i)}{\Gamma(i+1)^2\ (bk+i+1)} (R/\delta)^{2i} \tag{3.13}$$

which is similar to the expression of $\frac{1}{6}(\frac{\delta}{R})^{2bk} A_1(b)$.

DL to UL *ISR* $U_{\downarrow}(z_0)$

The signal coming from neighboring cells is often very strong with respect to mobile transmit power, especially if neighboring cells' antennas are in LOS condition or inter-site distance is lower (path loss is low). Contrary to the UL to UL interference, here the interfering signals come from cells, which have fixed positions. Hence, under the same system model assumptions, $U_{\downarrow}$ is given by

$$U_{\downarrow}(z_0) = \sum_{s \in \Lambda^*} \frac{P\,|s|^{-2b}}{P^*\ r^{2b(k-1)}} = A_2(b) x^{2b(1-k)} \tag{3.14}$$

where $A_2(b) = \frac{P\ \omega(b)}{P^*\ \delta^{2bk}}$.

Fig. 3.4 shows the developed *ISR* in DL transmission direction for different values of path loss exponent (2b=2.4, 2b=3.5). The first obvious observation is that the DL interference level decreases in the studied cell when other cells use more frequently the UL transmission cycle. This means that the impact of DL interference coming from other cells is relatively higher than the impact of interference coming from mobiles. Consequently, one can conclude that DL interference level in DL cycle for D-TDD should be lower than Static TDD.

The system behavior during the UL cycle is completely different. As shown in Fig. 3.5, interference level significantly increases when 25% or 50% of cells switched to the opposite direction, i.e., DL transmission. The UL performance degradation is mainly related to the higher DL transmit power of other cells, especially when they are in LOS conditions. This makes D-TDD system very limited by DL to UL interference. These conclusions are in agreement with the results of [24], which showed that there is an improvement of 10dB in the DL *SINR* of the serving cell when 50% of other cells switch from DL to UL transmission cycle; whereas the UL *SINR* of the same serving cell degrades by 20dB. This UL performance loss is expected to be more significant in macro-cell deployment. Therefore, DL to UL interference can seriously deteriorate system performance if no action is taken to mitigate it.

3.3.3 Coverage probability

The coverage probability (CCDF of *SINR*) is the probability that a mobile user is able to achieve a threshold *SINR*, denoted by γ, in UL and DL transmissions.

$$\Theta(\gamma) = P(SINR > \gamma) \tag{3.15}$$

For any scenario of user location distributions, the coverage probability is given by

$$\Theta(\gamma) = \int_{s_0} \mathbb{1}(SINR > \gamma) dt(z) \tag{3.16}$$

such that $\int_{s_0} dt(z) = 1$ (e.g., $dt(z) = \frac{rdrd\theta}{\pi R^2}$ for uniform user locations distribution).

Based on the expressions of the DL and UL *ISR* derived previously, we define the DL and UL *SINR*, denoted respectively by Π_{DL} and Π_{UL}, as follows

$$\Pi_{DL}(x) = \frac{1}{\eta\ D(x) + y_0 x^{2b}} = \frac{1}{d(x)} \tag{3.17}$$

$$\Pi_{UL}(x) = \frac{1}{\eta\ U(x) + y_0^{'} x^{2b(1-k)}} = \frac{1}{u(x)} \tag{3.18}$$

where $y_0 = \frac{P_N \delta^{2b}}{P}$, $y_0^{'} = \frac{P_N \delta^{2b(1-k)}}{P^*}$, P_N is the thermal noise power and η is the average load over the interfering cells.

Under a uniform user locations distribution, the expression of the coverage probability is given by

$$\Theta(\gamma) = \frac{2}{R^2} \int_0^R \mathbb{1}(r < \delta g^{-1}(\frac{1}{\gamma}))\ rdr = \frac{\Theta^2(\gamma)}{R^2} \tag{3.19}$$

where

$$\Theta(\gamma) = \min\left(\delta \times g^{-1}(\frac{1}{\gamma}), R\right)$$

with $g = d$ for the DL coverage probability and $g = u$ for the UL coverage probability.

The explicit formulas of the coverage probability require the inverse functions of d and u. This can be calculated by using series reversion methods; see for instance [8]. The inverse of u is easy to derive, and it is given by

$$u^{-1}(y) = (\frac{y}{\eta\,\alpha_u A_1(b) + \eta\,\alpha_d A_2(b) + y_0^{'}})^{\frac{1}{2b(1-k)}} \tag{3.20}$$

Now, to derive the inverse function of d, we shall follow the same approach as in [8]. To do so, let $y = d(x)$, using the series expansion of $D_{\downarrow}(m)$ in (3.5) and the simplified expression of $D_{\uparrow}(m)$ given in (3.10), it is clear that d admits an analytic expansion on $x = r/\delta$ and can be expressed as follows

$$y = x^{2b} f(b) \left(1 + \sum_{h=1}^{+\infty} c_h x^{2h}\right) \tag{3.21}$$

where

$$f(b) = 6\eta\,\alpha_d \omega(b) + \frac{6\eta P^* R^{2bk} \beta_0}{P\Gamma^2(b)} + y_0 \tag{3.22}$$

and

$$c_h = \frac{6\eta\alpha_d\Gamma(b+h)^2\omega(b+h)\beta_h}{f(b)\Gamma(b)^2\Gamma(h+1)^2} \tag{3.23}$$

Equation (3.21) can be transformed to

$$\begin{aligned}\left(\frac{y}{f(b)}\right)^{\frac{1}{b}} &= x^2\left(1+\sum_{h=1}^{+\infty} c_h x^{2h}\right)^{\frac{1}{b}} \\ &= x^2 + \frac{c_1}{b}x^4 + O(x^6)\end{aligned} \tag{3.24}$$

Eliminating the error terms in equation (3.24) gives a second-order equation in x^2 that admits two solutions:

$$x_{\pm}^2 = \frac{V(y,b)^2}{\frac{1}{2} \pm \sqrt{\frac{1}{4} + \frac{c_1}{b}V(y,b)^2}} \tag{3.25}$$

where

$$V(y,b) = \left(\frac{y}{f(b)}\right)^{\frac{1}{2b}} \tag{3.26}$$

Since $x = r/\delta$ is a positive real number, only the positive solution is valid. Hence we obtain the following approximation of $x = d^{-1}(y)$

$$d^{-1}(y) \approx \frac{V(y,b)^2}{\sqrt{\frac{1}{2} + \sqrt{\frac{1}{4} + \frac{c_1}{b}V(y,b)^2}}}. \tag{3.27}$$

3.4 Small-cells' network performance analysis

Let $\tilde{s}_0 = z_0 + Re^{i\theta}$ be the complex location of a typical small-cell that serves a typical mobile z_0. Thanks to the stationarity of the PPP Φ, we can evaluate interference in the mobile location $z_0 = 0$ having a random distance R to its closest serving BS. To simplify calculations, we denote hereafter by R_s, the distance between an interfering small-cell $\tilde{s}$ and the typical mobile location z_0, by R_z the distance between an interfering mobile z and z_0, by D_s the distance between an interfering small-cell $\tilde{s}$ and the typical cell $\tilde{s}_0$ and by D_z the distance between an interfering mobile z and $\tilde{s}_0$; see Fig. 3.6.

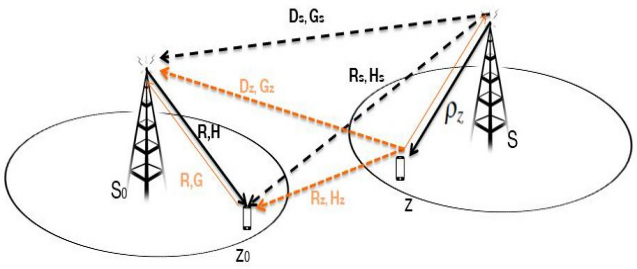

Figure 3.6 – Parameters recapitulation.

Based on the heterogeneous system model provided previously, The DL interference $\mathscr{I}_{DL}$, perceived by a mobile operating in DL, is expressed by

$$\begin{aligned}\mathscr{I}_{DL} &= \mathscr{I}_{DL->DL} + \mathscr{I}_{UL->DL} \\ &= \sum_{z\in\Phi\setminus\{z_0\}} \left(R_s^{-2b} H_s \tilde{P} \chi_d(z) + R_z^{-2b} H_z \rho_z^{2bk} \tilde{P}^* (1-\chi_d(z))\right). \end{aligned} \tag{3.28}$$

Similarly, the UL interference $\mathscr{I}_{UL}$ experienced by a mobile z_0, operating in UL transmission cycle and received at the serving small-cell BSs position, is given by

$$\begin{aligned}\mathscr{I}_{UL} &= \mathscr{I}_{UL->UL} + \mathscr{I}_{DL->UL} \\ &= \sum_{z\in\Phi\setminus\{z_0\}} \left(D_z^{-2b} G_z \rho_z^{2bk} \tilde{P}^* \chi_u(z) + D_s^{-2b} G_s \tilde{P} (1-\chi_u(z))\right). \end{aligned} \tag{3.29}$$

Therefore, the DL and UL *SINR* can be defined respectively by

$$\Pi_{DL} = \frac{\tilde{P} H R^{-2b}}{\mathscr{I}_{DL} + P_N} \tag{3.30}$$

$$\Pi_{UL} = \frac{\tilde{P}^* G R^{-2b(1-k)}}{\mathscr{I}_{UL} + P_N}. \tag{3.31}$$

with H and G are the fading coefficients between the typical mobile and its serving small-cell.

Once again, the DL (UL) coverage probability is defined as the CCDF of the DL (UL) *SINR*. It gives the percentage of locations in which Π_{DL} (Π_{UL}) is greater than a threshold value γ. It can be expressed for the DL and UL transmission directions as

$$\Theta_{DL} = \mathbb{E}_{\{R\}}\left[\mathbb{P}(\Pi_{DL} > \gamma)|R = r\right] \tag{3.32}$$

$$\Theta_{UL} = \mathbb{E}_{\{R\}}\left[\mathbb{P}(\Pi_{UL} > \gamma)|R = r\right]. \tag{3.33}$$

3.4.1 DL coverage probability derivation

Starting from the definition of the DL coverage probability and the DL *SINR*, we have

$$\Theta_{DL}(\gamma) = \int_0^{+\infty} \mathbb{P}\left[H > \frac{\gamma(\mathscr{I}_{DL} + P_N)}{\tilde{P}R^{-2b}}|R = r\right] f_R(r)dr \tag{3.34}$$

with $f_R(r)$ is the distribution of R which is the distance between z_0 and the closest small-cell. Using the null probability of a PPP, it has been shown that this distance is Rayleigh distributed [9] and its probability density function is given by

$$f_R(r) = 2\pi\lambda r e^{-\lambda\pi r^2} \tag{3.35}$$

Using the fact that H follows an exponential distribution of mean 1 and the definition of the Laplace transform, it follows that

$$\Theta_{DL}(\gamma) = 2\pi\lambda \int_0^{+\infty} e^{-\lambda\pi r^2} e^{-\gamma\tilde{P}^{-1}P_N r^{2b}} \mathscr{L}_{\mathscr{I}_{DL}}(\frac{\gamma r^{2b}}{\tilde{P}}) r dr \tag{3.36}$$

with $\mathscr{L}_{\mathscr{I}_{DL}}(v)$ is the Laplace transform of $\mathscr{I}_{DL}$ conditionally on R. It is defined by

$$\begin{aligned}\mathscr{L}_{\mathscr{I}_{DL}}(v) &= \mathbb{E}\left[e^{-v\mathscr{I}_{DL}}\right] \\ &= \mathbb{E}_{\{R_s,R_z,\rho_z,H_s,H_z,\chi_d(z)\}}\Bigg[\exp\big(-v\times \\ &\qquad \sum_{z\in\Phi\setminus\{z_0\}} R_s^{-2b}H_s\tilde{P}\chi_d(z) + R_z^{-2b}H_z\rho_z^{2bk}\tilde{P}^*(1-\chi_d(z))\big)\Bigg]\end{aligned} \tag{3.37}$$

From the complex geometry, the distance R_s between a small-cell $\tilde{s}$ and the typical mobile $z_0 = 0$ can be written in terms of R_z and ρ_z as

$$R_s^2 = R_z^2 + \rho_z^2 + 2R_z\rho_z\cos(\arg(z) - \phi_z). \tag{3.38}$$

with $\arg(z)$ is the complex argument of z relatively to the origin of the plane $z_0 = 0$.

Thus, replacing R_s by its expression and using the fact that H_s and H_z are i.i.d RVs and follow an exponential distribution of mean 1, (3.37) can be simplified to

$$\begin{aligned}
&\mathscr{L}_{\mathscr{I}_{DL}}(v) = \mathbb{E}_{\{R_z,\rho_z,\chi_d(z)\}}\Bigg[\prod_{z\in\Phi\setminus\{z_0\}} \mathbb{E}_{\{H_s,H_z\}}\big[\\
&\exp\big(-v(R_z^2+\rho_z^2+2R_z\rho_z\cos(\arg(z)-\phi_z))^{-b}H_s\tilde{P}\chi_d(z)\big)\times \\
&\exp\big(-vR_z^{-2b}H_z\rho_z^{2bk}\tilde{P}^*(1-\chi_d(z))\big)\big]\Bigg] \\
&= \mathbb{E}_{\{R_z\}}\Bigg[\prod_{z\in\Phi\setminus\{z_0\}} \mathbb{E}_{\{\chi_d(z),\rho_z\}}\big[\\
&\frac{1}{1+v(R_z^2+\rho_z^2+2R_z\rho_z\cos(\arg(z)-\phi_z))^{-b}\tilde{P}\chi_d(z)}\times \\
&\qquad \frac{1}{1+vR_z^{-2b}\rho_z^{2bk}\tilde{P}^*(1-\chi_d(z))}\big]\Bigg]
\end{aligned} \tag{3.39}$$

Now, using the Probability Generating Functional (PGFL) of PPP Φ with respect to the function inside the product, (3.39) becomes

$$\begin{aligned}
&\mathscr{L}_{\mathscr{I}_{DL}}(v) = \exp\Bigg(-\lambda\int_r^{+\infty}\int_0^{2\pi}\big(1-\mathbb{E}_{\{\chi_d(z),\rho_z\}}\big[\\
&\frac{1}{1+v(x^2+\rho_z^2+2x\rho_z\cos(\theta))^{-b}\tilde{P}\chi_d(z)}\times \\
&\frac{1}{1+vx^{-2b}\rho_z^{2bk}\tilde{P}^*(1-\chi_d(z))}\big]\big)xdxd\theta\Bigg) \\
&= \exp\Bigg(-\lambda\int_r^{+\infty}\int_0^{2\pi}\big(1-\mathbb{E}_{\{\rho_z\}}\big[\\
&\frac{\alpha_d}{1+v(x^2+\rho_z^2+2x\rho_z\cos(\theta))^{-b}\tilde{P}}+ \\
&\frac{\alpha_u}{1+vx^{-2b}\rho_z^{2bk}\tilde{P}^*}\big]\big)xdxd\theta\Bigg)
\end{aligned} \tag{3.40}$$

We have made the assumption that each user is associated with the nearest BS. Hence, following the same analysis provided in [71], we can approximate the distribution of ρ_z by the same distribution as R i.e., Rayleigh. It follows that

$$f_{\rho_z}(\rho) = 2\pi\lambda\rho e^{-\lambda\pi\rho^2}, \ \ \rho \geq 0. \tag{3.41}$$

Finally, by using (3.41), it follows that

$$\begin{aligned}\mathscr{L}_{\mathscr{I}_{DL}}(v) = \exp\Bigg(-\lambda \int_r^{+\infty} \int_0^{2\pi} \big(1- \\ \int_0^{+\infty} 2\pi\lambda e^{-\lambda\pi\rho^2} \big[\frac{\alpha_d}{1+v(x^2+\rho^2+2x\rho\cos(\theta))^{-b}\tilde{P}} + \\ \frac{\alpha_u}{1+vx^{-2b}\rho^{2bk}\tilde{P}^*}\big]\rho d\rho\big)xdxd\theta\Bigg).\end{aligned} \tag{3.42}$$

3.4.2 UL coverage probability derivation

The derivation of the UL coverage probability is quite similar to the DL one. The typical cell $\tilde{s}_0$ is operating in UL cycle and perceives interference coming from the other small-cells operating in DL and also from the mobiles transmitting in UL. Interference in this case is received at the location of $\tilde{s}_0$. Since the small-cells are distributed also as a PPP, denoted hereafter by Φ_s and constructed by the displacement of Φ, we can perform the analysis at the location $\tilde{s}_0 = 0$ (The stationarity of the PPP). Therefore, using the definition of the UL coverage probability given by (3.33), we get

$$\begin{aligned}\Theta_{UL}(\gamma) &= \int_0^{+\infty} \mathbb{P}\big[G > \frac{\gamma(\mathscr{I}_{UL}+P_N)}{\tilde{P}^* R^{-2b(1-k)}} | R = r\big] f_R(r)dr \\ &= 2\pi\lambda \int_0^{+\infty} e^{-\lambda\pi r^2} e^{-\gamma\tilde{P}^{*-1}P_N r^{2b(1-k)}} \times \\ &\qquad \mathscr{L}_{\mathscr{I}_{UL}}(\frac{\gamma r^{2b(1-k)}}{\tilde{P}^*})rdr,\end{aligned} \tag{3.43}$$

with $\mathscr{L}_{\mathscr{I}_{UL}}(v)$ is the Laplace transform of $\mathscr{I}_{UL}$ calculated conditionally on R.

Once again, the distance D_s represents the distance between an interfering small-cell $\tilde{s}$ and the typical one taken at the origin ($\tilde{s}_0 = 0$). Hence using the complex notations, we get

$$D_z^2 = D_s^2 + \rho_z^2 + 2D_s\rho_z\cos(\arg(s) - \phi_z). \tag{3.44}$$

Thus, by following the same steps as we did in the derivation of $\mathscr{L}_{\mathscr{I}_{DL}}(v)$, the Laplace transform of $\mathscr{I}_{UL}$ is given by

$$\mathscr{L}_{\mathscr{I}_{UL}}(v) = \exp\Bigg(-\lambda \int_r^{+\infty} \int_0^{2\pi} \big(1- \int_0^{+\infty} 2\pi\lambda e^{-\lambda\pi\rho^2} \big[\frac{\alpha_u}{1+v\rho^{2bk}(x^2+\rho^2-2x\rho\cos(\theta))^{-b}\tilde{P}^*} + \frac{\alpha_d}{1+vx^{-2b}\tilde{P}}\big]\rho d\rho\big) x dx d\theta \Bigg). \tag{3.45}$$

3.4.3 Average spectral efficiency

The instantaneous spectral efficiency (SE) is defined as the maximum information rate that can be transmitted in a given bandwidth. Using the upper-bound of the well known Shannon's formula, the instantaneous spectral efficiency is expressed by

$$SE_s = \log_2(1+\Pi_s) \tag{3.46}$$

with $s = DL$ when the serving small-cell is operating in DL and $s = UL$ when the serving small-cell is operating in UL.

The average spectral efficiency (ASE) is obtained by averaging over (3.46). It follows that

$$\begin{aligned} ASE_s &= \mathbb{E}[\log_2(1+\Pi_s)] \\ &= \int_0^{+\infty} \mathbb{P}(\log_2(1+\Pi_s) > t) dt \\ &\overset{(a)}{=} \frac{1}{\ln(2)} \int_0^{+\infty} \frac{\Theta_s(\gamma)}{(\gamma+1)} d\gamma \end{aligned} \tag{3.47}$$

with (a) comes from the change of variable $\gamma = e^t - 1$.

3.5 Simulation results

We simulate in MATLAB the proposed Macro-cell and small-cell models, for both DL and UL transmission directions, using the parameters summarized in Table. 3.1.

Macro-cells power P	60dBm
Small cells power $\tilde{P}$	26dBm
Target power cell specific P^*	20dBm
Noise power P_N	-93dBm
Number of rings (Macro-cells)	4 (60 interfering BSs)
Inter-site distance δ	1km
Antennas gain	16dBi
User distributions	uniform
small-cells density	10 cells.km^{-2}
Propagation factor a	Outdoor: 130dB, Indoor: 160dB
System bandwidth	Macro:20Mhz, small:10Mhz
Path loss exponent $2b$	2.5, 3.5

Table 3.1 – D-TDD simulation parameters.

We plot, respectively in Fig. 3.7 and Fig. 3.8, the DL and UL empirical coverage probability curves obtained by using Monte Carlo simulations for 20000 mobile locations z_0 and for two path loss exponent different values ($2b = 2.5$ and $2b = 3.5$). As we can see in Fig. 3.7, starting from a static TDD configuration where all the macro-cells are transmitting in DL, the coverage probability increases when D-TDD is activated with $\alpha_d = 75\%$ and $\alpha_d = 50\%$. This behavior is expected since the macro-cell BSs transmit with high power level and generate strong interference compared to interfering mobiles z transmitting in UL. However, the system behavior is completely different during the UL cycle of the serving cell. As it is shown in Fig. 3.8, activating D-TDD with a mean number of neighboring UL macro-cells $\alpha_u = 75\%$ and $\alpha_u = 50\%$ deteriorates completely the coverage probability. For instance, with a threshold SINR of $-20dB$, the coverage probability undergoes a huge degradation of 80%. Hence, one can conclude that D-TDD has a tremendous effect on performance during UL transmission especially for macro-cell deployments. Those results are in agreement with simulation results provided in [24] and quite similar to the theoretical *ISR* curves of Fig. 3.1 and Fig. 3.2.

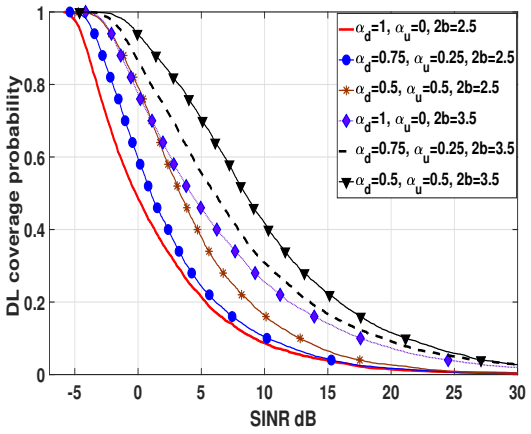

Figure 3.7 – Macro-cells network DL coverage probability.

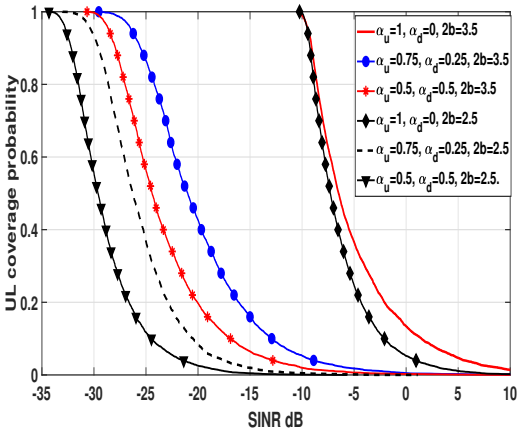

Figure 3.8 – Macro-cells network UL coverage probability.

In Fig. 3.9, we plot the DL and UL coverage probability curves, with different fractional power control factor values ($k = 0$, $k = 0.4$, $k = 0.8$ and $k = 1$), when D-TDD is activated and the number of DL and UL interfering cells is quite proportional (i.e., $\alpha_d = 50\%$ and $\alpha_u = 50\%$). When the serving cell is operating in DL, we notice that changing the power control factor has no impact on the coverage probability. This is mainly due to the fact that the principal interference impact comes from the DL BS signals where no power control mechanisms are considered. During the UL transmission cycle of the serving cell, one can notice that the coverage probability is decreasing when the fractional power control is increasing. Actually, FPC aims at providing the required *SINR* to UL users while controlling at the same time their interference. When FPC factor $k = 1$ the path loss is completely compensated and the target cell-specific power P^* is reached. Thus, the interference coming from mobiles z in UL is higher especially if a mobile is located in the edge of a neighboring cell. When FPC factor $0 < k < 1$, the scheme indemnifies partially the path loss. The higher is the path loss the lower is the received signal. This means that there is a compromise between the path loss and the *SINR* requirements. Therefore, interference are likely to be controlled, which explain the enhancement of the coverage probability. This enhancement is more obvious when $k = 0$. Which means that there is no compensation and the signal coming from the mobiles is weak.

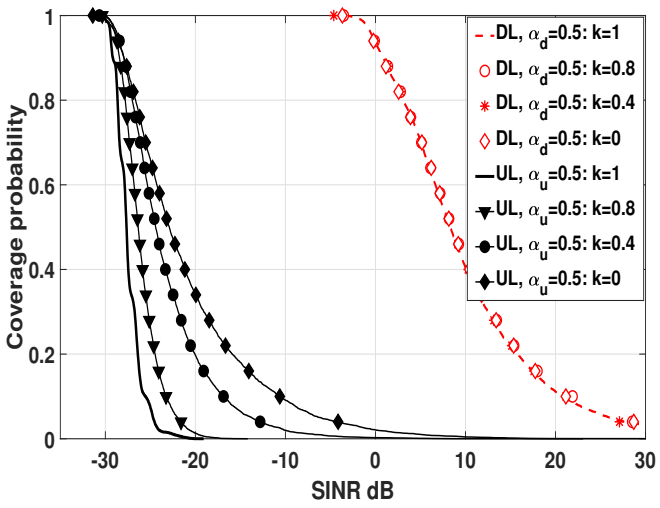

Figure 3.9 – Macro-cells network DL and UL coverage probability with different power control factors.

Fig. 3.10 shows the DL coverage probability obtained from the simulation of a heterogeneous network. First, small-cells operate with a static TDD configuration i.e., $\alpha_d = 1$, then the whole network switch to a D-TDD configuration during the ABS sub-frames. We plot the coverage probability curves for an outdoor environment with a propagation parameter $a = 130dB$ and a deep indoor environment with $a = 160dB$. For the outdoor environment, the comparison between the S-TDD and D-TDD shows that the behavior is quite similar to the macro-cells deployment. For instance, when 50% of small-cells switch from the DL to UL, there is an enhancement of the coverage probability by 15% for a threshold *SINR* of $-10dB$. However, for a deep indoor environment, one can notice that the coverage probability remains unchangeable even when 50% of the interfering small-cells switch to the opposite direction. In fact, signal propagation in a deep indoor environment suffers from high attenuation and delay factors because of the presence of obstacles and building penetration. During the DL transmission, the major interference comes from DL small-cells signal. In a deep indoor environment, not only the signal received from the serving cell is attenuated but also interference signal is subject to high attenuation. Similarly, Fig. 3.11 represents the comportment of the system during the UL transmission cycle. As expected, there is a degradation of the coverage probability when 50% of small-cells switch from DL to UL for an outdoor environment. This degradation is not severe like the case of macro-cells because small-cells transmit with low power and not highly elevated. Also, the comportment in a deep indoor environment is quite similar to the DL scenario for the same reasons stated previously.

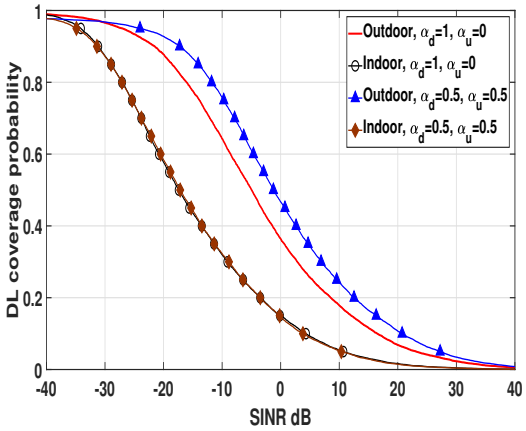

Figure 3.10 – Small-cells DL coverage probability : $2b = 3.5$, $k = 0.4$ and $\lambda = 10$ small-cell$/km^2$.

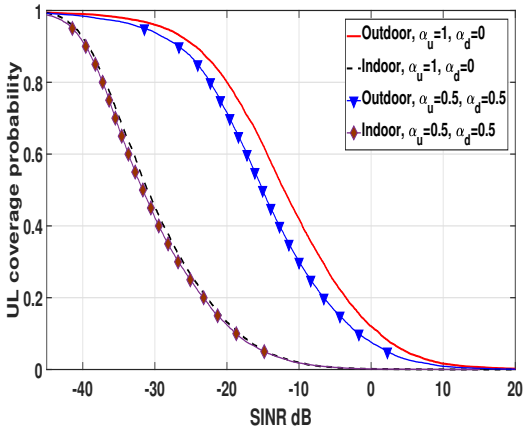

Figure 3.11 – Small-cells UL coverage probability : $2b = 3.5$, $k = 0.4$ and $\lambda = 10$ small-cell$/km^2$.

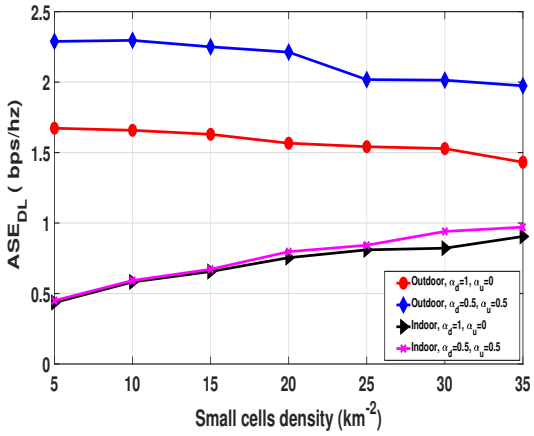

Figure 3.12 – DL average spectral efficiency : $2b = 3.5$, $k = 0.4$.

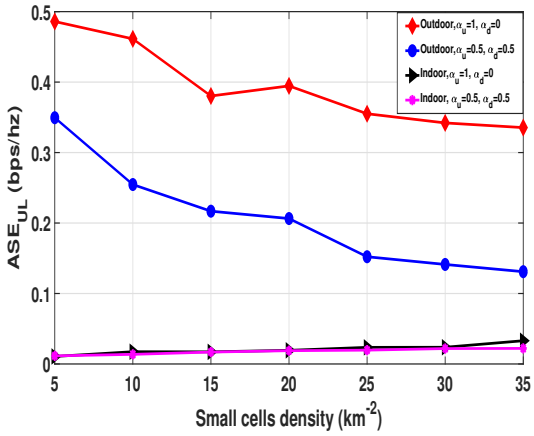

Figure 3.13 – UL average spectral efficiency : $2b = 3.5$, $k = 0.4$..

Additionally, we plot in Fig. 3.12 the average spectral efficiency in DL obtained from the simulation of the HetNet as a function of the small-cells' density. Once again, the comparison between the static TDD configuration and dynamic TDD, in an outdoor environment, shows that there is an enhancement of the ASE when D-TDD is activated with

$\alpha_d = 50\%$. Also, we observe that the ASE is slightly decreasing when small-cells density increases before it becomes almost constant. Actually, when small-cells density increases, the mean distance between the small-cells decreases because the density is inversely proportional to the mean distance between nodes. Hence, also the size of small-cells decreases and then both received signal power and interference increase simultaneously. Once we reach the interference limited scenario, the ASE becomes almost constant. For deep indoor environment, interference undergoes high attenuation as we have explained previously. When λ increases, the size of small-cells decrease. Thus, the received signal from the serving cell overcome interference undergoing bad propagation conditions. Similarly in Fig. 3.13, we plot the ASE during the UL cycle of a typical serving small-cell using the same parameters as in DL. Once again, we observe that the ASE is decreasing when D-TDD is activated with $\alpha_u = 50\%$ for the outdoor environment. Also, the ASE decreases as the small-cells density increases, especially when D-TDD is active. Moreover, for a deep indoor environment, the system experiences very bad performances in terms of ASE.

3.6 Conclusion

In this chapter we have investigated inter-cell interference in D-TDD based network. Explicit formulas of *ISR* covering different scenarios of interference have been derived. We have provided the explicit expressions of the coverage probability in macro-cell and small-cell deployments. The comparison between static-TDD configuration and D-TDD shows that performance are better with D-TDD during the DL. However, the UL transmission is severely limited by interference coming from other BSs DL signal. Also, we have compared two types of environment, outdoor and deep indoor. As expected, the system experiences bad performance in deep indoor environment for both static and dynamic TDD. Moreover, we have analyzed the impact of fractional power control mechanisms on the UL transmission. Results have shown that small FPC factors enhance the coverage probability for both D-TDD and S-TDD.

Chapter 4

A 3D beamforming scheme based on the spatial distribution of users' locations

4.1 Introduction

Massive Multiple antenna technologies including 3D beamforming have drawn recently the attention of telecommunication actors and research community. Actually, beamforming consists in forming a signal beam between the transmitter and the receiver by using an array of antennas. It enhances the signal strength at the receiver and minimize interference level so that high average data rate and high spectral efficiency can be achieved. Most existing base stations (BSs) are equipped with directional antennas that provides radiation patterns in the horizontal dimension, considering only the azimuth angle, and having a fixed vertical pattern and downtilt. Recently, there has been a trend to consider also the impact of the elevation and investigate how antennas' downtilt influences performance. It has been shown that the combination of the horizontal and the vertical dimensions can further improve the signal strength at the receiver location, enhances data rates and minimize interference in neighboring cells.

4.2 System model and notations

4.2.1 Network model

In this chapter, we consider a regular tri-sectorized hexagonal network denoted by Λ with an infinite number of sites s having an inter-site distance denoted by δ. Similarly to the

regural hexagonal network, for each site $s \in \Lambda$, there exists a unique (m,n) $\in \mathbb{Z}^2$ such that $s = \delta(m + ne^{i\frac{\pi}{3}})$. We denote by s_0 the serving cell located at the origin of $\mathbb{R}^2$. Unlike regular hexagonal network with omni-directional antennas where BSs are located in the center of hexagons, BSs of sites here are located at the corner of the hexagons. All BSs have the same height l_b, transmit with the same power level P and assumed to have directional antennas covering each one a hexagonal sector identified by $c \in \{1,2,3\}$. The azimuths of antennas ϑ_c in which the radiation is at its maximum is taken relative to the real axis such that

$$\vartheta_c = \frac{\pi}{3}(2c-1) \tag{4.1}$$

so that the azimuth of the first sector of each site has an angle of $\frac{\pi}{3}$ with the real axis relatively to the location of s.

We consider a typical mobile served by the first sector ($c = 1$) of s_0. Its location is denoted by z_0 such that $z_0 = re^{i\theta}$ where (r, θ) are the polar coordinates in the complex plane. We denote also by $z_{s,c}$ the location of a mobile served by a sector c of a site $s \in \Lambda^*$, where Λ^* is the lattice Λ without the serving cell s_0. Locations $z_{s,c}$ are written in the complex plane by $z_{s,c} = s + r_{s,c}e^{i\theta_{s,c}}$, where $r_{s,c}$ and $\theta_{s,c}$ represent respectively the distance and the angle (complex argument) between $z_{s,c}$ and s.

4.2.2 Beamforming model

As we mentioned previously, BSs are equipped with directional antennas with sectorized gain pattern. At each TTI (Time Transmit Interval), we assume that there is at most one user served by a sector c of site s using beamforming radiation pattern. This can be modeled by a Bernoulli RV $\rho_{s,c}$ such that $\mathbb{P}(\rho_{s,c} = 1) = \eta$ and $\mathbb{P}(\rho_{s,c} = 0) = 1 - \eta$. η represents the percentage of the occupied resources or the average load over the interfering sites s.

Furthermore, we assume that each antenna has a directional radiation that can be described by two planar patterns: the horizontal and the vertical one denoted respectively by H and V. We define the antenna radiation for each pattern by a 2π-periodic function U such that its restriction on $(-\pi,\pi] \to [0,1]$ has the following properties

- $U(\alpha) = U(-\alpha)$ for all $\alpha \in (-\pi,\pi]$,

- $U(\alpha) = 0$ if $\frac{\pi}{2} \leq |\alpha| \leq \pi$,

- U is decreasing on $[0, \frac{\pi}{2}]$ and increasing on $[\frac{-\pi}{2}, 0]$.

Numerous antenna radiation pattern models can be found in literature such as the 3GPP model, Mogensen model [79] and real antenna patterns provided by constructors (Kathrein antennas...). For reasons of tractability, we adopt in the reminder of this analysis Mogensen model to describe the antenna horizontal and vertical radiation patterns in the linear scale as follows

$$H(\alpha) = [\cos(\alpha)]^{-2w_h} \tag{4.2}$$

$$V(\phi) = [\cos(\phi)]^{-2w_v}, \tag{4.3}$$

with $w_h = \frac{ln(2)}{\ln(\cos(\frac{\theta_{h3dB}}{2})^2)}$ and $w_v = \frac{ln(2)}{\ln(\cos(\frac{\theta_{v3dB}}{2})^2)}$. θ_{h3dB} and θ_{v3dB} are respectively the horizontal and the vertical half power beam widths (HPBW).

This model can be adapted to beamforming radiation pattern by taking small values of HPBWs (θ_{h3dB} and θ_{v3dB}) to have narrow horizontal and vertical beams. Hence, the antenna radiation pattern received in a mobile location z_0 from an interfering site s is defined by

$$G_s(z_0) = \sum_{c=1}^{3} \rho_{s,c} H(\alpha_{s,c}) V(\phi_{s,c}), \tag{4.4}$$

with $\alpha_{s,c}$ is the angle between the mobile z_0 orientation and the beam axis directed to a mobile $z_{s,c}$ in the horizontal plane and $\phi_{s,c}$ is the angle between the beam direction in the vertical plane and the mobile z_0. The angle $\alpha_{s,c}$ can be expressed, based on the complex geometry, as

$$\alpha_{s,c} = \psi(z_0, s) - \theta_{s,c}, \tag{4.5}$$

where $\psi(z,s) = arg(z_0 - s)$ and $\theta_{s,c} = \psi(z_{s,c}, s)$ is the complex argument of $z_{s,c}$ relatively to s. Each $\theta_{s,c}$ is assumed to be uniformly distributed in the interval $[\vartheta_c - \frac{\pi}{3}, \vartheta_c + \frac{\pi}{3}]$, thus using a linear transformation of the RV $\theta_{s,c}$, we can easily prove that the angle $\alpha_{s,c}$ is a RV uniformly distributed in the interval $[\psi(z,s) - \frac{2\pi}{3}c, \psi(z,s) + \frac{2\pi}{3}(1-c)]$.

Similarly for the vertical dimension, the angle $\phi_{s,c}$ can be expressed as

$$\phi_{s,c} = atan(\frac{l_b}{|z_0 - s|}) - \tilde{\phi}_{s,c}, \tag{4.6}$$

with $\tilde{\phi}_{s,c} = atan(\frac{l_b}{r_{s,c}})$ refers to the antenna downtilt, which is variable in our case.

The distance $r_{s,c} = |z_{s,c} - s|$ between a mobile $z_{s,c}$ and s varies between 0, when $z_{s,c}$ is close to s location, and $\frac{2\delta}{3}$ when $z_{s,c}$ is located at the edge of a sector. This distance can be characterized using the antenna radiation pattern covering a whole hexagonal sector of s. Thus, $r_{s,c}$ is varying between 0 and $\frac{2\delta}{3}U(\theta_{s,c} - \vartheta_c)$, with $U(\theta_{s,c} - \vartheta_c)$ is the antenna radiation pattern of a sector (i.e., the horizontal half power beam width is equal to 65 degrees). So the mobile will be located at the far edge of a sector when the angle between $z_{s,c}$ and s is equal to the antenna azimuth in which the radiation is at its maximum. Moreover, since mobile locations $z_{s,c}$ are taken inside the serving hexagonal sector, we consider in the remainder that $r_{s,c}$ is a RV uniformly distributed on the interval $[0, \frac{2\delta}{3}U(\theta_{s,c} - \vartheta_c)]$. Fig. 4.1 illustrates the 3D beamforming model.

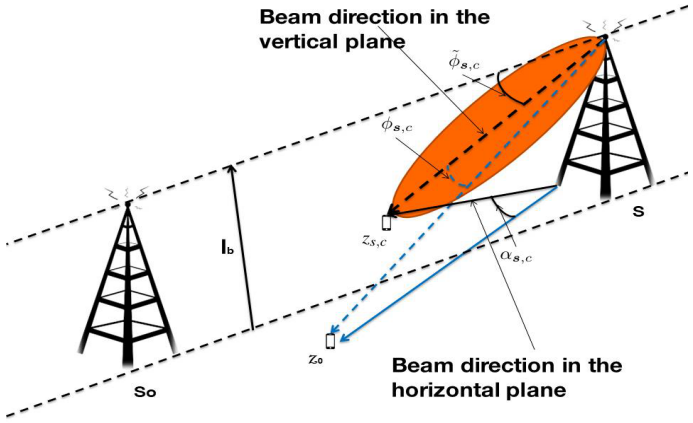

Figure 4.1 – 3D beamforming illustration

4.2.3 Propagation model

To model the wireless channel we consider the same power-law path loss as in chapter 3 and given by equation (3.1). Additionally, in this chapter we model the shadowing effect between a mobile location z_0 and an interfering site s by a log-normal RV $\chi_s(z_0) = 10^{\frac{Y_s(z_0)}{10}}$

with $Y_s(z_0)$ is a Normal RV with mean $\mathbb{E}(Y_s(z_0)) = 0$ and variance σ^2. The shadowing effect between z_0 and the serving site s_0 is denoted by χ_0. This sequence of RVs are assumed to be independent and identically distributed (i.i.d) for all (s, z_0).

Therefore, the received power from a BS s, transmitting with a power level P, in a mobile location z_0 is expressed by

$$P_r(z_0, s) = \frac{PAG_s(z_0)\chi_s(z_0)}{L(s, z_0)}, \tag{4.7}$$

with A is the antenna gain and $G_s(z_0)$ is the antenna radiation pattern from s received at the mobile location z_0.

4.3 Characterization of antenna beamforming radiation pattern

It is obvious from (4.4) that $G_s(z_0)$ is a RV that depends on the three RVs: $\alpha_{s,c}$, $\phi_{s,c}$ and $r_{s,c}$. Also, one can notice that $V(\phi_{s,c})$ is a RV that depends on the RV $H(\alpha_{s,c})$. Therefore, to characterize $G_s(z_0)$, we start first by deriving the probability density function (PDF) of $H(\alpha_{s,c})$ and the PDF of $V(\phi_{s,c})$ conditionally on $H(\alpha_{s,c})$, denoted respectively by $f_{H_{s,c}}(h)$ and $f_{V_{s,c}|H_{s,c}}(v)$. To do so, we shall use the following lemma that gives the PDF of a transformed RV by a bijective function.

Lemma 1. *Let X be a RV and f_X its PDF defined on an interval [a,b]. Let Y be a RV such that $Y = g(X)$ with g is a bijective function. The PDF of Y f_Y is given by*

$$f_Y(y) = f_X(g^{-1}(Y)) \left| \frac{dg^{-1}(y)}{dy} \right| \mathbb{1}_{[g(a)\wedge g(b), g(a)\vee g(b)]}(y) \tag{4.8}$$

where g^{-1} is the inverse function of g, $g(a) \wedge g(b) = min(g(a), g(b))$ and $g(a) \vee g(b) = max(g(a), g(b))$.

The proof of this lemma is not provided here. To obtain the result, one can calculate the PDF by distinguishing between the case when g is increasing and the case when it is decreasing.

Using lemma 1, the PDF $f_{\alpha_{s,c}}$ of the RV $\alpha_{s,c}$ is given by

$$f_{\alpha_{s,c}}(\alpha) = \frac{3}{2\pi}\mathbb{1}_{[\psi(z_0,s)-\frac{2\pi}{3}c,\psi(z_0,s)+\frac{2\pi}{3}(1-c)]}(\alpha). \tag{4.9}$$

Similarly, from equation (4.6), we can see that $\phi_{s,c}$ is the transformation of the uniform RV $r_{s,c}$ by the function $g(x) = atan(\frac{l_b}{|z_0-s|}) - atan(\frac{l_b}{x})$. Also, this RV depends on $\alpha_{s,c}$. One can easily verify that g is strictly increasing on the interval $[0, \frac{2\delta}{3}U(\theta_{s,c} - \vartheta_c)]$ and its inverse function g^{-1} is given by

$$g^{-1}(y) = \frac{l_b}{tan(atan(\frac{l_b}{|z_0-s|}) - y)}. \tag{4.10}$$

Hence, the PDF of $\phi_{s,c}$ conditionally on $\alpha_{s,c}$, denoted by $f_{\phi_{s,c}|\alpha_{s,c}}(\phi)$, is given by

$$f_{\phi_{s,c}|\alpha_{s,c}}(\phi) = \frac{3}{2\delta U(\theta_{s,c} - \vartheta_c)}\Big(1 + \frac{1}{\tan^2(\phi - atan(\frac{l_b}{|z_0-s|}))}\Big) \mathbb{1}_{[atan(\frac{-|z_0-s|}{l_b}),atan(\frac{2\delta l_b U(\theta_{s,c}-\vartheta_c)-3l_b|z_0-s|}{2\delta|z_0-s|U(\theta_{s,c}-\vartheta_c)+3l_b^2})]}(\phi) \tag{4.11}$$

Now, to characterize $G_s(z_0)$, we apply once again Lemma 1 to $\alpha_{s,c}$ and $\phi_{s,c}$ transformed by the function g such that $g = H$ for $\alpha_{s,c}$ and $g = V$ for $\phi_{s,c}$. Thence, using lemma 1 and equations (4.9) and (4.11) we obtain

$$f_{H_{s,c}}(h) = \frac{-3h^{\frac{-1-2w_h}{2w_h}}}{4\pi w_h\sqrt{1-h^{\frac{-1}{w_h}}}}\mathbb{1}_{[h_1\wedge h_2, h_1\vee h_2]}(h), \tag{4.12}$$

with $h_1 = H(arg(z_0 - s) - \frac{2\pi}{3}c)$ and $h_2 = H(arg(z_0 - s) + \frac{2\pi}{3}(1-c))$. And

$$f_{V_{s,c}|H_{s,c}}(v) = \Big(1 + \frac{1}{\tan^2(acos(v^{\frac{-1}{2w_v}}) - atan(\frac{l_b}{|z_0-s|}))}\Big)\times \frac{-3v^{\frac{-1-2w_v}{2w_v}}}{4w_v\delta U(\theta_{s,c} - \vartheta_c)\sqrt{1-v^{\frac{-1}{w_v}}}}\mathbb{1}_{[v_1\wedge v_2, v_1\vee v_2]}(v), \tag{4.13}$$

with $v_1 = V(atan(\frac{-|z_0-s|}{l_b}))$ and $v_2 = V(atan(\frac{2\delta l_b U(\theta_{s,c}-\vartheta_c)-3l_b|z_0-s|}{2\delta|z_0-s|U(\theta_{s,c}-\vartheta_c)+3l_b^2}))$.

Moreover, the joint PDF of $H(\alpha_{s,c})$ and $V(\phi_{s,c})$ denoted by $f_{H_{s,c},V_{s,c}}$ is given by

$$f_{H_{s,c},V_{s,c}}(h,v) = f_{V_{s,c}|H_{s,c}}(v) f_{H_{s,c}}(h). \tag{4.14}$$

To calculate the PDF of $Z_{h,v} = H(\alpha_{s,c})V(\phi_{s,c})$, one can use the Mellin transform of the distribution of $Z_{h,v}$, denoted by $f_{Z_{h,v}}$, defined by

$$\begin{aligned}\mathscr{M} f_{Z_{h,v}}(s) = \mathbb{E}[Z_{h,v}^{s-1}] &= \int\int h^{s-1} v^{s-1} f_{H_{s,c},V_{s,c}}(h,v) dh dv \\ &= \int h^{s-1} \Big(\int v^{s-1} f_{V_{s,c}|H_{s,c}}(v) dv \Big) f_{H_{s,c}}(h) dh \end{aligned} \tag{4.15}$$

Then, the PDF of the product of the horizontal and the vertical patterns $f_{Z_{h,v}}$ can be obtained by using the inverse Mellin transform as follows

$$f_{Z_{h,v}}(z) = \frac{1}{2\pi i} \int z^{-s} \mathscr{M} f_{Z_{h,v}}(s) ds. \tag{4.16}$$

Finally the distribution of $G_s(z_0)$ can be obtained by the convolution of $f_{Z_{h,v}}$ for $c \in \{1,2,3\}$.

The mathematical expectation of $G_s(z_0)$ is defined by

$$\mathbb{E}[Gs(z_0)] = \eta \sum_{c=1}^{3} \mathbb{E}[H(\alpha_{s,c})V(\phi_{s,c})], \tag{4.17}$$

where $\mathbb{E}[H(\alpha_{s,c})V(\phi_{s,c})]$ is calculated by taking $s = 2$ in equation (4.15).

When the downtilt is taken constant, the vertical antenna radiation pattern is no more a RV. Thus, the explicit expression of $\mathbb{E}[Gs(z_0)]$ conditionally on z_0 can be written as

$$\begin{aligned}\mathbb{E}[Gs(z_0)] &= \frac{3\eta V(\phi_{s,c})}{2\pi} \sum_{c=1}^{3} \int_{\upsilon_c - \frac{\pi}{3}}^{\upsilon_c + \frac{\pi}{3}} \cos^{-2w_h}(\theta - \psi(z_0, s)) d\theta \\ &= \frac{3\eta V(\phi_{s,c})}{\pi} \int_0^{\pi} \cos^{-2w_h}(\theta) d\theta. \end{aligned} \tag{4.18}$$

Equation (4.18) comes from the $2\pi-$periodicity of the function cos and Chasles's formula.

Finally, by using $\int_0^{\frac{\pi}{2}} cos^z(x) = \frac{\sqrt{\pi}\Gamma(\frac{z+1}{2})}{2\Gamma(\frac{z}{2}+1)}$ for all complex number z such that $\Re(z) > -1$, the explicit expression of the mathematical expectation of $G_s(z_0)$ is given by

$$\mathbb{E}[G_s(z_0)] = \frac{3\eta V(\phi_{s,c})\Gamma(\frac{1}{2} - w_h)}{\sqrt{\pi}\Gamma(1-w_h)} \tag{4.19}$$

with $\Gamma(.)$ is the Euler Gamma function.

4.4 Interference characterization

A mobile located at a position z_0 in the first sector ($c = 1$) of the serving site s_0 receives interference from the co-sectors and also from the other interfering sites in Λ^*. We define the individual *ISR*, denoted here by $\mathscr{I}_s(z_0)$, as the received power from an interfering site s divided by the useful power received by z_0 from the serving cell. Its expression is given by

$$\begin{aligned} \mathscr{I}_s(z_0) &= \frac{P_r(z_0, s)}{P_r(z_0, s_0)} \\ &= r^{2b}|s - z_0|^{-2b} G_s(z_0)\tilde{\chi}_s, \end{aligned} \tag{4.20}$$

where $\tilde{\chi}_s = 10^{\frac{\tilde{Y}_s}{10}}$ is a log-normal RV representing the ratio of the shadowing effect from interfering sites and the shadowing effect from the serving site (The ratio of two log-normal RVs is a log-normal RV), with $\tilde{Y}_s$ is a Normal RV with mean 0 and variance $\tilde{\sigma}^2$. Also, we define the cumulative *ISR* from all the interfering sites including the two other sectors of the serving site s_0 as the sum over $s \in \Lambda$ of all the individual ISRs. It is expressed as

$$\mathscr{I}(z_0) = -1 + \sum_{s \in \Lambda} r^{2b}|s - z_0|^{-2b} G_s(z_0) 10^{\frac{\tilde{Y}_s}{10}}. \tag{4.21}$$

$\mathscr{I}(z_0)$ is an infinite sum of independent positive RVs not identically distributed. As far is known, the distribution of a sum of log-normal RVs is not exactly known but there exists some approximations that can be found in the probability theory literature. Fenton-Wilkinson [80] approach appears to be a convenient approximation to deal with this sum of log-normal RVs. It consists in approximating a sum of log-normal RVs by a new log-normal RV by matching the mean and the variance. Consequently, according to Theorem 9.2.a of [81],

$$\mathbb{E}[\mathscr{I}(z_0)] = -1 + \mathbb{E}[10^{\frac{\tilde{Y}_s}{10}}] \sum_{s \in \Lambda} r^{2b}|s - z_0|^{-2b} \mathbb{E}[G_s(z_0)].$$

In [8], it has been shown that $\sum_{s\in\Lambda^*} r^{2b}|s-z_0|^{-2b}$ is a convergent series on $x=\frac{r}{\delta}$ that can be approximated as follows

$$\sum_{s\in\Lambda^*} r^{2b}|s-z_0|^{-2b} \approx \frac{6x^{2b}}{\Gamma(b)^2}\sum_{h=0}^{+\infty}\frac{\Gamma(b+h)^2}{\Gamma(h+1)^2}\omega(b+h)x^{2h} \tag{4.22}$$

with $\omega(z)$ is given by equation (3.6).

Since $G_s(z_0)\leq 1$, we have $\mathbb{E}(G_s(z_0))<1$. By using (4.22), we can easily prove that $\mathbb{E}[\mathscr{I}(z_0)]<\infty$. Hence, according to Theorem 9.2.b of [81], $\mathscr{I}(z_0)$ converges almost surely.

This result is very important, since the almost sure convergence implies convergence in probability and thus implies convergence in distribution which is the notion of convergence used in the strong law of large numbers. However, the central limit theorem (CLT) can not be applied in this case because the random variables in the sum are not identically distributed. Also, the generalized CLT known as Lyapunov CLT and Lindeberg CLT conditions are not verified here. Hence, $\mathscr{I}(z_0)$ can not be approximated by a Gaussian RV.

On the other hand, the coverage probability $\Theta(z_0)$ is defined according to (3.15) as follows

$$\Theta(\gamma)=\mathbb{P}(\Pi(z_0)>\gamma), \tag{4.23}$$

where $\Pi(z_0)$ is the *SINR* of z_0 and it can be expressed in terms of the cumulative *ISR* $\mathscr{I}(z_0)$ as follows

$$\Pi(z_0)=\frac{1}{\mathscr{I}(z_0)+y_0}, \tag{4.24}$$

with $y_0=\frac{aNr^{2b}}{AP\chi_0}$ and N is the thermal noise power.

Finally, the throughput is calculated using the upper bound of the well known Shannon's formula for a MIMO system $Tx\times Rx$, with Tx and Rx are respectively the number of transmit and receive antennas. Hence the throughput $C(z_0)$ of a user located at a position z_0 can be written as

$$C(z_0)=(Tx\wedge Rx)B_w log_2(1+\Theta(z_0)), \tag{4.25}$$

with B_w is the system bandwidth.

4.5 Numerical results and discussion

For numerical purpose, we consider 5 rings of interfering sites with an inter site distance $\delta = 0.750km$. All BSs are assumed to have the same height $l_b = 30m$, transmit with a power level $P = 40dBm$ and operate in a bandwidth B_w of $20MHz$. The antenna gain is set to be $A = 17dBi$. Also, the downlink thermal noise power is calculated for B_w and set to $N = -93dBm$. The path loss exponent is considered to be $2b = 3.5$, the propagation factor of an outdoor environment is $a = 130dB$ and the standard deviation of the log-normal shadowing is $\sigma = 5.5dB$. Finally, we assume that we have $2Rx$ antennas in user's terminals, the number of Tx antennas depends on the chosen HPBWs (θ_{h3dB} and θ_{v3dB}). This number with beamforming is greater than 2 and thus, the number of possible transmission layers is at most 2.

We simulate the 3D beamforming model in MATLAB considering four values of θ_{h3dB} (30°, 20°, 14° and 8°) and a vertical half power beam width $\theta_{v3dB} = 8°$. We compare it to a simulated hexagonal tri-sectorized network without beamforming mechanisms with $\theta_{h3dB} = 65$, $\theta_{v3dB} = 32$ and a fixed downtilt angle 8°.

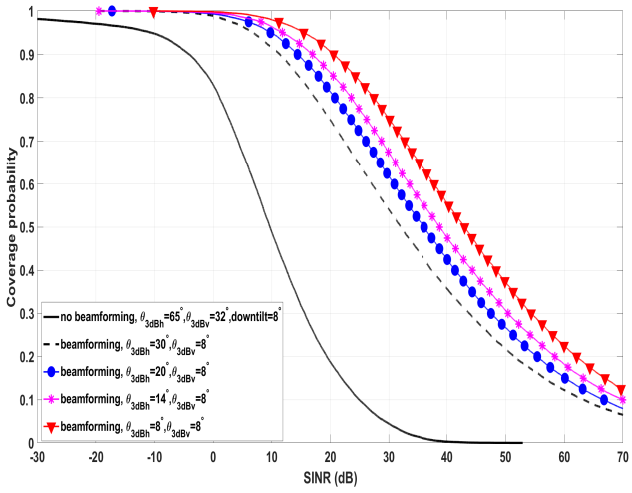

Figure 4.2 – Coverage probability variations: no beamforming vs 3D beamforming with different θ_{h3dB}.

We plot in Fig. 4.2 the empirical coverage probability (CCDF of *SINR*) curves obtained by using Monte Carlo simulations for 20000 mobile locations z_0. As we can see,

3D beamforming enhances significantly performance. For instance, with an *SINR* threshold of $10dB$, the coverage probability increases from 66% to 99% when 3D beamforming is deployed with a horizontal HPBW of $\theta_{h3dB} = 8°$. Moreover, it can be observed that the coverage probability increases as the horizontal HPBW decreases. Actually, the horizontal HPBW is related to the number of transmit antennas used by BSs. When this number increases, the signal is focused on a specific zone of the cell. Hence, interference coming from neighboring sites are reduced significantly as the HPBW decreases and the number of transmit antennas increases. This leads to an enhancement of *SINR* and thus an enhancement of the coverage probability.

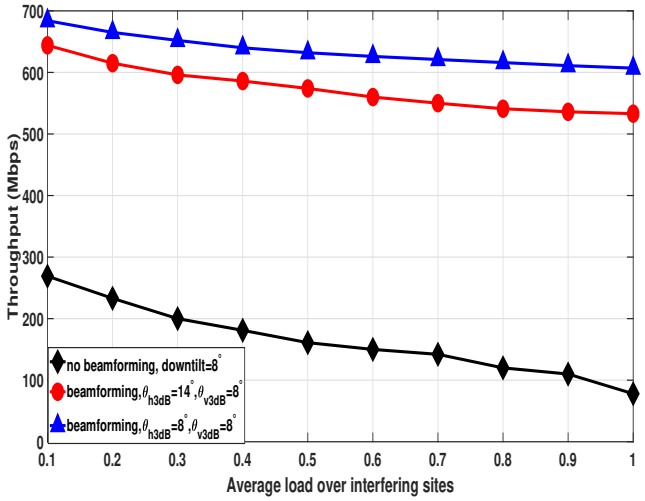

Figure 4.3 – Throughput variation with the average load over interfering sites: comparison between 3D beamforming model and hexagonal tri-sectorized network.

Similarly in Fig. 4.3, we plot the user throughput as a function of the average load over interfering sites considering the 3D beamforming with two values of θ_{h3dB} (14° and 8°) and $\theta_{v3dB} = 8°$. We compare results with the case of tri-sectorized hexagonal network without beamforming. As we can observe, with a tri-sectorized hexagonal network without 3D beamforming, the throughput is more sensitive to the average load variations over interfering sites and it decreases by almost 30% when the average load increases from 1% to 100%. With 3D beamforming, one can notice that the throughput increases significantly compared to the case without beamforming. Also, it increases as the horizontal HPBW decreases, which is in agreement with results of Fig. 4.2. Additionally, we can see that the sensitivity to the average load and interference decreases in the case where 3D beamform-

ing is used, especially with small values of the horizontal HPBW i.e., when the number of transmit antennas increases.

Fig. 4.4 shows a comparison between the coverage probability of a network adopting the 3D beamforming according to our model and the one of a network using a 2D beamforming where only a random horizontal radiation pattern is considered. The vertical component is taken constant and included in the antenna gain. Once again, we can notice that a small horizontal HPBW leads to an increase of the coverage probability for the both models. Moreover, it is obvious that performance in terms of *SINR* with 3D beamforming are better than 2D beamforming. Actually, most BSs use a linearly arranged array of antennas placed at the top of BSs. Unfortunately, the number of antennas can not be increased because of size constraints. Hence the interest of FD-MIMO, based on a 2D array of antennas, that offers the possibility to increase the number of transmit antennas and gives extra degrees of freedom in order to improve significantly the wireless system performance. Also, it provides the capability to adapt dynamically beam patterns in the horizontal and vertical dimensions, which leads to performance enhancement.

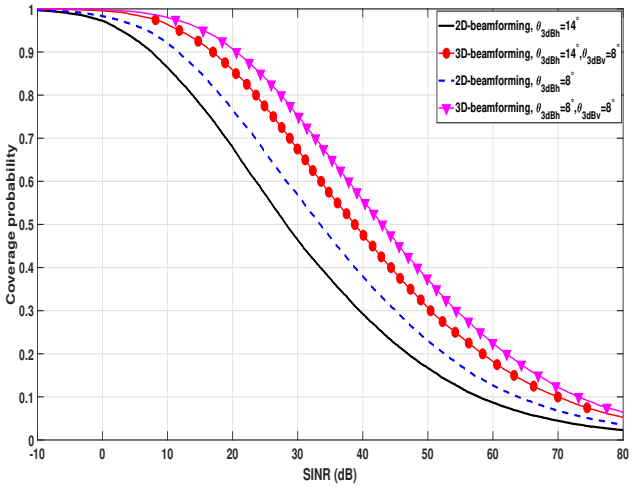

Figure 4.4 – Coverage probability comparison: 3D beamforming vs 2D beamforming.

Finally in Fig. 4.5, we plot the coverage probability considering the 3D beamforming model, presented in this chapter, for 2 values of θ_{h3dB} (8° and 14°) and $\theta_{v3dB} = 8°$. We compare it with the coverage probability of the same network, but instead of taking the downtilt angle $\tilde{\phi}_{s,c}$ as a function of the mobile location $z_{s,c}$, we consider two values

of this angle, $\tilde{\phi}_{s,c} = 4°$ and $\tilde{\phi}_{s,c} = 8°$, close to the values used in practical systems. One can observe that when the horizontal HPBW is set to be 14°, the 3D beamforming model with variable downtilt angle has better performance than the case of fixed downtilt for the two values of $\tilde{\phi}_{s,c}$. However, with a horizontal HPBW of 8°, we can notice that the coverage probability when $\tilde{\phi}_{s,c} = 8°$ is getting closer to the one of the network with 3D beamforming. Hence, using a large number of transmit antennas to concentrate the beam to a specific location, especially in the horizontal dimension, leads to a significant enhancement of performance. Moreover, for the vertical dimension, it has been shown in several papers that there exists an optimal downtilt angle for which the performance are enhanced significantly. In practical systems, we take always a downtilt close to 6°.

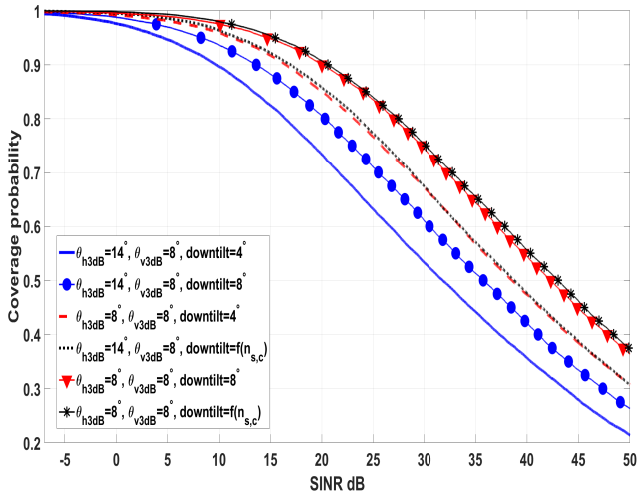

Figure 4.5 – Downtilt $\tilde{\phi}_{s,c}$ impact: variable vs fixed downtilt.

4.6 Conclusion

In this chapter, we have proposed an analytical model for 3D beamforming, in DL transmission, where antenna radiation patterns depend on the spatial distribution of users' locations in the plane. We have shown, through system level simulations, that the 3D beamforming reduces significantly interference and thus enhances the *SINR* and users throughput in downlink. A comparison between the proposed 3D model and the traditional 2D beamforming, where only the azimuthal plane is considered, shows better performance with 3D beamforming.

Chapter 5

D-TDD interference mitigation schemes

As we have seen in chapter 3, D-TDD shows better performance than S-TDD during the DL transmission cycle of a typical cell. However, The UL performance undergoes a huge degradation because of interference, mainly DL to UL interference. The aim of this chapter is to study the applicability of the 3D beamforming scheme, introduced in the previous chapter, to DL transmitting cells in a D-TDD based tri-sectorized hexagonal network. Additionally, we propose a cell clustering interference mitigation scheme based on the hexagonal tessellation and applied to a small-cell deployment that intends also to reduce the DL to UL interference.

5.1 D-TDD based macro-cell deployment interference mitigation scheme

In the remainder of this chapter, we adopt the same tri-sectorized hexagonal network model, propagation model, notations and 3D beamforming model presented in chapter 4. Additionally, to model D-TDD system, we proceed as we did in chapter 3. We assume that all cells initially operate synchronously in DL or UL with S-TDD mode. Once D-TDD is activated, each cell selects randomly the cycle of the transmission. Also, we assume that the transmission direction is the same in the three sectors of each site s and it is modeled by two Bernoulli RVs $\beta_d(s)$ and $\beta_u(s)$, such that $\mathbb{P}(\beta_d(s)=1)=\alpha_d$, $\mathbb{P}(\beta_u(s)=1)=\alpha_u$ and $\beta_u(s)=1-\beta_d(s)$

Additionally, We consider the 3D beamforming model, introduced in the previous chapter, as an interference mitigation scheme devoted to reduce DL to DL and DL to UL interference in D-TDD scenarios. Actually, to support 3D beamforming based CLI mit-

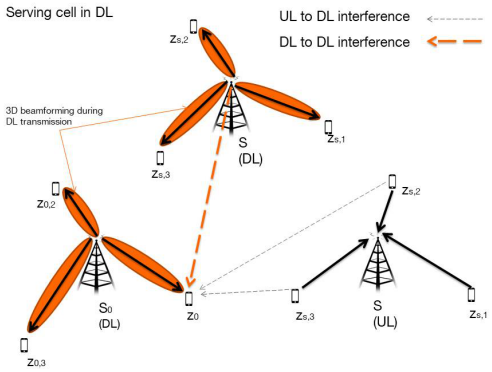

Figure 5.1 – D-TDD DL transmission cycle

.

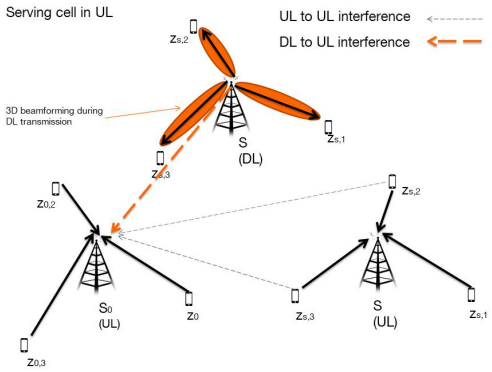

Figure 5.2 – D-TDD UL transmission cycle

.

igation, it is necessary to have coordination between BSs through signaling information exchange between cells. Also, the knowledge of channel properties in both horizontal and vertical planes can facilitate the design of coordinated 3D beamforming. With TDD mode, it is much easier to design the coordination between BSs, thanks to channel reciprocity property, than FDD. Besides, BSs have fixed locations in the plane, thus the interference between them can be determined, based on some static measurements over a long period of time, by using relevant metrics such as the mutual coupling loss or the level of RSRP (Reference Signal Receive Power). For instance, each BS can obtain the channel state information reference signal in the neighboring cells by exchanging information via the backhaul signaling or over the air interface signaling. Once an UL user vulnerable to be interfered by the DL signal of a BS is detected, the DL transmitting BSs can activate the 3D beamforming during the sub-frame of interest to serve a DL user. Furthermore, it can be found in the available scientific literature several works that propose beamforming coordination and interference management schemes in cellular networks and for D-TDD based networks in particular; see for instance [25, 26, 82, 83]. Since beamforming coordination is not the subject matter of this work, we assume that during the sub-frames where cells are allowed to use dynamic resources' allocation, transmitting cells in DL adopt 3D beamforming to serve DL users.

Moreover, we model the shadowing effect between a transmitting node t and a receiving one r by a log-normal RV $\chi(t,r) = 10^{\frac{Y(t,r)}{10}}$, with $Y(t,r)$ is a normal RV with mean $\mathbb{E}(Y(t,r)) = 0$ and variance σ^2. This sequence of RVs are assumed to be independent and identically distributed for all (t,r).

5.1.1 Interference characterization

Once again, we define the Interference to Signal Ratio *ISR* as the received power from an interfering source (interfering mobile or BS) divided by the useful signal power received by z_0 (or s_0) from the serving cell (or UL transmitting mobile z_0). In DL transmission, the mobile z_0 receives interference from other BSs operating in DL and from mobiles transmitting in UL. Hence, we define the DL *ISR* denoted by $\mathscr{I}_{DL}(z_0)$ by

$$\mathscr{I}_{DL}(z_0) = D_{\downarrow}(z_0) + D_{\uparrow}(z_0) \tag{5.1}$$

where $D_{\downarrow}(z_0)$ refers to DL to DL *ISR* and $D_{\uparrow}(z_0)$ refers to UL to DL *ISR*. $D_{\downarrow}(z_0)$ and $D_{\uparrow}(z_0)$ can be defined for a tri-sectorized hexagonal network considering 3D beamforming radiation patterns in DL, respectively as follows

$$\mathbb{E}[D_{\downarrow}(z_0)] = -1 + \sum_{s\in\Lambda} \beta_d(s) G_s(z_0) |s - z_0|^{-2b} r^{2b} \tilde{\chi}(s, z_0) \tag{5.2}$$

$$\mathbb{E}[D_{\uparrow}(z_0)] = \sum_{s\in\Lambda^*} \beta_u(s) \sum_{c=1}^{3} \frac{r^{2b} P^* r_{s,c}^{2bk} \tilde{\chi}(z_{s,c}, z_0)}{P |z_{s,c} - z_0|^{2b}}, \tag{5.3}$$

where $\tilde{\chi}(t, z_0) = 10^{\frac{\tilde{Y}(t,z_0)}{10}}$ is a log-normal RV representing the ratio of $\chi(t, z_0)$ ($t = s$ or $t = z_{s,c}$) and $\chi(s_0, z_0)$ (The ratio of two log-normal RVs is a log-normal RV). $\tilde{Y}(t, z_0)$ is a Normal RV with mean 0 and variance $\tilde{\sigma}^2$.

$D_{\downarrow}(z_0)$ is an infinite sum of independent positive RVs not identically distributed. As we have shown previously, this RV is an almost sure convergent series and its mathematical expectation, conditionally on z_0, can be obtain by averaging over all the RVs inside the sum. It is written as follows

$$\mathbb{E}[D_{\downarrow}(z_0)] = -1 + \alpha_d e^{\frac{\ln^2(10)\tilde{\sigma}^2}{200}} \sum_{s\in\Lambda} \mathbb{E}[G_s(z_0)] |s - z_0|^{-2b} r^{2b}. \tag{5.4}$$

Now to calculate the average UL to DL *ISR*, we average first over all the cells operating in UL. Then we average over the shadowing log-normal RVs and over the mobiles $z_{s,c}$ random locations conditionally on z_0. It follows that

$$\mathbb{E}[D_{\uparrow}(z_0)] = \frac{9P^* \alpha_u e^{\frac{\ln^2(10)\tilde{\sigma}^2}{200}}}{4\pi\delta P} \sum_{c=1}^{3} \sum_{s\in\Lambda^*} \int_{\vartheta_c - \frac{\pi}{3}}^{\vartheta_c + \frac{\pi}{3}} \Bigg[\int_0^{\frac{2\delta}{3}\cos^{-2\omega_h}(\phi - \vartheta_c)} \frac{r^{2b} x^{2bk}}{\cos^{-2\omega_h}(\phi - \vartheta_c) |s - re^{i\theta} - xe^{i\phi}|^{2b}} dx \Bigg] d\phi. \tag{5.5}$$

One can simplify equation (5.5) by proceeding analogously to the simplification of (3.7) in chapter 3.

During the UL cycle of the serving cell s_0, the UL transmitted signal by the mobile z_0 is interfered by the DL signal of cells transmitting in DL and also by the signal of mobiles transmitting in UL. We define the UL *ISR* as

$$\mathscr{I}_{UL}(z_0) = U_{\uparrow}(z_0) + U_{\downarrow}(z_0) \tag{5.6}$$

where $U_{\downarrow}(z_0)$ is DL to UL *ISR* and $U_{\uparrow}(z_0)$ refers to UL to UL *ISR*.

The interfering signal coming from BSs in DL, which have fixed positions, is received at the location of the serving cell s_0. Hence, by averaging conditionally on z_0, over all DL transmitting cells, shadowing and beamforming radiation pattern RVs, the expectation of $U_{\downarrow}(z_0)$ is expressed by

$$\mathbb{E}[U_{\downarrow}(z_0)] = \frac{P\alpha_d}{P^*} e^{\frac{\ln^2(10)\tilde{\sigma}^2}{200}} \sum_{s\in\Lambda^*} |s-s_0|^{-2b} r^{2b(1-k)} \mathbb{E}[G_s(s_0)], \tag{5.7}$$

with $G_s(s_0)$ is the 3D beamforming antenna radiation patterns coming from the DL sites and received at the location of s_0.

$\sum_{s\in\Lambda^*} |s-s_0|^{-2b} r^{2b(1-k)}$ is a convergent series on $x = \frac{r}{\delta}$ and its expression is recalled from equation (3.14):

$$\sum_{s\in\Lambda^*} |s-s_0|^{-2b} r^{2b(1-k)} = \frac{\omega(b)}{\delta^{2bk}} x^{2b(1-k)}. \tag{5.8}$$

Hence by using the same reasoning as we did for the DL to DL *ISR*, we can show that $U_{\downarrow}(z_0)$ converges almost surely.

UL to UL interference is generated by mobiles $z_{s,c} = s + r_{s,c}e^{i\theta_{s,c}}$ in neighboring cells transmitting in UL and also from the UL transmission in the two co-sectors of s_0. Recalling the fact that $r_{s,c}$ is a RV uniformly distributed in $[0, \frac{2\delta}{3}U(\theta_{s,c} - \vartheta_c)]$, $\theta_{s,c}$ is uniform RV in $[\vartheta_c - \frac{\pi}{3}, \vartheta_c + \frac{\pi}{3}]$ and considering the fractional power control model applied to the UL

transmission, it follows that

$$\mathbb{E}[U_{\uparrow}(z_0)] = -1 + \frac{9}{4\pi\delta} e^{\frac{\ln^2(10)\tilde{\sigma}^2}{200}} \sum_{s\in\Lambda} \int_{\vartheta_c-\frac{\pi}{3}}^{\vartheta_c+\frac{\pi}{3}} \left[\int_0^{\frac{2\delta}{3}\cos^{-2\omega_h}(\phi-\vartheta_c)} \frac{|s+xe^{i\phi}|^{-2b} x^{2bk}}{\cos^{-2\omega_h}(\phi-\vartheta_c) r^{2b(k-1)}} dx \right] d\phi. \tag{5.9}$$

Based on the expressions of the DL and UL *ISR* derived previously, we define the DL and UL *SINR*, denoted respectively by Π_{DL} and Π_{UL}, as follows

$$\Pi_{DL}(z_0) = \frac{1}{\eta\ \mathscr{I}_{DL}(z_0) + y_0 x^{2b}} \tag{5.10}$$

$$\Pi_{UL}(z_0) = \frac{1}{\eta\ \mathscr{I}_{UL}(z_0) + y_0^{'} x^{2b(1-k)}} \tag{5.11}$$

where $y_0 = \frac{P_N a \delta^{2b}}{P\chi(s_0,z_0)}$, $y_0^{'} = \frac{P_N a \delta^{2b(1-k)}}{P^{*}\chi(z_0,s_0)}$, P_N is the thermal noise power and η is the average load over the interfering cells.

Finally, the coverage probability is defined by

$$\Theta_s(\gamma) = P(SINR > \gamma), \tag{5.12}$$

with $s = DL$ for DL coverage probability and $s = UL$ for the UL one.

5.1.2 Simulation results

Once again, we simulate in MATLAB the 3D beamforming model considering static and dynamic TDD scenarios. Table. 5.1 shows the different parameters used to perform this simulations.

Macro-cells power P	43dBm
Target power cell specific P^*	20dBm
Noise power P_N	-93dBm
Number of rings (Macro-cells)	5 (90 interfering sites)
Inter-site distance δ	0.75km
Antennas gain	17.5dBi
BSs height l_b	$0.02km$
Antenna downtilt	8°
Shadowing standard deviation	6dB
Propagation factor a	Outdoor: 130dB
System bandwidth	Macro-cells:20Mhz
Path loss exponent $2b$	3.5

Table 5.1 – 3D beamforming based D-TDD network simulation parameters.

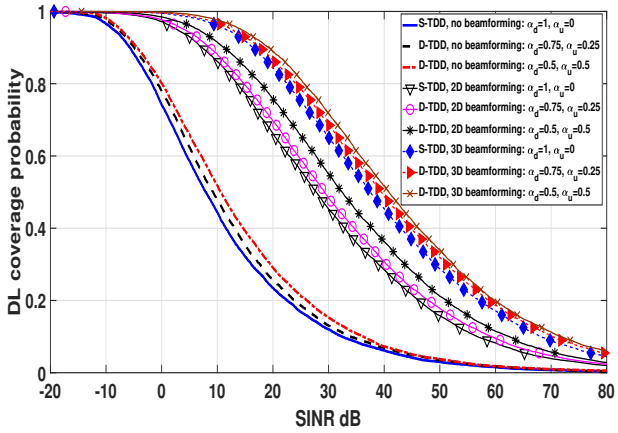

Figure 5.3 – DL Coverage probability ($2b = 3.5$, $k = 0.4$).

We plot in Fig. 5.3 the coverage probability curves in DL obtained by using Monte Carlo simulations for 20000 mobile locations z_0. We compare the static TDD and Dynamic TDD for three scenarios: without beamforming mechanisms, 2D beamforming and 3D beamforming. Starting from a static TDD configuration where all the sites s are transmitting in DL, Fig. 5.3 shows that the coverage probability increases when D-TDD is activated, with $\alpha_d = 75\%$ and $\alpha_d = 50\%$, for the three scenarios. This behavior is expected since the macro-cells BSs transmit with high power level and generate strong in-

terference compared to interfering mobiles z transmitting in UL. In the second scenario, we contemplate 2D beamforming where only the horizontal radiation pattern with a half power beam-width $\theta_{h3dB} = 14°$ and a fixed antenna downtilt are considered. As expected, there is an important enhancement in system performance, translated by an increase in the coverage probability, for both S-TDD and D-TDD, compared to the first case. This enhancement becomes more obvious in the third scenario when 3D beamforming is implemented with $\theta_{h3dB} = 14°$ and a vertical half power beam-width $\theta_{v3dB} = 8°$. Therefore, D-TDD is more convenient with DL transmission direction and adding 3D beamforming results in a gain in performance.

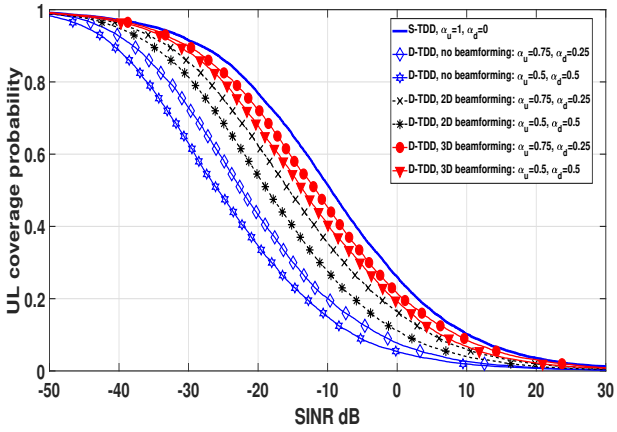

Figure 5.4 – UL coverage probability ($2b = 3.5$, $k = 0.4$).

To analyze the system behavior during the UL transmission direction, we plot in Fig. 5.4 the UL coverage probability considering the same scenarios as in DL. It is worth mentioning that for S-TDD UL transmission, there is no beamforming mechanisms since all BSs are in UL and mobiles are equipped with omni-directional antennas. Hence, we consider only one S-TDD scenario and we compare it to the three scenarios raised in the previous paragraph. The main obvious observation from Fig. 5.4 is that when 3D and 2D beamforming are not implemented, the coverage probability undergoes a huge degradation when the system switch from the static configuration to the dynamic one with $\alpha_u = 75\%$ and $\alpha_u = 50\%$. This degradation is mainly coming from the strong interfering signals of DL BSs and makes the system very limited if no interference mitigation schemes are setting up. Moreover, with 2D beamforming, one can observes from Fig. 5.4 that there is an enhancement in the UL coverage probability when D-TDD is activated compared to the static configuration. This enhancement becomes more significant when 3D beamforming

is considered for DL BSs. In this case, the UL coverage probability is getting closer to the one of S-TDD.

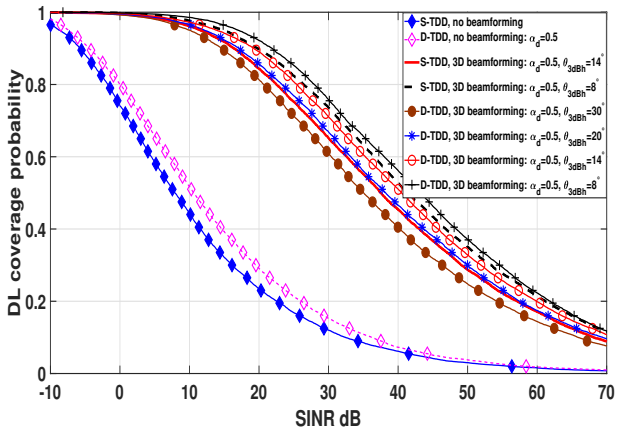

Figure 5.5 – DL coverage probability: D-TDD vs S-TDD with 3D beamforming considering different half power beam-widths ($2b = 3.5$, $k = 0.4$).

In Fig. 5.5 and Fig. 5.6 we plot respectively the DL and UL coverage probability curves when D-TDD is considered, with 3D beamforming having different horizontal half power beam-widths ($\theta_{h3dB} = 30°, 20°, 14°, 8°$) and a vertical half power beam-width $\theta_{v3dB} = 8°$. When the serving site s_0 is operating in DL, it can be observed that the DL coverage probability increases as the beam width decreases in both D-TDD and S-TDD. Also, one can notice that the gain obtained with D-TDD is quite important than S-TDD without beamforming. Moreover, the coverage probability of a S-TDD network with 3D beamforming having small θ_{h3dB} is getting closer to the one of a D-TDD system. Actually, the beam-width is related to the number of transmit antennas used by BSs. When this number increases, the signal is focused on a specific zone of the cell. Hence, interference coming from neighboring sites are reduced significantly. This leads to an enhancement of *SINR* and thus an enhancement of the coverage probability. Similar results are observed for the UL scenario as shown in Fig. 5.6. With 3D beamforming based D-TDD, as the horizontal half power beam-width is getting smaller, the UL coverage probability is enhanced and getting closer to the one of S-TDD. This means that 3D beaforming reduces significantly the DL to UL interference and can make D-TDD feasible for macro-cells' network.

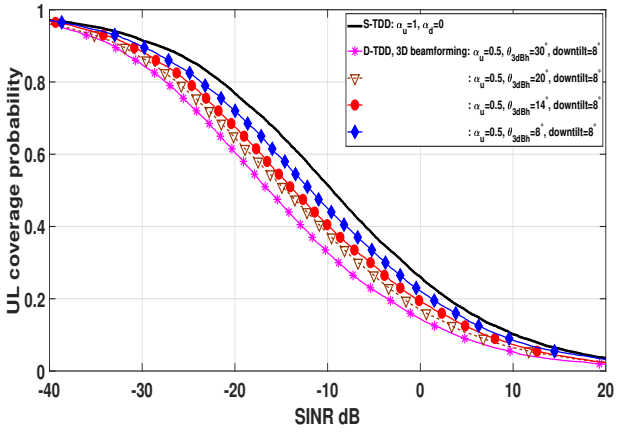

Figure 5.6 – UL coverage probability: D-TDD vs S-TDD with 3D beamforming considering different half power beam-widths ($2b = 3.5$, $k = 0.4$).

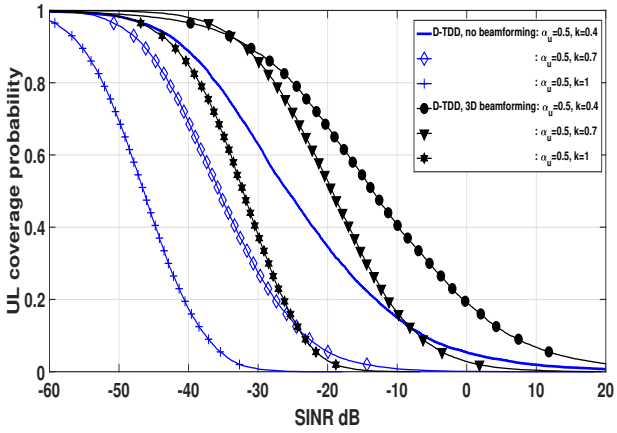

Figure 5.7 – UL coverage probability: fractional power control effect: $2b = 3.5$, $k = 0.4$.

Finally, to analyze the effect of the fractional power control considered for the UL transmission direction, we plot in Fig. 5.7 the UL coverage probability of a D-TDD system, with and without 3D beamforming, considering different FPC factor values ($k = 0.4$, $k = 0.7$ and $k = 1$). One can notice that the coverage probability is decreasing when the FPC factor is increasing for both 3D beamforming based D-TDD network and D-TDD without 3D beamforming. Also, performance of 3D beamforming with small FPC factors are better than the case where no beamforming scheme is applied. The interpretation of

those results follows likely the same interpretation of the results of Fig. 3.9. When the FPC factor $0 < k < 1$, the scheme indemnifies partially the path loss. The higher is the path loss the lower is the received signal which means that UL to UL interference are controlled. With 3D beamforming, minimizing also the DL to UL interference results in better performance.

5.2 D-TDD interference mitigation in small-cell deployment

Additional types of interferences that occur in D-TDD systems are the prime concerns to minimize. As mentioned in chapter 1, 3GPP advices new approach for interference mitigation in dynamic environment such as cell clustering. Furthermore, small-cells are a good candidates for D-TDD because they can be considered well isolated from each others since they transmit with a low power level and the base stations are not highly elevated. In this section we analyze D-TDD performance considering a cell clustering scheme applied to a small-cell deployment.

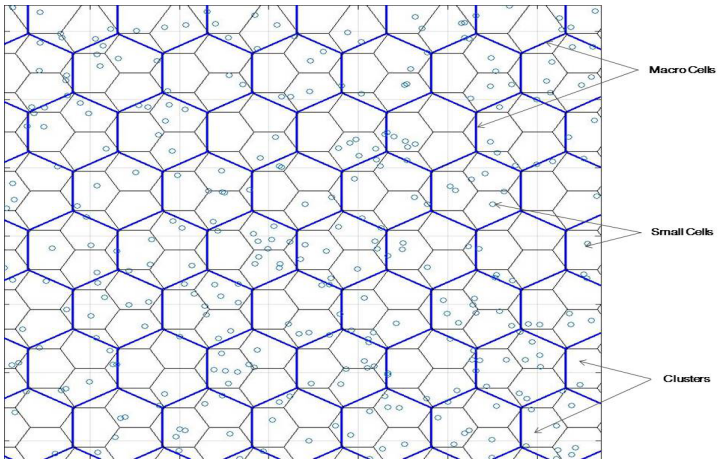

Figure 5.8 – Cell clustering model

The main idea of cell clustering is to gather small-cells in different clusters based on specific metrics e.g., Mutual Coupling Loss (MCL) threshold between cells. Small-cells in the same cluster adopt the same UL-DL configurations and the transmission inside a cluster can be coordinated by a central unit, which decides the more convenient frame

configuration according to traffic conditions. Moreover, cells belonging to different clusters can choose the configuration independently from each others. The problem of cross link interference still exists even with cell clustering scheme. Actually, the dense deployment of small cells certainly induces severe interference between small cells belonging to neighboring clusters when they transmit in opposite directions. Hence, users served by small-cells located in cluster edges, especially during the UL cycle, can be interfered by other small-cell DL signals .

To evaluate this clustering scheme, we consider the same network architecture, propagation and power control models used previously. We assume that clusters form a new hexagonal lattice denoted by C as shown in Fig. 5.8, with inter-cluster distance $\tilde{\delta}$ such that $\tilde{\delta} = \delta/\sqrt{3}$. Every cluster center c is uniquely identified by the complex variable $c = \tilde{\delta}(u + ve^{i\frac{\pi}{3}})$ with $(u,v) \in \mathbb{Z}^2$ and c_0 is the new origin of the plane $\mathbb{R}^2$. Cluster radius is denoted by $\tilde{R}$. Each cluster contains N small cells uniformly and independently distributed with the same intensity λ. Small cell location $\tilde{s}$ is determined by $\tilde{s} = c + \tilde{\rho}e^{i\tilde{\phi}}$ where $\tilde{\rho}$ is the distance between $\tilde{s}$ and the cluster center. The small-cell of interest is denoted by $\tilde{s_0}$ such that $\tilde{s_0} = \tilde{\rho_0}e^{i\tilde{\phi_0}}$. Small-cell radius is designated by $\tilde{R}_s$. A mobile location $\tilde{z_0}$, served by $\tilde{s_0}$ in UL transmission, is identified by the complex variable $\tilde{z_0} = \tilde{s_0} + \tilde{r}e^{i\tilde{\theta}}$, where $\tilde{r}$ is the distance between $\tilde{z_0}$ and $\tilde{s_0}$. We assume also that small-cells transmit with the same power level denoted by $\tilde{P}$. The small-cell target power in UL transmission will be denoted $\tilde{P}^*$. In the remainder of this section, we assume that macro and small-cells operate in different frequency bands, hence interference from macro-cell layers will not be considered. Also in the remainder, UL to UL interference is neglected and the DL cycle is not analyzed, since cell clustering schemes intend to minimize DL to UL interference in D-TDD system.

5.2.1 DL to UL *ISR* derivation

Let $ISR(\tilde{s}_{\downarrow}, \tilde{s_0}_{\uparrow})$ be the individual relative interference received from small cell $\tilde{s}$ and impacting useful signal at $\tilde{s_0}$ when it is in UL communication with mobile location $\tilde{z_0}$. Small cell $\tilde{s}$ is of course assumed to belong to another cluster c of cells operating in DL transmission. The expression of $ISR(\tilde{s}_{\downarrow}, \tilde{s_0}_{\uparrow})$ can be formulated by

$$\begin{aligned} ISR(\tilde{s}_{\downarrow}, \tilde{s_0}_{\uparrow}) &= \frac{\tilde{P}\, L(\tilde{z_0}, \tilde{s_0})}{P(\tilde{z_0}, \tilde{s_0})\, L(\tilde{s}, \tilde{s_0})} \\ &= \frac{\tilde{P}\, |\tilde{s} - \tilde{s_0}|^{-2b}}{\tilde{P}^*\ |\tilde{z_0} - \tilde{s_0}|^{2bk}\ |\tilde{z_0} - \tilde{s_0}|^{-2b}} \end{aligned}$$

Recalling the fact that small cells are uniformly distributed in clusters with the intensity λ (For numerical results, we will take $\lambda = \frac{3}{\pi\tilde{R}^2}$, i.e., three small cells per cluster), DL to

UL *ISR* can be obtained by summing over all small cells belonging to all clusters except the one containing $\tilde{s_0}$. It follows that

$$U_{\downarrow}(\tilde{z_0}) = \lambda \sum_{c \in C^*} \int_c ISR(\tilde{s}_{\downarrow}, \tilde{s_{0\uparrow}}) d\tilde{s} \tag{5.13}$$

To evaluate equation (5.13), we can proceed analogously to the derivation of $D_{\uparrow}$ in chapter 3. Take $\tilde{x} = \tilde{r}/\tilde{\delta}$, then for $\tilde{x} < 1$ and $b > 1$, the DL to UL *ISR* $U_{\downarrow}(z_0)$ is explicitly written as

$$U_{\downarrow}(\tilde{z_0}) = \tilde{A}_2(b)\, \tilde{x}^{2b(1-k)} \tag{5.14}$$

where

$$\tilde{A}_2(b) = \frac{6\pi\tilde{R}^2\tilde{P}\lambda}{\tilde{P}^*\,\Gamma(b)^2\tilde{\delta}^{2bk}} \sum_{h=0}^{+\infty} \sum_{n=0}^{\lfloor \frac{h}{2} \rfloor} \sum_{i=0}^{h-2n} \frac{\Gamma(b+h)^2\omega(b+h)}{\Gamma(n+1)^2\Gamma(h+1)} \times \frac{(\frac{\tilde{R}}{\tilde{\rho_0}})^{2n+2i}\,(\frac{\tilde{\rho_0}}{\tilde{\delta}})^{2h}}{\Gamma(i+1)\Gamma(h-2n-i+1)(n+i+1)}$$

5.2.2 Coverage probability

Coverage probability is identified by the percentage of locations having their SINR higher that a given threshold γ. Let $\Pi(\tilde{x})$ be the UL *SINR* experienced by small cell $\tilde{s_0}$ when it communicates with mobile location $\tilde{z_0}$, such that $|\tilde{z_0}| = \tilde{x}\tilde{\delta}$.

$$\Pi(\tilde{x}) = \frac{1}{U_{\downarrow}(\tilde{x}) + \tilde{y}_0 \tilde{x}^{2b(1-k)}} \tag{5.15}$$

where $\tilde{y}_0 = \frac{P_N \tilde{\delta}^{2b(1-k)}}{P^*}$, with P_N is the noise power.

Assuming that location $\tilde{z_0}$ is uniformly distributed in small cell $\tilde{s}_0$, the UL coverage probability is evaluated as in [8] by:

$$\begin{aligned} \Phi(\gamma) =& \mathbb{P}(\Pi(\tilde{x}) > \gamma) \\ =& \min\left[\left(\frac{\tilde{\delta}}{\tilde{R}_s} g(\frac{1}{\gamma})\right)^2 ; 1\right] \end{aligned} \tag{5.16}$$

where $g(y)$ is the inverse function of $y(\tilde{x}) = 1/\Pi(\tilde{x})$. It is given by

$$g(y) = (\frac{y}{\tilde{A}_2(b) + \tilde{y}_0})^{\frac{1}{2b(1-k)}}. \tag{5.17}$$

The strong DL to UL interference, which is the dominant interference in a D-TDD system, comes from the large coupling between small-cells. It can be observed from Fig. 5.9 that the clustering scheme minimizes its impact, mainly for favored propagation condition, i.e., low value of parameter *b*.

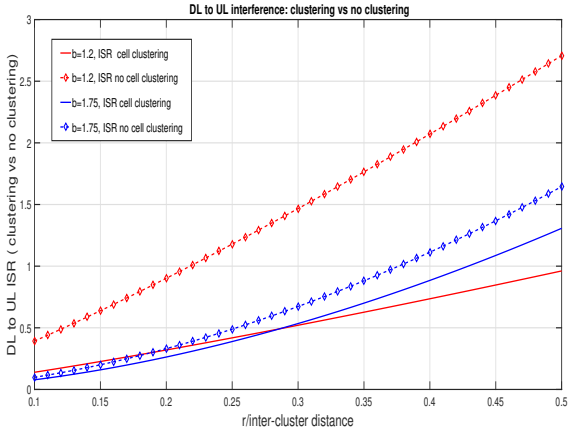

Figure 5.9 – D-TDD DL to UL ISR with cell clustering scheme

5.3 Conclusion

In this chapter, we have investigated the applicability of 3D beamforming scheme to a D-TDD based macro-cell deployments. We have shown that the gain in performance, during the DL transmission cycle of a typical cell, is important when 3D beamforming is deployed. For the UL transmission cycle, the impact of DL to UL interference is significantly reduced, when 3D beamforming is applied to DL transmitting cells, and performance gets closer to S-TDD based systems. 3D beamforming appears to be an efficient solution to reduce the strong interference coming from BSs' signals. Nevertheless, applying this feature requires beam and frequency resources management mechanisms between interfering BSs. Furthermore, we have introduced a tractable cell clustering scheme, that can be applied to small-cell deployments, by exploiting the mathematical framework of hexagonal network tractability. It has been shown that this scheme reduces the impact of DL to UL interference and thus enhances UL performance.

Chapter 6

OFDM based 5G-NR dimensioning approach

6.1 Introduction

5G NR interface design takes in consideration the wide array of emerging use cases and also future requirements. Therefore, The 3GPP has chosen an optimized OFDM based waveform for 5G NR known as scalable OFDM and having different subcarriers' spacing ($\Delta f = 2^{\nu}15$ kHz, where $\nu = 0$ to 4). OFDM radio dimensioning is an important task. It consists in assessing the network resources required to carry a predicted data traffic with a satisfactory QoS. This later is often summarized in some metrics such as the average user throughput or the target congestion probability.

In this chapter, we tackle the problem of OFDM dimensioning. In contrast with some recent works, where the dimensioning process is performed to satisfy a minimum user throughput in the cell, we use the cell congestion as the target QoS, instead. Besides, dimensioning is performed assuming mobile users distributed in roads or located in buildings. The first kind of users are modeled by Cox point process driven by PLP whereas the second kind is described by a spatial PPP. Such mobile users are granted some radio resources, called Physical Resource Blocks (PRB), at each Time Transmit Interval (TTI) and according to a predefined scheduling algorithm. The choice of the scheduling algorithm is mainly related to the fairness level made between users, i.e., the way that resources are allocated to users according to their channel qualities and their priorities, defined by the operator. Moreover, we show that the total requested PRBs follows a compound Poisson distribution and we attempt to derive the explicit expression of the congestion probability by introducing a mathematical tool from combinatorial analysis called the exponential

Bell polynomials. Finally we show how to dimension radio resources, for a given target congestion probability, by solving an implicit relation between the necessary resources and the forecast data traffic expressed in terms of cell throughput. Different numerical results are presented to justify this dimensioning approach.

6.2 System model and notations

6.2.1 Indoor users model

A PPP in $\mathbb{R}^2$ with intensity ζ is a point process that satisfies: *i*) the number of points inside every bounded closed set $B \in \mathbb{R}^2$ follows a Poisson distribution with mean $\zeta|B|$, where $|B|$ is the Lebesgue measure on $\mathbb{R}^2$; *ii*) the number of points inside any disjoint sets of $\mathbb{R}^2$ are independent [11]. Actually, spatial PPP has been widely used to model BSs and users locations in cellular network. In this chapter, indoor users are considered to be distributed in buildings according to a spatial PPP φ of intensity κ, which means that their locations are uniformly distributed in the studied cell coverage area and their number follows a Poisson distribution.

6.2.2 Outdoor users model

As we mentioned previously, outdoor users are considered to be distributed along a random system of roads. To model the random tessellation of roads, we consider the so-called PLP which is mathematically derived from the spatial PPP. Instead of points, the PLP is a random process of lines distributed in the plane $\mathbb{R}^2$. Each line in $\mathbb{R}^2$ is parametrized in terms of polar coordinates (r,θ) obtained from the orthogonal projection of the origin on that line, with $r \in \mathbb{R}^+$ and $\theta \in (-\pi,\pi]$. Now we can consider an application T that maps each line to a unique couple (r,θ), generated by a PPP in the half-cylinder $\mathbb{R}^+ \times (-\pi,\pi]$; Fig. 6.1. The distribution of lines in $\mathbb{R}^2$ is the same as points' distribution in this half-cylinder; see [15] and [65] for more details.

In the sequel, we assume that roads are modeled by a PLP ϕ with roads' intensity denoted by λ. The number of roads that lie inside a disk s of radius R is a Poisson random variable, denoted by Y. It corresponds to the number of points of the equivalent spatial PPP in the half-cylinder $[0,R] \times (-\pi,\pi]$ having an area of $2\pi R$. Hence, the expected number of roads that lie inside s is $\mathbb{E}(Y) = 2\pi\lambda R$. Then, conditionally on ϕ (i.e., conditionally on roads), outdoor users are assumed to be distributed on each road according to independent linear PPPs with the same intensity δ. This model is known as Cox point process. The mean number of users on a given road j is δL_j, with L_j is the length of road j. Besides, the

number of roads that lie between two disks of radius R_1 and R_2 respectively, with $R_1 \leqslant R_2$, is $2\pi\lambda(R_2 - R1)$. Also, the number of distributed users in a road, parametrized by (r,θ) and delimited by the two disks, is $2\delta(\sqrt{R_2^2 - r^2} - \sqrt{R_1^2 - r^2})$. Additionally, the average number of outdoor users in the disk of radius R can be calculated using the equivalent homogeneous spatial PPP with intensity $\lambda\delta$ in the disk area. For illustration, Fig. 6.1 presents the line parametrization described above and Fig. 6.2 shows a realization of a Cox Point Process driven by PLP.

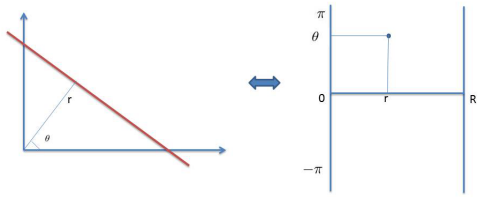

Figure 6.1 – Line parametrization.

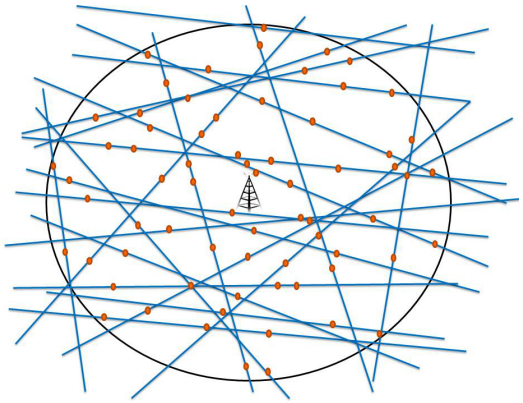

Figure 6.2 – A realization of Cox Point Process driven by PLP.

Additionally, we assume that outdoor and indoor users processes are independent and they form respectively two processes with intensities $\lambda\delta$ and κ. Therefore, the average

number of users (outdoor and indoor), denoted by u, inside s coverage area can be calculated by

$$u = (\lambda\delta + \kappa)\pi R^2. \tag{6.1}$$

Table 6.1 summarizes the basic notations used in this chapter.

Symbols	Definition
φ	spatial PPP of indoor users with intensity κ
ϕ	PLP of roads with intensity λ
δ	The linear PPP intensity on each road (outdoor)
r_j	The short distance between a road j and the origin
Y	number of roads that lie inside s
$\delta\lambda$	Spatial PPP intensity on half-cylinder $[0,R]\times(-\pi,\pi]$
u	Average number of users in s

Table 6.1 – Chapter 6 notations.

6.2.3 Network model

We consider a circular cell s of radius R with a BS, denoted also s and positioned at its center, transmitting with a power level P. The received power by a user located at distance x from s is Px^{-2b}/a, where $2b$ is the path loss exponent and a is the propagation constant. We assume that BS s allocates PRBs to its users at every TTI (e.g., 1 ms). Each PRB has a bandwidth denoted by W (e.g., W =180kHz for scalable OFDM with subcarriers spacing of 15kHz).

Active users in the cell compete to have access to the available dimensioned PRBs. Their number is denoted by M. The BS allocates a given number n of PRBs to a given user depending on: *i*) the class of services he belongs to (i.e.,the transmission rate he requires) and *ii*) his position in the cell (i.e., the perceived radio conditions). Without loss of generality, we assume that there is just one class of services with a required transmission rate denoted by C^*.

A user located at distance x from s decodes the signal only if the metric "Signal to Interference plus Noise Ratio (SINR)" $\Theta(x) = \frac{Px^{-2b}/a}{I+\sigma^2}$ is above a threshold $\Theta^* = \Theta(R)$, where I is the received co-channel interference and σ^2 is the thermal noise power. For performance analysis purpose, SINR $\Theta(x)$ is often mapped to the user throughput by a

link level curve. For simplicity of calculation, we use hereafter the upper bound of the well known Shannon's formula for MIMO system $Tx \times Rx$, with Tx and Rx are respectively the number of transmit and receive antennas. Hence, the throughput of a user located at distance x from s is

$$C(x) = \vartheta W \log_2 (1 + \Theta(x)), \tag{6.2}$$

with $\vartheta = min(Tx, Rx)$.

Then, the number of PRBs required by a user located at distance x from s is

$$n(x) = \lceil \frac{C^*}{C(x)} \rceil \leq N, \tag{6.3}$$

where $N = min(N_{max}, \lceil C^*/(\vartheta W log_2(1+\Theta^*)) \rceil)$, N_{max} is the maximum number of PRBs that a BS can allocate to a user (fixed by the operator) and $\lceil . \rceil$ stands for the Ceiling function.

It is obvious from (6.3) that users are fairly scheduled because a user with bad radio conditions (with low value of $C(x)$) gets higher number of PRBs to achieve its transmission rate C^*.

Let d_n be the distance from s that verifies, for all $x \in (d_{n-1}, d_n]$, $n(x) = n$ with

$$n = \frac{C^*}{C(d_n)} \tag{6.4}$$

is an integer and

$$d_n = \begin{cases} 0 \text{ if } n = 0, \\ \left[\frac{a(I+\sigma^2)}{P} (2^{\frac{C^*}{n\vartheta W}} - 1) \right]^{\frac{-1}{2b}} \text{ otherwise,} \end{cases}$$

From (6.4), the cell s area can be divided into rings with radius d_n such that for $1 \leqslant n \leqslant N$, $0 \leqslant d_{n-1} < d_n \leqslant R$. The area between the ring of radius d_n and the ring of radius d_{n-1} characterizes the region of the cell where users require n PRBs to achieve the transmission rate C^*. Given that d_n depends on the propagation parameter, it is worth to mention that there is a difference between d_n values for outdoor and indoor environments. Thus to avoid confusion, we denote in the remainder, for indoor environment, the ring radius by $\tilde{d}_n$ and

the propagation parameter by $\tilde{a}$. Finally, we define the cell throughput by the sum over all transmission rates of users:

$$\tau = uC^*, \tag{6.5}$$

with u is recalled the average number of users inside s and expressed by (6.1).

On the other hand, inter-cell interference is one of the main factors that compromise cellular network performance. The analysis of this factor level go through the SINR evaluation that depends on the geometry of the network as well as the distribution of users' locations. The analytical random models that can be found in literature, such as Homogeneous PPP, assume that BSs are randomly distributed according to a spatial point process. Thus it becomes hard to estimate the interference level in each user location and only its distribution is determined; see for instance [9].

Besides, interference level estimation is of utmost importance in link adaptation procedure. In practical systems, the SINR is mapped to an indicator called Channel Quality Indicator (CQI) (e.g., 15 CQI indexes for LTE). This indicator is used by the BSs to determine the Modulation and Coding Schemes (MCS) and hence the transmission rate. Actually, the level of interference varies from one location to another in the same cell. Practically cell edge users experience high interference level compared to users that are close to the BS in the cell middle or cell center. for this purpose, in the remainder of this analysis, we consider three range of CQI indexes with a constant interference level for each range. The first range (i.e., low CQI indexes) stands for bad channel quality with high interference level, the second range (i.e., medium CQI indexes) stands for low interference level and the last range (i.e., high CQI indexes) refers to good channel quality with a negligible interference level.

Furthermore, when interference level is non negligible, we use the notion of interference margin (IM) or Noise Rise in link budget. IM is defined as the increase in the thermal noise level caused by other-cell interference. IM can be expressed in the linear scale as

$$IM = \frac{I + \sigma^2}{\sigma^2} \tag{6.6}$$

In the remainder of this study, we evaluate interference level by using three margins for each region of the studied cell. We consider three regions in s coverage area: the cell center that stands for the disk having a radius of $\frac{R}{3}$, the cell middle that represents the region between the disk B$(0,\frac{R}{3})$ and the disk B$(0,\frac{2R}{3})$. Finally, the cell edge refers to the region of the cell where the distance to s is above $\frac{2R}{3}$.

6.3 Presentation of the dimensioning approach

Dimensioning process consists in evaluating the required radio resources that allow to carry a forecast data traffic given a target QoS. The QoS can be measured by the congestion probability metric or even by a target average user throughput. The present approach assesses the congestion probability as a function of many key parameters, in particular the number of PRBs M and the cell throughput τ. To characterize this congestion probability, we need to evaluate the total requested PRBs by all users. In the remainder, we will state some analytical results regarding the explicit expression of the congestion probability under the system model presented in the previous sections.

6.3.1 Qualification of the total number of requested PRBs

Outdoor users are distributed on each road L_j according to a linear PPP of intensity δ. Now, if we consider a disk B(0,d_n) of radius d_n, the number of users in the portion of L_j that lies inside B(0,d_n) is a Poisson random variable (this comes from the definition of the linear PPP) with mean $2\delta\sqrt{d_n^2 - r_j^2}$ (Pythagoras' theorem). Hence, conditionally on ϕ, the mean number of users $\alpha_n(Y)$ inside B(0,d_n) is the sum over all roads L_j that intersect with B(0,d_n) and it can be expressed by

$$\alpha_n(Y) = 2\delta \sum_{j=1}^{Y} \mathbb{1}_{(d_n > r_j)} \sqrt{d_n^2 - r_j^2}. \tag{6.7}$$

Moreover, the number of users in the portion of L_j that lies between two rings B(0,d_n) and B(0,d_{n-1}) is also a Poisson random variable with parameter (i.e, the mean number of users) $2\delta(\sqrt{d_n^2 - r_j^2} - \sqrt{d_{n-1}^2 - r_j^2})$. Finally, the mean number of users $\mu_n(Y)$ in all roads that lie between the rings B(0,d_n) and B(0,d_{n-1}) can be expressed by

$$\mu_n(Y) = \alpha_n(Y) - \alpha_{n-1}(Y). \tag{6.8}$$

Similarly, the mean number of indoor users, that are distributed according to a spatial PPP of intensity κ, can be expressed by

$$\tilde{\mu}_n = \kappa\pi(\tilde{d}_n^2 - \tilde{d}_{n-1}^2). \tag{6.9}$$

To qualify the number of requested PRBs by outdoor and indoor users, we consider two independent Poisson random variables denoted respectively by X_n and $\tilde{X}_n$ with parameters $\mu_n(Y)$ and $\tilde{\mu}_n$. X_n and $\tilde{X}_n$ represent the number of users (outdoor and indoor) that

request n PRBs with $1 \leq n \leq N$.

Finally, we can define the total number of requested PRBs in the cell as the sum of demanded PRBs by outdoor and indoor users in each ring. It can be expressed as

$$\Gamma = \mathscr{F} + \tilde{\mathscr{F}}, \tag{6.10}$$

where $\mathscr{F} = \sum_{n=1}^{N} nX_n$ and $\tilde{\mathscr{F}} = \sum_{n=1}^{N} n\tilde{X}_n$ are the total demanded PRBs by outdoor and indoor users respectively.

The random variable Γ is the sum of weighted Poisson random variables and it is called compound Poisson sum. The evaluation of its distribution requires extensive numerical simulation. It is important to mention that the parameter μ_n of X_n depends on Y, which is a Poisson random variable. Hence all calculations should be done conditionally on ϕ. The following proposition gives the explicit expression of the first-order moment (i.e., the mathematical expectation) of Γ.

Proposition 1. *Let Γ be a compound Poisson sum as in (6.10). Let ϕ be a PLP with Y is the Poisson random variable that represents the number of lines that lie inside s coverage area. The first-order moment of Γ is given by*

$$\mathbb{E}(\Gamma) = \frac{4\delta\omega}{3R} \sum_{n=1}^{N} n \frac{d_n^3 - d_{n-1}^3}{R} + \kappa\pi \sum_{n=1}^{N} n(\tilde{d}_n^2 - \tilde{d}_{n-1}^2), \tag{6.11}$$

with $\omega = 2\pi\lambda R$ is the mathematical expectation of Y.

Proof. Let Γ be defined as in (6.10). X_n and $\tilde{X}_n$ are two Poisson random variables with parameters $\mu_n(Y)$ and $\tilde{\mu}_n$. The random variable X_n is dependent on the PLP ϕ i.e., depends on Y. Hence, the mathematical expectation of Γ can be written as

$$\begin{aligned} \mathbb{E}(\Gamma) &= \mathbb{E}_{\phi}(\Gamma|\phi) \\ &= \sum_{n=1}^{N} n\mathbb{E}_{\phi}(\mu_n(Y)) + \sum_{n=1}^{N} n\tilde{\mu}_n \end{aligned} \tag{6.12}$$

To evaluate equation (6.12), we need to calculate first the mathematical expectation of $\mu_n(Y)$. Let $\omega = 2\pi\lambda R$ be the mathematical expectation of the Poisson random variable Y. $\mathbb{E}_{\phi}(\mu_n(Y))$ can be expressed as

$$\mathbb{E}_{\phi}(\mu_n(Y)) = 2\delta \sum_{k=1}^{+\infty} \frac{\omega^k e^{-\omega}}{k!} \sum_{j=1}^{k} \mathbb{E}_{r_j}\left[\mathbb{1}_{(d_n > r_j)}\sqrt{d_n^2 - r_j^2}\right] - \mathbb{E}_{r_j}\left[\mathbb{1}_{(d_{n-1} > r_j)}\sqrt{d_{n-1}^2 - r_j^2}\right]. \tag{6.13}$$

$\{r_j\}$ follow a uniform distribution in the cell coverage area. Thus

$$\mathbb{E}_{r_j}\left[\mathbb{1}_{(d_n > r_j)}\sqrt{d_n^2 - r_j^2}\right] = \frac{2}{R^2}\int_0^{d_n} \sqrt{d_n^2 - r^2} r dr. \tag{6.14}$$

Finally, by using a change of variable $x = r^2$ and the expression of $\tilde{\mu}_n$, we get the result of proposition 1, which completes the proof. □

6.3.2 Congestion probability and dimensioning approach

The congestion probability, denoted by Π, is defined as the probability that the number of total requested PRBs in the cell is greater than the available PRBs fixed by the operator. In other words, it measures the probability of failing to achieve an output number of PRBs M required to guarantee a predefined quality of services:

$$\Pi(M, \tau) = \mathbb{P}(\Gamma \geq M). \tag{6.15}$$

The following proposition gives the explicit expression of the congestion probability for a given process of users.

Proposition 2. *Let Λ be a random variable such that $\Lambda = \sum_{n=1}^{N} nV_n$, with V_n are Poisson random variables of intensity w_n. The probability that Λ exceeds a threshold M is*

$$\mathbb{P}(\Lambda \geq M) = 1 - \frac{1}{\pi} e^{-\sum_{n=1}^{N} w_n} \times \int_0^{\pi} e^{p_n(\theta)} \frac{\sin(\frac{M\theta}{2})}{\sin(\frac{\theta}{2})} \cos(\frac{M-1}{2} - q_n(\theta)) d\theta, \tag{6.16}$$

where

$$p_n(\theta) = \sum_{n=1}^{N} w_n \cos(n\theta) \text{ and } q_n(\theta) = \sum_{n=1}^{N} w_n \sin(n\theta).$$

Proof. To prove proposition 2, we firstly calculate the moment generating function (i.e., Z-Transform) $f(z)$ of the discrete random variable Λ.

$$\begin{aligned} f(z) = \mathbb{E}(z^{\Lambda}) &= \sum_{k=0}^{+\infty} z^k \mathbb{P}(\Lambda = k) \\ &= \prod_{n=1}^{N} \sum_{k=0}^{+\infty} z^{nk} \mathbb{P}(V_n = k). \end{aligned} \tag{6.17}$$

Since V_n is a Poisson random variable with parameter w_n, (6.17) is simplified to

$$f(z) = e^{-\sum_{n=1}^{N} w_n} e^{\sum_{n=1}^{N} z^n w_n}, \tag{6.18}$$

It is obvious that f is analytic on $\mathbb{C}$ and in particular inside the unit circle ω. Cauchy's integral formula gives then the coefficients of the expansion of f in the neighborhood of $z = 0$:

$$\mathbb{P}(\Lambda = k) = \frac{1}{2\pi i} \int_{\omega} \frac{f(z)}{z^{k+1}} dz. \tag{6.19}$$

In (6.19), replacing f by its expression (6.18) and parameterizing z by $e^{i\theta}$ lead to

$$\mathbb{P}(\Lambda = k) = \frac{1}{2\pi} e^{-\sum_{n=1}^{N} w_n} \int_0^{2\pi} \frac{e^{\sum_{n=1}^{N} w_n e^{in\theta}}}{e^{ik\theta}} d\theta. \tag{6.20}$$

Since the congestion probability is defined by the CCDF (Complementary Cumulative Distribution Function) of Λ, then

$$\begin{aligned} \mathbb{P}(\Lambda \geq M) &= 1 - \sum_{k=0}^{M-1} \mathbb{P}(\Lambda = k) \\ &= 1 - \frac{1}{2\pi} e^{-\sum_{n=1}^{N} w_n} \int_0^{2\pi} e^{\sum_{n=1}^{N} w_n e^{in\theta}} \sum_{k=0}^{M-1} e^{-ik\theta} d\theta. \end{aligned} \tag{6.21}$$

The sum inside the right hand integral of (6.21) can be easy calculated to get the explicit expression of (6.16) after some simplifications. □

This formula is valid for every process of user distribution including spatial PPP which represents here the distribution of indoor users. The congestion probability $\mathbb{P}(\tilde{\mathscr{F}} \geq M)$ in this case can be explicitly determined by taking $w_n = \tilde{\mu}_n$ and using $\sum_{n=1}^{N} \tilde{\mu}_n = \kappa \pi R^2$ in (6.16).

Similarly, for outdoor users process which is a Cox point process, conditionally on the PLP ϕ, by taking $w_n = \mu_n(Y)$ and using $\sum_{n=1}^{N} \mu_n(Y) = \alpha_N(Y)$, proposition 2 remains valid. The explicit expression of the congestion probability $\mathbb{P}(\mathscr{F} \geq M)$ in this case is calculated by averaging over the PLP.

Moreover, from the superposition theorem of Poisson process, the congestion probability, considering the combination of outdoor and indoor users, can be calculated by applying proposition 2 to the random variable $\Gamma = \sum_{n=1}^{N} nV_n$, with $V_n = X_n + \tilde{X}_n$ is a Poisson random variable with parameter $w_n = \mu_n(Y) + \tilde{\mu}_n$.

The congestion probability expressions above can be developed even further by introducing a mathematical tool from combinatorial analysis called the exponential Bell polynomials [84] and [85]. This tool is widely used for the evaluation of integrals and alternating sums.

In the following part, we introduce some key results and properties regarding Bell Polynomials.

Key background on the exponential Bell Polynomials

The exponential complete Bell polynomials B_p are defined by

$$B_p(x_1, x_2, ..., x_p) = \sum_{k_1+2k_2+...=p} \frac{p!}{k_1!k_2!....} (\frac{x_1}{1!})^{k_1} (\frac{x_2}{2!})^{k_2} ....$$

and verify the following formula given by the generating function

$$e^{\sum_{j=1}^{+\infty} x_j \frac{t^j}{j!}} = \sum_{p=0}^{+\infty} \frac{t^p}{p!} B_p(x_1, x_2, ...x_p). \tag{6.22}$$

Also, if we consider the following matrix $A_p = (a_{i,j})_{1 \leq i,j \leq p}$ defined by

$$\begin{cases} a_{i,j} = \binom{p-i}{j-i} x_{j-i+1} & \text{if } i \leq j, \\ a_{i,i-1} = -1 & \text{if } i \geq 2 \\ a_{i,j} = 0 & \text{if } i \geq j+2, \end{cases}$$

such that

$$A_p = \begin{bmatrix} x_1 & \binom{p-1}{1}x_2 & \binom{p-1}{2}x_3 & \binom{p-1}{3}x_4 & \dots & x_p \\ -1 & x_1 & \binom{p-2}{1}x_2 & \binom{p-2}{2}x_3 & \dots & x_{p-1} \\ 0 & -1 & x_1 & \binom{p-3}{1}x_2 & \dots & x_{p-2} \\ 0 & 0 & -1 & x_1 & \dots & x_{p-3} \\ \vdots & \vdots & \vdots & \ddots & \ddots & \vdots \\ 0 & 0 & 0 & \dots & -1 & x_1 \end{bmatrix}$$

then the complete exponential Bell Polynomial $B_p(x_1,....x_p)$ can be define as the determinant of this matrix.

$$B_p(x_1,..,x_p) = det(A_p). \tag{6.23}$$

For instance, the first few Bell Polynomials are given by

$$\begin{aligned} &B_0 = 1 \\ &B_1(x_1) = x_1 \\ &B_2(x_1,x_2) = x_1^2 + x_2 \\ &B_3(x_1,x_2,x_3) = x_1^3 + 3x_1x_2 + x_3 \\ &B_4(x_1,x_2,x_3,x_4) = x_1^4 + 6x_1^2x_2 + 4x_1x_3 + 3x_2^2 + x_4 \\ &\vdots \end{aligned}$$

Also, the Complete Bell polynomials satisfy the binomial type relation:

$$B_p(x_1+y_1,..,x_p+y_p) = \sum_{i=0}^{p} \binom{p}{i} B_{p-i}(x_1,..,x_{p-i})B_i(y_1,..,y_i). \tag{6.24}$$

The following proposition gives the expression of the congestion probability as a function of the exponential complete Bell Polynomials.

Proposition 3. *Let Λ be a random variable such that $\Lambda = \sum_{n=1}^{N} nV_n$, with V_n are Poisson random variables of intensity w_n. Let x_j be defined as*

$$x_j = \begin{cases} w_j j! & \text{if } 1 \le j \le N, \\ 0 & \text{otherwise.} \end{cases}$$

The probability that Λ exceeds a threshold M can be expressed as a function of the exponential complete Bell polynomials by

$$\mathbb{P}(\Lambda \geq M) = 1 - H \sum_{k=0}^{M-1} \frac{B_k(x_1,...,x_k)}{k!} \tag{6.25}$$

with $H = e^{-\sum_{n=1}^{N} w_n}$.

Proof. By using the definition of x_j, the Z-Transform of Λ given by equation (6.18) becomes

$$f(z) = He^{\sum_{j=0}^{+\infty} z^j \frac{x_j}{j!}}, \tag{6.26}$$

with $H = e^{-\sum_{n=1}^{N} w_n}$.

The second exponential term in (6.26) can be evaluated by using the generating function of the complete Bell Polynomials given in equation (6.22), it follows that

$$f(z) = H \sum_{p=0}^{+\infty} \frac{z^p}{p!} B_p(x_1,...,x_p) \tag{6.27}$$

On the other hand, by using the definition of Z-Transform of Λ and the Taylor expansion of $f(z)$ in 0, we get

$$\mathbb{P}(\Lambda = p) = \frac{H}{p!} B_p(x_1,...,x_p). \tag{6.28}$$

Finally, from the definition of the CCDF, we obtain

$$\mathbb{P}(\Lambda \geq M) = 1 - \sum_{k=0}^{M-1} \mathbb{P}(\Lambda = k), \tag{6.29}$$

which completes the proof.. □

Now, to derive the expression of the congestion probability, we can apply proposition 3 to the random variable Γ defined in (6.10) as the superposition of two independent discrete random variables $\mathscr{F}$ and $\tilde{\mathscr{F}}$. Γ can be written as

$$\Gamma = \sum_{n=1}^{N} nV_n, \tag{6.30}$$

with $V_n = X_n + \tilde{X}_n$ is a Poisson random variable of parameter $w_n = \mu_n(Y) + \tilde{\mu}_n$. Hence, by using proposition 3, the congestion probability conditionally on ϕ (PLP) can be expressed as

$$P(\Gamma \geq M|\phi) = 1 - H \sum_{k=0}^{M-1} \frac{B_k(x_1,...,x_k)}{k!}, \tag{6.31}$$

where $x_j = (\mu_j(Y) + \tilde{\mu}_j)/\,j!$ and $H = e^{(-\alpha_N(Y) - \kappa\pi R^2)}$.

Once again, the final expression of the congestion probability is calculated by averaging over the PLP ϕ as

$$\Pi(M,\tau) = \mathbb{E}_\phi[\mathbb{P}(\Gamma \geq M|\phi)]. \tag{6.32}$$

Once we have the expression of the congestion probability, we set a target value Π^* and then, the required number of PRBs M is written as a function of τ through the implicit equation $\Pi(M,\tau) = \Pi^*$. The output M of the implicit function constitutes the result of the dimensioning process.

6.4 Numerical results

For numerical purpose, we consider a cell of radius $R = 0.7km$ with a transmit power level $P = 60dBm$ (corresponds to $43dBm$ from the transmitter power amplifier and $17dBi$ for the antenna gain of the transmitter) and operating with TDD mode having bandwidth of $20MHz$. The downlink thermal noise power including the receiver noise figure is calculated for $20MHz$ and set to $\sigma^2 = -93dBm$. For outdoor environment, the propagation parameter is $a = 130dB$ and for deep indoor environment we take $\tilde{a} = 166dB$. The path loss exponent is considered to be $2b = 3.5$. We assume also that we have 8Tx antennas in the BS and 2Rx antennas in users' terminals. So, the number of possible transmission layers is at most 2. The SINR threshold is set to $\Theta^* = -10dB$.

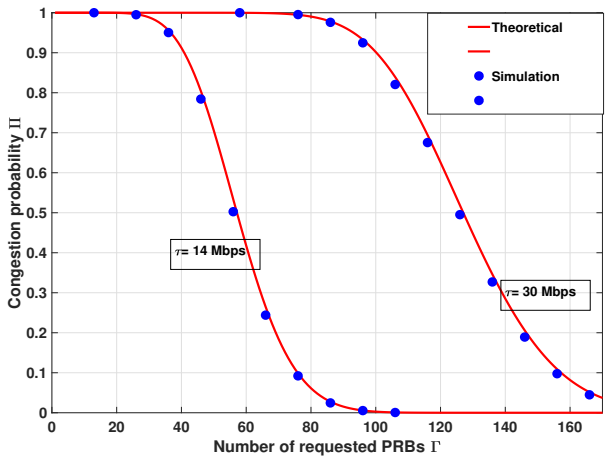

Figure 6.3 – Congestion probability theoretical vs simulation for two values of τ

In Fig. 6.3, we simulate the described model in MATLAB for two values of cell throughput $\tau = 14Mbps$ and $\tau = 30Mbps$. We notice that the explicit expression of the congestion probability fits the empirical one obtained by using Monte-Carlo simulations. Moreover, it is obvious that an increase in cell throughput τ generates an increase in the congestion probability because τ is related to the number of users in the cell and depends on 3 intensities: outdoor users' intensity δ, roads' intensity λ and indoor users' intensity κ. When those intensities increase, the number of required PRBs by users in the cell coverage area increases, thus the system experiences a high congestion. An other important factor that can impact system performance is the path loss exponent. The variations of this parameter has tremendous effect on the congestion probability: when $2b$ goes up, radio conditions become worse and consequently the number of demanded PRBs to guarantee the required QoS increases.

To see how users' random distribution impacts performance, we plot in Fig. 6.4 the congestion probability first, considering only outdoor users in a random system of roads according to Cox process with roads intensity $\lambda = 9km/km^2$ and users intensity $\delta = 6users/km$, and we compare it with the congestion probability of a spatial PPP outdoor users model with an equivalent intensity of $\lambda\delta = 54users/km^2$. We observe that the number of requested PRBs by users is always higher, for every target value of the congestion probability, when users are modeled by Cox process driven by PLP. In other words, even if the mean number of users in the cell is the same, the random tessellations of roads i.e., the geometry of the area covered by the cell has a significant impact on performance. Also, one can notice that if we consider a Cox model with high roads' intensity, users

appear to be distributed every where in the cell as in spatial PPP model with high users' intensity. In this case, Cox process driven by PLP can be approximated by a spatial PPP.

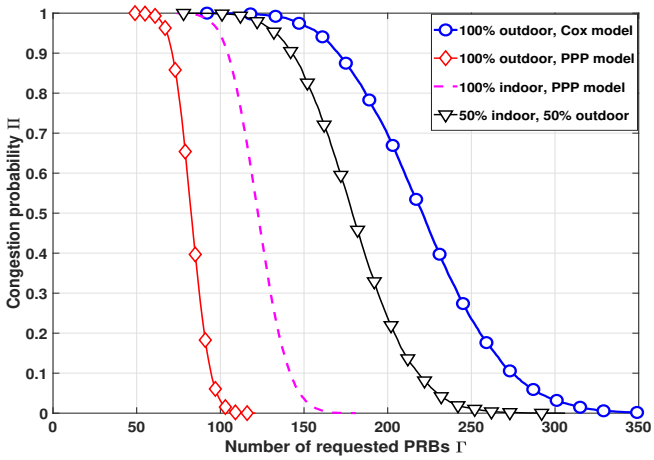

Figure 6.4 – Comparison between different user distributions

Also in Fig. 6.4, we compare the congestion probability of indoor users modeled according to a spatial PPP and the one of outdoor users modeled according to a spatial PPP having the same intensity. We notice that indoor users required more PRBs than outdoor users and this comes from the difference between outdoor and indoor environment. Actually, signal propagation in indoor environment suffers from high attenuation and delay factors because of the presence of obstacles such as buildings and walls. Hence, indoor users always experience high path loss and bad performance in terms of SINR, which means that they need always more PRBs than outdoor users to achieve a required transmission rate.

During resource dimensioning process, the operator starts by defining a target congestion probability that can be tolerated for a given service. For different traffic forecasts, the number of PRBs is set to ensure that the congestion probability never exceeds its target value. Fig. 6.5 shows the number of required PRBs that the operator should make it available, when the expected cell throughput is known, for two target values of the congestion probability ($\Pi^* = 1\%$ and $\Pi^* = 5\%$) and for two roads' intensity values ($\lambda = 2km/km^2$ and $\lambda = 10km/km^2$) with a fixed transmission rate of $500kbps$. We can observe that for each forecast cell throughput value, the threshold number of resources required in the cell decreases when road intensity increases. For instance, when λ increases from $2km/km^2$ to

$10km/km^2$ (i.e., from 9 expected roads to 44), the number of dimensioned PRBs decreases by 32, for the same cell throughput value $\tau = 25Mbps$. Also, for a given value of τ, we can notice from (6.5) that the user intensity on roads δ is inversely proportional to roads' intensity λ. Thus for fixed τ, if λ increases, δ decreases and consequently the number of required PRBs decreases.

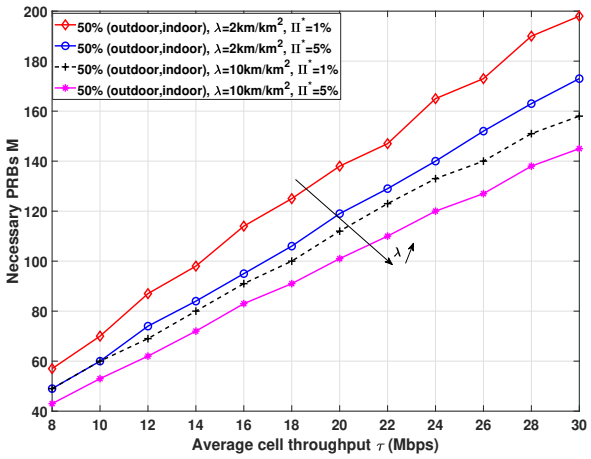

Figure 6.5 – Required PRB M as a function of cell Throughput τ, for fixed transmission rate $C^* = 500kbps$.

Moreover, in Fig. 6.6 we compare dimensioning results of three models: Outdoor users according to Cox process driven by PLP, outdoor users according to a spatial PPP model and indoor users with spatial PPP model (having the same intensities). We notice that the number of dimensioned PRBs for outdoor users is always higher when users are modeled according to Cox process driven by PLP than spatial PPP model. Also, we can see that indoor users need more PRBs than outdoor users (when the both are modeled by the spatial PPP) which is in agreement with the previous results. Besides, we have mentioned previously that when λ is very high, the distribution of users becomes similar to the one of a spatial PPP. Thus, with a spatial PPP model, one can have small values of dimensioned PRBs, which is considered optimistic compared to the real geometry of the area covered by a cell in dense urban environment where more PRBs are required to guarantee the desired quality of services.

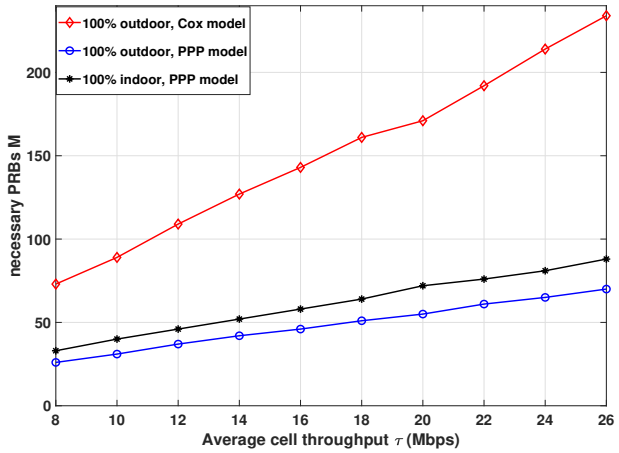

Figure 6.6 – Dimensioned PRBs comparison: outdoor users with Cox model, outdoor users with spatial PPP and indoor users with spatial PPP, for a fixed transmission rate $C^* = 500kbps$

To see interference impact on the dimensioning process, we consider three regions of the cell: cell center with a radius of $R/3$, cell middle represented by the ring between $R/3$ and $2R/3$ and cell edge identified by a distance from the BS that exceeds $2R/3$. Each region of the cell experiences a given level of interference evaluated in terms of IM (Interference Margin or Noise Rise). Cell edge users always experience high interference level and IM is set to be $15dB$. In cell middle we consider an interference margin of $8dB$, whereas in the cell center where users perceive good radio conditions, the interference margin is set to be $IM = 1dB$.

Fig. 6.7 shows the congestion probability in a noise-limited scenario (Interference level is neglected) and its comparison with the one where interference is considered as we have described above. We consider a scenario with 50% of outdoor users modeled according to Cox process driven by the PLP and 50% of indoor users modeled according to a spatial PPP, with an average cell throughput of $30Mbps$ and a fixed transmission rate of $500kbps$. As expected, interference has a tremendous impact on the number of required PRBs. For instance, when the target congestion probability is set to 5%, the number of required PRBs increases by almost 80 because of the presence of interference. Similarly in Fig. 6.8, we plot dimensioning curves i.e., the threshold number of PRBs in the cell as a function of the forecast average cell throughput, for a noise-limited environment and an environment with interference. As we can see, the number of PRBs that the operator should make it available is higher when interference impact is considered. For instance,

for a forecast average cell throughput of 26Mbps and a target QoS $\Pi^* = 5\%$, the number of dimensioned PRBs increases by almost 50 PRBs when the three interference margins are considered.

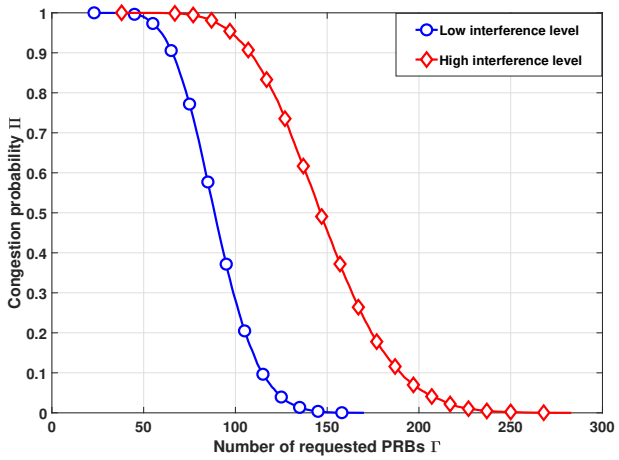

Figure 6.7 – Interference impact ($\tau = 30Mbps$).

Besides, interference level varies from one location to another in the same cell. Practically cell edge users experience high interference level compared to users that are close to the BS in the cell middle or cell center. Fig. 6.9 shows a comparison between radio resource dimensioning results for the three regions of the cell: cell center, cell middle and cell edge. As we can observe, the high demand on PRBs comes especially from cell edge users that perceive bad radio conditions because of their far distance from the BS and the presence of interference. Hence, for a predicted average cell throughput, the number of dimensioned PRBs should be set always by considering a probable presence of traffic hotspots at cell edges.

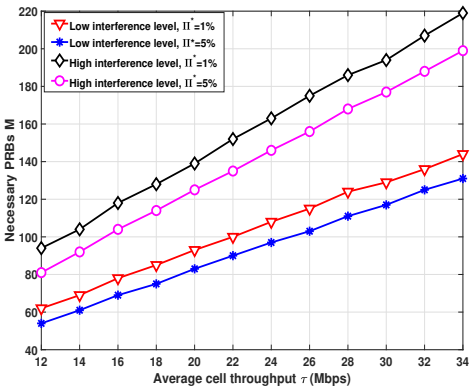

Figure 6.8 – Interference impact on dimensioned PRBs M.

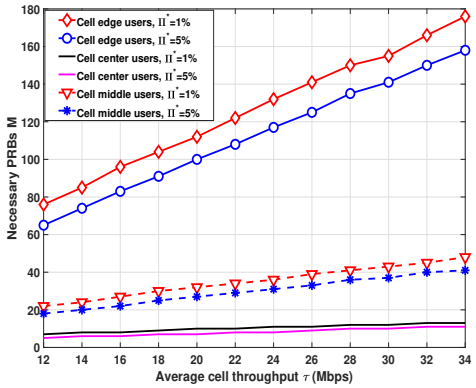

Figure 6.9 – Comparison between dimensioned PRBs M for cell edge, cell middle and cell center users.

Dimensioning phase is very important because it gives the operators a vision on how they should manage the available spectrum. If the dimensioned number of resources exceeds the available one, the operator can for instance:

- aggregate fragmented spectrum resources into a single wider band in order to increase the available PRBs,
- activate capacity improvement features like carrier aggregation or dual connectivity between 5G and legacy 4G networks in order to delay investment on the acquisition of new spectrum bands,
- change the TDD (Time Division Duplexing), configuration to relieve the congested link,
- or even buy new spectrum bands.

6.5 Conclusion

In this chapter, we have presented a resource dimensioning model for OFDM based systems that can be applied also for scalable OFDM based 5G NR interface. We have considered two spatial random distributions in order to distinguish between outdoor users distributed along a random system of roads in a typical cell coverage area (Cox Point Process driven by PLP) and indoor users distributed in buildings according to the widely used

spatial PPP. The comparison between the two spatial distributions showed that results are more optimistic when spatial PPP is used. Also, we have shown that the geometry of the area covered by a cell can impact the results. Moreover, we have derived an analytical model to qualify the number of required PRBs in a typical cell with two explicit formulas of the congestion probability. Moreover, we have established an implicit relationship between the required resources and the forecast traffic given a target congestion probability. This relationship translates the dimensioning problem that an operator can perform to look for the amount of necessary spectrum resources to satisfy a predefined QoS. Finally, a comparison between an interfered environment and a noise-limited one has been provided. Besides, we have shown that the high requirement in terms of radio resources comes from cell edge users that perceive bad radio conditions.

Chapter 7

Conclusions and perspectives

7.1 Conclusions

In this dissertation, D-TDD interference problematic in macro-cell and small-cell networks has been discussed. We have chosen a regular hexagonal network to model the macro-cells' layer and a spatial PPP to model the distribution of small-cells. We have derived the explicit expressions of ISR covering different interference scenarios in a D-TDD based network. This metric is very important from an engineering point of view since it gives an estimation of the average perceived interference in each location of the studied cell and can be used in link budget tools. Also, we have derived the explicit formulas of the coverage probability for both macro-cells and small cells. Results have shown that D-TDD results in a gain during the DL cycle of cells since reducing the number of DL transmitting cells minimizes in turn the perceived interference. However, the UL transmission undergoes a huge degradation in performance because of the strong interference coming from DL transmitting BSs. Small-cells performance are better than macro-cells since they are well isolated from each others and can be isolated from the macro-cell layer by using an interference coordination technique such as FeICIC. In spite of that, small-cells still suffer from DL to UL interference. Therefore, implementing an interference mitigation scheme, when D-TDD feature is activated, for the UL transmission is a must for both macro-cell and small-cell networks.

To this intend, we have proposed a 3D beamforming scheme where antenna horizontal and radiation patterns depend on the spatial distribution of users' locations and dedicated to reduce DL interference in macro-cell networks. With this scheme, we have shown that ISR is an almost sure convergent series which is an important results since the almost sure convergence implies convergence in probability and thus implies convergence in distribu-

tion. Moreover, combining the 3D beamforming and D-TDD leads to an enhancement of the coverage probability in both DL and UL transmission directions which makes D-TDD feasible for macro-cell deployments. Additionally we have shown that using FPC mechanisms, with small power control factors, during the UL transmission enhances performance especially when 3D beamforming is used for DL transmitting BSs. For D-TDD based small-cells network, we have proposed a cell-clustering scheme based on the hexagonal tessellation. Results have shown that this scheme reduces DL to UL interference and enhances the UL performance in terms of ISR.

On the other hand, we have assessed in the third part of this dissertation the problematic of OFDM radio resource dimensioning. We have considered two spatial models for users in a typical cell coverage area. The first one is the spatial PPP which is convenient to model the spatial distribution of indoor users, usually located inside buildings. The second one is Cox process driven by PLP to model the random distribution of roads in the cell coverage area and the distribution of users located on this random system of roads. This model can be adequate to outdoor users often located along roads. We have evaluated the congestion probability, considered as a relevant metric for the QoS, by using a mathematical tool from the combinatorial analysis which is Bell polynomials. Furthermore, the proposed dimensioning approach remains valid for the scalable OFDM that will be a key feature of 5G networks and can be used with other spatial processes that describes the spatial distribution of users. Results have shown that the network geometry has impact on dimensioning results. We have reached the conclusion that dimensioning results are optimistic with spatial PPP comparing to Cox process driven by PLP. Also, we have shown that the the high requirement in terms of radio resources comes from cell edge users that usually perceive bad radio conditions because of the high received interference and their distance from the serving BS.

7.2 Perspectives

Although the proposed 3D beamforming scheme deals efficiently with DL to UL and DL to DL interference in D-TDD based macro-cell networks, the problem of UL to DL interference still exists and has an impact on performance during the DL cycle of cells. Actually, this interference is difficult to deal with because the sources of interference are mobiles that move around randomly. The first extension of this work could include a study of a 3D beamforming scheme dedicated to reduce the impact of UL interference. The second extension could focus on beam coordination between BSs and mobiles. Coordination between BSs appears to be possible by using a long term CSI measurements since BSs

have fixed locations and interference between them can be static. However, coordination between users is difficult to perform because of their randomness and requires more investigations. The third extension could focus on studying the imperfection of beam steering to indoor users. Actually, indoor users suffer from a strong signal attenuation because of buildings' penetration. This bad propagation environment can impact the precision of beam steering which is based on users' localization. Finally, regarding OFDM radio resource dimensioning, more attention could be focused on other random models to describe the spatial distribution of users and the random tessellation of roads' systems.

Bibliography

[1] E. Dahlman, S. Parkvall, and J. Skold, *5G NR: The next generation wireless access technology*. Academic Press, 2018.

[2] D. Astely, E. Dahlman, G. Fodor, S. Parkvall, and J. Sachs, "Lte release 12 and beyond [accepted from open call]," *IEEE Communications Magazine*, vol. 51, no. 7, pp. 154–160, 2013.

[3] A. D. Gandhi, "Significant Gains in Coverage and Downlink Capacity From Optimal Antenna Downtilt for Closely-Spaced cells in wireless networks," in *Wireless and Optical Communication Conference (WOCC), 2014 23rd*. IEEE, 2014, pp. 1–6.

[4] 3GPP, "Technical specification group radio access network (nr) ; physical layer procedures for data," 3rd Generation Partnership Project (3GPP), TS 38.214, 12 2017, version 15.0.0.

[5] R. D. Trivedi and M. Patel, "Comparison of different scheduling algorithm for lte," *International Journal of Emerging Technology and Advanced Engineering*, vol. 4, no. 5, pp. 334–339, 2014.

[6] S. Sadr, A. Anpalagan, and K. Raahemifar, "Radio resource allocation algorithms for the downlink of multiuser ofdm communication systems," *IEEE Communications Surveys & Tutorials*, vol. 11, no. 3, 2009.

[7] E. Yaacoub and Z. Dawy, "A survey on uplink resource allocation in ofdma wireless networks," *IEEE Communications Surveys & Tutorials*, vol. 14, no. 2, pp. 322–337, 2012.

[8] R. Nasri and A. Jaziri, "Analytical tractability of hexagonal network model with random user location," *IEEE Transactions on Wireless Communications*, vol. 15, no. 5, pp. 3768–3780, May 2016.

[9] J. G. Andrews, F. Baccelli, and R. K. Ganti, "A tractable approach to coverage and rate in cellular networks," *Communications, IEEE Transactions on*, vol. 59, no. 11, pp. 3122–3134, 2011.

[10] B. Błaszczyszyn and M. K. Karray, "Spatial Distribution of The SINR in Poisson Cellular Networks With Sector Antennas," *IEEE Transactions on Wireless Communications*, vol. 15, no. 1, pp. 581–593, 2016.

[11] R. Nasri and A. Jaziri, "Tractable approach for hexagonal cellular network model and its comparison to poisson point process," in *Proc. IEEE Globecom 2015, Wireless Communications Symposium*, 2015.

[12] Y. Wang, K. Venugopal, R. W. Heath, and A. F. Molisch, "Mmwave vehicle-to-infrastructure communication: Analysis of urban microcellular networks," *IEEE Transactions on Vehicular Technology*, 2018.

[13] C. Gloaguen, F. Fleischer, H. Schmidt, and V. Schmidt, "Analysis of shortest paths and subscriber line lengths in telecommunication access networks," *Networks and Spatial Economics*, vol. 10, no. 1, pp. 15–47, 2010.

[14] F. Voss, C. Gloaguen, F. Fleischer, and V. Schmidt, "Distributional properties of euclidean distances in wireless networks involving road systems," *IEEE Journal on Selected Areas in Communications*, vol. 27, no. 7, 2009.

[15] V. V. Chetlur and H. S. Dhillon, "Coverage analysis of a vehicular network modeled as cox process driven by poisson line process," *IEEE Transactions on Wireless Communications*, 2018.

[16] S. Chen, S. Sun, Y. Wang, G. Xiao, and R. Tamrakar, "A comprehensive survey of tdd-based mobile communication systems from td-scdma 3g to td-lte (a) 4g and 5g directions," *China Communications*, vol. 12, no. 2, pp. 40–60, 2015.

[17] W. Jeong and M. Kavehrad, "Cochannel interference reduction in dynamic-tdd fixed wireless applications, using time slot allocation algorithms," *IEEE Transactions on Communications*, vol. 50, no. 10, pp. 1627–1636, 2002.

[18] H. Holma, S. Heikkinen, O.-A. Lehtinen, and A. Toskala, "Interference considerations for the time division duplex mode of the umts terrestrial radio access," *IEEE Journal on Selected Areas in communications*, vol. 18, no. 8, pp. 1386–1393, 2000.

[19] H. Ji, Y. Kim, S. Choi, J. Cho, and J. Lee, "Dynamic resource adaptation in beyond lte-a tdd heterogeneous networks," in *2013 IEEE International Conference on Communications Workshops (ICC)*. IEEE, 2013, pp. 133–137.

[20] P. Pirinen, "Challenges and possibilities for flexible duplexing in 5g networks," in *2015 IEEE 20th International Workshop on Computer Aided Modelling and Design of Communication Links and Networks (CAMAD)*. IEEE, 2015, pp. 6–10.

[21] J. Nasreddine and S. E. H. Hassan, "Interference mitigation and traffic adaptation using cell clustering for lte-tdd systems," in *Multidisciplinary Conference on Engineering Technology (IMCET), IEEE International*. IEEE, 2016, pp. 155–159.

[22] Y. Zhong, P. Cheng, N. Wang, and W. Zhang, "Dynamic tdd enhancement through distributed interference coordination," in *2015 IEEE International Conference on Communications (ICC)*. IEEE, 2015, pp. 3509–3515.

[23] M. S. ElBamby, M. Bennis, W. Saad, and M. Latva-Aho, "Dynamic uplink-downlink optimization in tdd-based small cell networks," in *2014 11th International Symposium on Wireless Communications Systems (ISWCS)*. IEEE, 2014, pp. 939–944.

[24] A. Khoryaev, A. Chervyakov, M. Shilov, S. Panteleev, and A. Lomayev, "Performance analysis of dynamic adjustment of tdd uplink-downlink configurations in outdoor picocell lte networks," in *Ultra Modern Telecommunications and Control Systems and Workshops (ICUMT), 2012 4th International Congress on*. IEEE, 2012, pp. 914–921.

[25] A. Lukowa and V. Venkatasubramanian, "Centralized ul/dl resource allocation for flexible tdd systems with interference cancellation," *IEEE Transactions on Vehicular Technology*, 2019.

[26] A. Łukowa and V. Venkatasubramanian, "On the performance of 5g flexible tdd systems with coordinated beamforming," in *2018 14th International Conference on Wireless and Mobile Computing, Networking and Communications (WiMob)*. IEEE, 2018, pp. 175–180.

[27] B. Yu, L. Yang, H. Ishii, and S. Mukherjee, "Dynamic tdd support in macrocell-assisted small cell architecture," *IEEE Journal on Selected Areas in Communications*, vol. 33, no. 6, pp. 1201–1213, 2015.

[28] T. Ding, M. Ding, G. Mao, Z. Lin, A. Y. Zomaya, and D. López-Pérez, "Performance analysis of dense small cell networks with dynamic tdd," *IEEE Transactions on Vehicular Technology*, vol. 67, no. 10, pp. 9816–9830, 2018.

[29] H. Sun, M. Wildemeersch, M. Sheng, and T. Q. Quek, "D2d enhanced heterogeneous cellular networks with dynamic tdd," *IEEE Transactions on Wireless Communications*, vol. 14, no. 8, pp. 4204–4218, 2015.

[30] M. N. Kulkarni, J. G. Andrews, and A. Ghosh, "Performance of dynamic and static tdd in self-backhauled millimeter wave cellular networks," *IEEE Transactions on Wireless Communications*, 2017.

[31] Y. Gao, L. Cheng, Y. Li, X. Zhang, and D. Yang, "Performance evaluation on cell clustering interference mitigation and comp in multi-pico network with dynamic tdd," in *Vehicular Technology Conference (VTC Spring), 2015 IEEE 81st*. IEEE, 2015, pp. 1–5.

[32] Y.-T. Lin, C.-C. Chao, and H.-Y. Wei, "Dynamic tdd interference mitigation by using soft reconfiguration," in *Heterogeneous Networking for Quality, Reliability, Security and Robustness (QSHINE), 2015 11th International Conference on*. IEEE, 2015, pp. 352–357.

[33] T. L. Marzetta, "Massive mimo: an introduction," *Bell Labs Technical Journal*, vol. 20, pp. 11–22, 2015.

[34] E. G. Larsson, O. Edfors, F. Tufvesson, and T. L. Marzetta, "Massive mimo for next generation wireless systems," *IEEE communications magazine*, vol. 52, no. 2, pp. 186–195, 2014.

[35] J. Hoydis, S. ten Brink, and M. Debbah, "Massive mimo in the ul/dl of cellular networks: How many antennas do we need?" *IEEE Journal on Selected Areas in Communications*, vol. 31, no. 2, pp. 160–171, 2013.

[36] A. L. Swindlehurst, E. Ayanoglu, P. Heydari, and F. Capolino, "Millimeter-wave massive mimo: The next wireless revolution?" *IEEE Communications Magazine*, vol. 52, no. 9, pp. 56–62, 2014.

[37] A. F. Molisch, V. V. Ratnam, S. Han, Z. Li, S. L. H. Nguyen, L. Li, and K. Haneda, "Hybrid beamforming for massive mimo: A survey," *IEEE Communications Magazine*, vol. 55, no. 9, pp. 134–141, 2017.

[38] A. Kammoun, M.-S. Alouini *et al.*, "Elevation beamforming with full dimension mimo architectures in 5g systems: A tutorial," *IEEE Communications Surveys & Tutorials*, 2019.

[39] T. L. Marzetta, "How much training is required for multiuser mimo?" in *2006 Fortieth Asilomar Conference on Signals, Systems and Computers*. IEEE, 2006, pp. 359–363.

[40] A. Tall, Z. Altman, and E. Altman, "Multilevel beamforming for high data rate communication in 5g networks," *arXiv preprint arXiv:1504.00280*, 2015.

[41] J. Ramiro-Moreno, K. I. Pedersen, and P. E. Mogensen, "Capacity gain of beamforming techniques in a wcdma system under channelization code constraints," *IEEE Transactions on Wireless Communications*, vol. 3, no. 4, pp. 1199–1208, 2004.

[42] T. Bai and R. W. Heath, "Coverage and Rate Analysis for Millimeter-Wave Cellular Networks," *IEEE Transactions on Wireless Communications*, vol. 14, no. 2, pp. 1100–1114, 2015.

[43] S. Singh, M. N. Kulkarni, A. Ghosh, and J. G. Andrews, "Tractable model for rate in self-backhauled millimeter wave cellular networks," *IEEE Journal on Selected Areas in Communications*, vol. 33, no. 10, pp. 2196–2211, 2015.

[44] H. Elkotby and M. Vu, "Interference modeling for cellular networks under beamforming transmission," *IEEE Transactions on Wireless Communications*, vol. 16, no. 8, pp. 5201–5217, 2017.

[45] S. Ak, H. Inaltekin, and H. V. Poor, "Gaussian approximation for the downlink interference in heterogeneous cellular networks," in *2016 IEEE International Symposium on Information Theory (ISIT)*. IEEE, 2016, pp. 1611–1615.

[46] J. Anastasov, G. Djordjevic, and M. Stefanovic, "Outage probability of interference-limited system over weibull-gamma fading channel," *Electronics letters*, vol. 48, no. 7, pp. 408–410, 2012.

[47] J. Koppenborg, H. Halbauer, S. Saur, and C. Hoek, "3d Beamforming Trials With an Active Antenna Array," in *Smart Antennas (WSA), 2012 International ITG Workshop on*. IEEE, 2012, pp. 110–114.

[48] H. Halbauer, S. Saur, J. Koppenborg, and C. Hoek, "Interference Avoidance With Dynamic Vertical Beamsteering in Real Deployments," in *Wireless Communications and Networking Conference Workshops (WCNCW), 2012 IEEE*. IEEE, 2012, pp. 294–299.

[49] J. Yang, M. Ding, G. Mao, Z. Lin, D.-g. Zhang, and T. H. Luan, "Optimal Base Station Antenna Downtilt in Downlink Cellular Networks," *arXiv preprint arXiv:1802.07479*, 2018.

[50] N. Seifi, M. Coldrey, M. Matthaiou, and M. Viberg, "Impact of Base Station Antenna Tilt on The Performance of Network MIMO Systems," in *IEEE 75th Vehicular Technology Conference, VTC Spring 2012, Yokohama, 6 May-9 June 2012*, 2012.

[51] J.-M. Kelif, M. Coupechoux, and M. Mansanarez, "A 3d beamforming analytical model for 5g wireless networks," in *2016 14th International Symposium on Modeling and Optimization in Mobile, Ad Hoc, and Wireless Networks (WiOpt)*. IEEE, 2016, pp. 1–8.

[52] Y. Huang, B. Jalaian, S. Russell, and H. Samani, "Technical report on efficient integration of dynamic tdd with massive mimo," *arXiv preprint arXiv:1804.06143*, 2018.

[53] A. A. Zaidi, R. Baldemair, V. Moles-Cases, N. He, K. Werner, and A. Cedergren, "Ofdm numerology design for 5g new radio to support iot, embb, and mbsfn," *IEEE Communications Standards Magazine*, vol. 2, no. 2, pp. 78–83, 2018.

[54] Z. Shen, J. G. Andrews, and B. L. Evans, "Adaptive resource allocation in multiuser ofdm systems with proportional rate constraints," *IEEE transactions on wireless communications*, vol. 4, no. 6, pp. 2726–2737, 2005.

[55] A. M. El Hajj and Z. Dawy, "Dynamic joint switching point configuration and resource allocation in tdd-ofdma wireless networks," in *Global Telecommunications Conference (GLOBECOM 2011), 2011 IEEE*. IEEE, 2011, pp. 1–6.

[56] A. M. El-Hajj, Z. Dawy, and W. Saad, "A stable matching game for joint uplink/downlink resource allocation in ofdma wireless networks," in *Communications (ICC), 2012 IEEE International Conference on*. IEEE, 2012, pp. 5354–5359.

[57] R. Agarwal, V. R. Majjigi, Z. Han, R. Vannithamby, and J. M. Cioffi, "Low complexity resource allocation with opportunistic feedback over downlink ofdma networks," *IEEE Journal on Selected Areas in Communications*, vol. 26, no. 8, 2008.

[58] A. K. Khattab and K. M. Elsayed, "Opportunistic scheduling of delay sensitive traffic in ofdma-basedwireless," in *proceedings of the 2006 International Symposium on on World of Wireless, Mobile and Multimedia Networks*. IEEE Computer Society, 2006, pp. 279–288.

[59] L. Decreusefond, E. Ferraz, P. Martins, and T.-T. Vu, "Robust methods for lte and wimax dimensioning," in *Performance Evaluation Methodologies and Tools (VALUETOOLS), 2012 6th International Conference on*. IEEE, 2012, pp. 74–82.

[60] B. Blaszczyszyn and M. K. Karray, "Dimensioning of the downlink in ofdma cellular networks via an erlang's loss model," in *Wireless Conference, 2009. EW 2009. European*. IEEE, 2009, pp. 157–161.

[61] M. K. Karray, "Analytical evaluation of qos in the downlink of ofdma wireless cellular networks serving streaming and elastic traffic," *IEEE Transactions on Wireless Communications*, vol. 9, no. 5, 2010.

[62] R. Giuliano and F. Mazzenga, "Dimensioning of ofdm/ofdma-based cellular networks using exponential effective sinr," *IEEE Transactions on Vehicular Technology*, vol. 58, no. 8, pp. 4204–4213, 2009.

[63] J. G. Andrews, A. K. Gupta, and H. S. Dhillon, "A primer on cellular network analysis using stochastic geometry," *arXiv preprint arXiv:1604.03183*, 2016.

[64] V. V. Chetlur and H. S. Dhillon, "Success probability and area spectral efficiency of a vanet modeled as a cox process," *IEEE Wireless Communications Letters*, vol. 7, no. 5, pp. 856–859, 2018.

[65] C.-S. Choi and F. Baccelli, "An analytical framework for coverage in cellular networks leveraging vehicles," *arXiv preprint arXiv:1711.09453*, 2017.

[66] N. Deng, W. Zhou, and M. Haenggi, "The Ginibre point process as a model for wireless networks with repulsion," *Wireless Communications, IEEE Transactions on*, vol. 14, no. 1, pp. 107–121, 2015.

[67] H. S. Dhillon, R. K. Ganti, F. Baccelli, and J. G. Andrews, "Modeling and analysis of k-tier downlink heterogeneous cellular networks," *arXiv preprint arXiv:1103.2177*, 2011.

[68] ——, "Modeling and analysis of K-tier downlink heterogeneous cellular networks," *Selected Areas in Communications, IEEE Journal on*, vol. 30, no. 3, pp. 550–560, 2012.

[69] H. ElSawy, E. Hossain, and M. Haenggi, "Stochastic geometry for modeling, analysis, and design of multi-tier and cognitive cellular wireless networks: A survey," *IEEE Communications Surveys & Tutorials*, vol. 15, no. 3, pp. 996–1019, 2013.

[70] J.-M. Kelif, M. Coupechoux, and P. Godlewski, "A fluid model for performance analysis in cellular networks," *EURASIP Journal on Wireless Communications and Networking*, vol. 2010, p. 1, 2010.

[71] T. D. Novlan, H. S. Dhillon, and J. G. Andrews, "Analytical modeling of uplink cellular networks," *IEEE Transactions on Wireless Communications*, vol. 12, no. 6, pp. 2669–2679, 2013.

[72] F. Morlot, "A population model based on a poisson line tessellation," in *2012 10th International Symposium on Modeling and Optimization in Mobile, Ad Hoc and Wireless Networks (WiOpt)*. IEEE, 2012, pp. 337–342.

[73] M. Coupechoux and J.-M. Kelif, "How to set the fractional power control compensation factor in lte?" in *Sarnoff Symposium, 2011 34th IEEE*. IEEE, 2011, pp. 1–5.

[74] K. Han, K. Huang, Y. Cui, and Y. Wu, "The connectivity of millimeter-wave networks in manhattan-type regions," in *GLOBECOM 2017-2017 IEEE Global Communications Conference*. IEEE, 2017, pp. 1–6.

[75] C.-S. Choi and F. Baccelli, "An analytical framework for coverage in cellular networks leveraging vehicles," *IEEE Transactions on Communications*, 2018.

[76] P. Mogensen, W. Na, I. Z. Kovács, F. Frederiksen, A. Pokhariyal, K. Pedersen, T. Kolding, K. Hugl, M. Kuusela *et al.*, "LTE capacity compared to the shannon bound," in *IEEE 65th Vehicular Technology Conference, VTC2007-Spring*. IEEE, 2007, pp. 1234–1238.

[77] C. U. Castellanos, D. L. Villa, C. Rosa, K. I. Pedersen, F. D. Calabrese, P.-H. Michaelsen, and J. Michel, "Performance of uplink fractional power control in utran lte," in *Vehicular Technology Conference, 2008. VTC Spring 2008. IEEE*. IEEE, 2008, pp. 2517–2521.

[78] M. Abramowitz and I. A. Stegun, *Handbook of mathematical functions: with formulas, graphs, and mathematical tables*. Courier Corporation, 1964, no. 55.

[79] P. E. Mogensen, K. Pedersen, P. Leth-Espensen, B. Fleury, F. Frederiksen, K. Olesen, S. L. Larsen *et al.*, "Preliminary measurement results from an adaptive antenna array testbed for GSM/UMTS," in *IEEE 47th Vehicular Technology Conference*, vol. 3. IEEE, 1997, pp. 1592–1596.

[80] L. F. Fenton, "The sum of log-normal probability distributions in scatter transmission systems," *Communications Systems, IRE Transactions on*, vol. 8, no. 1, pp. 57–67, 1960.

[81] J. Jacod and P. Protter, *Probability Essentials*. Springer Science & Business Media, 2012.

[82] N. Seifi, J. Zhang, R. W. Heath, T. Svensson, and M. Coldrey, "Coordinated 3d beamforming for interference management in cellular networks," *IEEE Transactions on Wireless Communications*, vol. 13, no. 10, pp. 5396–5410, 2014.

[83] Q. Tang, N. Ma, S. Guo, and X. Hou, "A beam coordination based interference mitigation scheme for 5g dynamic tdd," in *2017 3rd IEEE International Conference on Computer and Communications (ICCC)*. IEEE, 2017, pp. 36–40.

[84] S. Roman, "" the exponential polynomials" and" the bell polynomials", 4.1. 3 and 4.1. 8," *The Umbral Calculus*, pp. 63–67, 1984.

[85] M. Mihoubi, "Bell polynomials and binomial type sequences," *Discrete Mathematics*, vol. 308, no. 12, pp. 2450–2459, 2008.

INSTITUT POLYTECHNIQUE DE PARIS

Titre: Analyse des Performances et Dimensionnement des Réseaux Mobiles 5G basés sur le TDD avec Différent Modèles Géométriques.

Mots clés : D-TDD, Probabilité de couverture, ISR, OFDMA, PLP, Dimensionnement.

Résumé : La nouvelle génération des réseaux mobiles 5G-NR est en cours de standardisation à travers des améliorations apportées à son prédécesseur 4G/4G+. 5G-NR va introduire un nouveau niveau de flexibilité, scalabilité et efficacité afin de satisfaire plusieurs classes de services. Le mode de duplexage TDD est le plus favorable pour 5G-NR grâce aux avantages qu'il représente par rapport au mode FDD en termes de capacité, flexibilité et convenance de déploiement avec les autres technologies attendues dans le cadre de la 5G comme FD-MIMO. Une variante du TDD, connue sous le nom du dynamique TDD (D-TDD), attire de plus en plus l'attention. D-TDD est désigné pour l'adaptation des configurations des sous-trames DL et UL en se basant sur une estimation instantanée du trafic. Cependant, l'utilisation de ce mode nécessite l'implémentation des mécanismes capable de réduire deux types d'interférence additionnelles : l'interférence générée par les stations de bases qui impacte le signal UL des utilisateurs et l'interférence générée par les mobiles en UL qui interfère avec le signal DL des stations de base.

La première partie de cette thèse est consacrée à l'analyse des performances du mode D-TDD en termes d'ISR et de probabilité de couverture dans 2 types de déploiement : macro-cells et small-cells. Ensuite, nous proposons deux techniques de mitigation des interférences dont la première est destinée aux macro-cells et basée sur le 3D beamforming. La 2ème est le cell clustering statique appliquée au small-cells afin de réduire l'impact de l'interférence DL to UL. Dans la 2ème partie de cette thèse, nous étudions la problématique du dimensionnement de l'OFDMA scalable qui sera une technologie de base pour la 5G-NR. Etant donné que le dimensionnement des ressources radio est une tâche primordiale dans l'ingénierie radio, nous proposons un modèle analytique qui permet la réalisation de cette tâche en considérant un scheduling proportional fair. Nous distinguons entre 2 types d'utilisateurs : utilisateurs indoor qui sont modélisés par un PPP spatial et utilisateurs outdoor qui sont modélisés selon un processus de Cox conduit par un PLP. L'objectif c'est d'étudier l'impact de la géométrie de la zone de couverture d'une cellule et la distribution aléatoire des utilisateurs sur les performances.

Title: TDD Based 5G Networks Performance Analysis and Radio Resource Dimensioning with Different Network Geometry Models.

Keywords : D-TDD, Coverage Probability, ISR, OFDMA, PLP, Dimensioning.

Abstract : A new generation of cellular networks, known as 5G new radio (NR), has been standardized through improvements in the current 4G/4G+ concepts and features in order to bring a new level of flexibility, scalability and efficiency. Time division duplex (TDD) is expected to be one of the key features of 5G NR since it offers more advantages than frequency division duplex (FDD) mode in terms of capacity, flexibility and implementation adequacy with other features, such as full dimension multiple input multiple output antenna (FD-MIMO) technology. A variant operational mode of TDD, known as D-TDD, is in the scope. It is designed to deal with uplink (UL) and downlink (DL) traffic asymmetry since it is based on instantaneous traffic estimation and offers more flexibility in resource assignment. However, the use of D-TDD requires new interference mitigation schemes capable to handle two additional types of interference called cross link interference (CLI) and stands for DL to UL and UL to DL interference. The first part of this thesis is devoted to the problem of interference modeling in D-TDD based macro-cell and small-cell deployments. We provide a complete analytical approach to derive relevant metrics, such as interference-to-signal-ratio (ISR) and the coverage probability formulas, considering adequate geometry models for each type of deployment. Then, we propose an interference mitigation scheme based on 3D beamforming for macro-cells and a cell-clustering scheme for small-cells. Additionally, we investigate another problematic which is Orthogonal Frequency Division Multiplex (OFDM) radio resource dimensioning. Since 5G NR takes in consideration a wide array of emerging use cases and also the possibility of having future requirements, the third Generation Partnership Project (3GPP) comes up with a variant of OFDM known as scalable OFDM and having different sub carriers' spacing. This feature appears to be an ideal choice for 5G NR since it offers a high spectral efficiency, robustness to selective fading channels, convenience with diverse spectrum bands and compatibility with other features. Therefore, dimensioning OFDM is a major task to accomplish in the context of NR. To this purpose, we provide an analytical model to dimension OFDM based systems with a proportional fair resources' allocation policy. We model indoor users by a spatial PPP and outdoor users according to a Cox process driven by PLP. Different analytical and numerical results are provided to justify the accuracy of this model.

Institut Polytechnique de Paris
91120 Palaiseau, France